2021

Development And Evaluation Of A Functional Human Cardiac Tissue Equivalent Fabricated From Multi-Lineage Human Induced Pluripotent Stem Cell Derived Cells

Danielle Pretorius
University of Alabama at Birmingham

DEVELOPMENT AND EVALUATION OF A FUNCTIONAL HUMAN CARDIAC TISSUE EQUIVALENT FABRICATED FROM MULTI-LINEAGE HUMAN INDUCED PLURIPOTENT STEM CELL DERIVED CELLS

by

DANIELLE PRETORIUS

JIANYI ZHANG, CHAIR
JOEL L. BERRY, CO-MENTOR
ALAN W. EBERHARDT, CO-MENTOR
PALANIAPPAN SETHU
CHAO ZHAO
WUQIANG ZHU

A DISSERTATION

Submitted to the graduate faculty of The University of Alabama at Birmingham,
in partial fulfillment of the requirements for the degree of
Doctor of Philosophy

BIRMINGHAM, ALABAMA

2021

DEVELOPMENT AND EVALUATION OF A FUNCTIONAL HUMAN CARDIAC TISSUE EQUIVALENT FABRICATED FROM MULTI-LINEAGE HUMAN INDUCED PLURIPOTENT STEM CELL DERIVED CELLS

DANIELLE PRETORIUS

BIOMEDICAL ENGINEERING

ABSTRACT

The human heart is an exceptionally complex muscular organ that is vital for survival. Electrical impulses signal activation of mechanical contractions, pumping blood through the entire body and allowing for oxygen-exchange to occur. Unfortunately, certain disease states or traumatic injuries such as myocardial infarctions hamper the heart's efficiency and function by damaging its structure. Ideal treatment would allow for the replacement or regeneration of the damaged tissue with cells and material harvested from the patient, thus avoiding the potential for immune rejection. Engineered cardiac tissues fabricated from human induced pluripotent stem cells have shown great promise for restoring function in infarcted left ventricular myocardium, and since these induced pluripotent stem cells originate from reprogrammed somatic cells, they also skirt the ethical issues associated with the use of embryonic stem cells.

For engineered cardiac tissue constructs to reach their translational potential, they need to be of a clinically relevant volume and thickness, while also being capable of generating synchronous and forceful contraction to assist the pumping action of the recipient heart. Design requirements necessitate a thickness sufficient to produce a useful contractile force, prevascularization to overcome diffusion limitations and sufficient structural

development to allow for optimal cell communication. Previous attempts to meet these requirements have been hampered by diffusion limits of oxygen and nutrients, which occur within 100-200 μm of the boundary conditions, resulting in necrosis. Herein we develop a viable three dimensional engineered cardiac tissue model of the left ventricular myocardium fabricated from multi-lineage human induced pluripotent stem cell-derived cells. A novel layer-by-layer fabrication method will be employed to mimic the native myocardium in both form and function, while also minimizing the potential for necrosis. The engineered constructs will be evaluated and characterized in terms of cell fate and migration, extracellular matrix development, viscoelastic properties, ultrastructure development as well as their electrophysiological properties.

Keywords: stem cells, cardiac, regeneration, layer-by-layer, tissue engineering

ACKNOWLEDGMENTS

First and foremost, I would like to thank the University of Alabama at Birmingham (UAB) and the Department of Biomedical Engineering (BME) Graduate Committee for giving me the opportunity to realize my pipe dream of coming to the US and studying tissue engineering.

I cannot begin to describe my gratitude towards my mentor, Dr. Jay Zhang, who took a chance on me. Through his guidance, patience, and fantastic mentorship I have not only grown, but flourished. I would like to express my sincere gratitude towards my committee members for always making time to brainstorm, provide advice and guidance and mold me into a much more well-rounded scientist during my time as a graduate student.

I would like to thank all of the people who work tirelessly behind the scenes in the BME department – Keri, Huantao, Tomeka and Julie – thank you for always answering all my questions, helping with all the endless paperwork, always being supportive, and making it possible for me to focus on my work in the lab. A massive thank you goes out to each member of the Zhang lab for always being willing to help, brainstorm, be a peer-mentor when needed, be a supportive friend when needed, and guide me to this point in my research career. I will always be grateful.

I would like to thank my family and friends for their support and understanding of the requirements of graduate school. The friends I have made during my time in graduate

school have been vital to my success and have enriched my life more than I could possibly express. To my parents, I say a special thank you for being my anchors, but also teaching me to adjust my sails when necessary.

Lastly, but certainly not least, I would like to thank my husband, Taylor, who has been on this journey with me, through all the ups and downs. Thank you for your patience, support and unwavering love.

TABLE OF CONTENTS

Page

LIST OF TABLES

Table *Page*

FABRICATION AND CHARACTERIZATION OF A THICK, VIABLE BI-LAYERED STEM CELL-DERIVED SURROGATE FOR FUTURE MYOCARDIAL TISSUE REGENERATION

LAYER-BY-LAYER FABRICATION OF LARGE AND THICK HUMAN CARDIAC MUSCLE PATCH CONSTRUCTS WITH SUPERIOR ELECTROPHYSIOLOGICAL PROPERTIES

LIST OF FIGURES

Figures *Page*

INTRODUCTION

FABRICATION AND CHARACTERIZATION OF A THICK, VIABLE BI-LAYERED STEM CELL-DERIVED SURROGATE FOR FUTURE MYOCARDIAL TISSUE REGENERATION

LAYER-BY-LAYER FABRICATION OF LARGE AND THICK HUMAN CARDIAC MUSCLE PATCH CONSTRUCTS WITH SUPERIOR ELECTROPHYSIOLOGICAL PROPERTIES

DISCUSSION

LIST OF ABBREVIATIONS

2D	two-dimensional
3D	three-dimensional
A	surface area
A.U.	arbitrary units
AMI	acute myocardial infarction
ANOVA	analysis of variance
APD	action potential duration
AVN	atrioventricular node
BME	biomedical engineering
BSA	bovine serum albumin
CAD	computer-aided design
cDNA	complementary deoxyribonucleic acid
CMs	cardiomyocytes
CO2	carbon dioxide
Col1	collagen 1
Col3	collagen 3
Col4	collagen 4
CSDs	cardiac support devices
cTnI	cardiac troponin I

cTnT	cardiac troponin T
CV	conduction velocity
CVD	cardiovascular disease
Cx43	connexin 43
DAPI	4′,6-diamidino-2-phenylindole
DI	deionized
DMEM	Dulbecco’s Modified Eagle Medium
E	elastic modulus
ECM	extracellular matrix
ECs	endothelial cells
EDTA	ethylenediamine tetra-acetic acid
ESC	embryonic stem cell
F	force
FBs	fibroblasts
FDA	Food and Drug Administration
FN	fibronectin
GAPDH	glyceraldehyde 3-phosphate dehydrogenase
GJ	gap junction
GJIC	gap junction intracellular communication
HBSS	Hank’s balanced salt solution
hCMP	human cardiac muscle patch
HF	heart failure
Hg/Xe	mercury/xenon

HSCs	hematopoietic stem
IACUC	Institutional Animal Care and Use Committee
iPSC	induced pluripotent stem cell
JP2	junctophilin
Lam	laminin
LbL	layer-by-layer
LCST	lower critical solution temperature
LVADs	left ventricular assist devices
MC	mitochondria
MI	myocardial infarction
MLC2a	atrial myosin light chain 2
MLC2v	ventricular myosin light chain 2
N-Cad	N-cadherin
OCT	optical cutting temperature
PBS	phosphate buffered saline
PBST	phosphate buffered saline + Tween 20
PDMS	polydimethylsiloxane
PETE	polyethylene terephthalate
PFA	paraformaldehyde
PIPAAm	poly(N-isopropylacrylamide)
PLGA	poly(lactic-co-glycolic acid)
RNA	ribonucleic acid
RT-qPCR	quantitative reverse transcription polymerase chain reaction

RYR2	ryanodine receptor 2
SAN	sinoatrial node
SEM	standard error of the mean
SERCA2	sarco/endoplasmic reticulum calcium-ATPase 2
SMCs	smooth muscle cells
SR	sarcoplasmic reticulum
TEM	transmission electron microscopy
UAB	University of Alabama at Birmingham
ZL	Z-line
αMHC	myosin heavy chain alpha
βMHC	myosin heavy chain beta
ε	strain
η	viscosity
σ	stress

CHAPTER 1

INTRODUCTION

Through this piece of work, we have developed a viable three dimensional (3D) engineered cardiac tissue model of the left ventricular (LV) myocardium in both form and function, fabricated from multi-lineage human induced pluripotent stem cell (hiPSC) derived cells. The model is dynamic and has the ability to demonstrate various characteristics associated with the form and function of viable LV myocardial tissue, including, but not limited to extracellular matrix (ECM) composition, cellular representation, viscoelastic properties, vascularization, ultrastructure development, as well as the development of physiologically relevant conduction velocities. The overarching goal of the development of this *in vitro* model was to recapitulate the cellular architecture and ECM makeup of native human myocardium with hiPSC-derived cells while also reproducing the response to mechanical and electrical stimuli experienced *in vivo*.

Precision healthcare

In 2015, President Barack Obama announced that the United States (US) would embark on a government funded precision medicine initiative that would enroll over 1 million people. This approach to the diagnosis and treatment of diseases shifts the focus from a one-size-fits-all treatment approach to tailoring the medical treatment to the individual characteristics of each patient [1]. The power of precision medicine, thus, lies in its

ability to guide health care decisions toward the most effective treatment for a given patient, and subsequently improve care quality, while reducing the need for unnecessary diagnostic testing and therapies.

Of special interest is the potential for reducing and even elimination of allograft immune responses and potential rejection [2, 3]. Internationally, there is an annual donor organ shortage, compounded by the prerequisites for donor-recipient matching associated with many organs and systems [4-7] with only around 2000 heart transplants performed in the US annually [8]. Certain cases could potentially allow for the use of artificial or bio-artificial organ use, but even then, limitations exist, including the potential for rejection and limited lifespans associated with most biocompatible materials [9, 10]. Current advancements in cell harvesting and reprogramming have, however, made it possible to utilize patient-specific cells and with the advancements in precision medicine as well as tissue engineering, might make it possible to fabricate a whole, functioning organ from a patient's own cells within the next decade or two, especially considering the fact that researchers are fabricating vascularized, complex structures at this point [11]. Unfortunately, the heart is an extremely complex organ with regard to its structure and heterogonous cell population, making it a particularly challenging task to reproduce as a fully functional bio-artificial organ.

The human heart

Structure and function

A healthy human heart consists of four distinct chambers, each with its own unique function – two thin-walled atrial chambers, and two thick-walled ventricular chambers. The cellular makeup of these chambers differ by the type of chamber and its

function, with fibroblasts (FBs) and cardiomyocytes (CMs) for example, specific to each chamber possessing distinct properties, including but not limited to electrical conduction, metabolic properties and mechanical force generation [12-15]. These distinct electrical and mechanical properties are vital, since the heart functions as an electrically excitable pump in the body, circulating blood, and subsequently oxygen and nutrients through the systemic circuit.

To induce normal (sinus) rhythms in the heart, electrical excitation is generated in the sinoatrial node (SAN), located in the right atrium. Along with the cardiac conduction system, consisting of the atrioventricular node (AVN), and the His-Purkinje system, the SAN is seen as the primary pacemaker system of the heart [16]. Activation of the SAN initiates the contraction of the atria, pumping blood into the ventricles. There is a delay between atrial and ventricular systole due to decreased AVN conduction facilitating the filling of the ventricles before contracting, finally pumping the blood throughout the body [17].

Further complication is added to this already complex organ by the fact that the heart wall consists of three distinct layers. The inner and outer layers, both specialized forms of mesothelial tissue, known as the endocardium and epicardium, respectively, sandwich the much thicker layer of cardiac muscle tissue known as the myocardium (**Figure 1**) [18]. Moreover, muscle fiber bundles in the ventricular myocardium are arranged in three separate sublayers, allowing for the unique push-pull-torque movements associated with the heart [19].

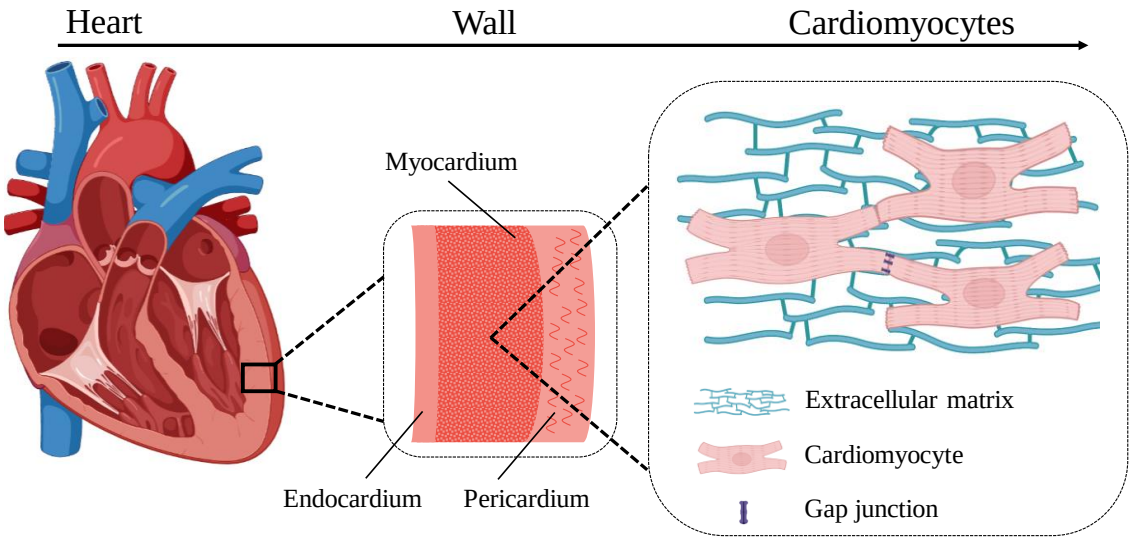

Figure 1: Organizational levels of the heart, from organ to structural to cellular level. Representative schematic of a healthy heart, its wall structure, as well as the cardiomyocytes, extracellular matrix and gap junctions in healthy, well-organized myocardial tissue.

Cardiovascular disease

Reduced efficiency in the transport of oxygenated blood by the heart through the circuitry of the body, whether due to unhealthy habits like smoking, being overweight or genetic issues, can have dire results. Cardiovascular disease (CVD) is one of the leading causes of death worldwide annually [20, 21], with more than 840 000 deaths in the US alone being attributed to CVD in 2016 [22]. The majority of CVD-associated deaths, a staggering 49.8%, is more specifically associated with ischemic heart disease, also known as coronary heart disease [21]. Ischemic heart disease occurs when one or more branches of the heart's coronary arteries become inflamed or blocked, subsequently decreasing or preventing consistent supply of oxygen-rich blood to the muscular tissue of the heart. This imbalance between the supply and demand in oxygen results in localized cell death, known as a myocardial infarction (MI), or more commonly, a heart attack [23].

Myocardial infarction (MI) and its prognosis

Arterial blockage caused by plaque build-up or thrombi are some of the primary causes of MI's [24]. This arterial blockage not only leads to a loss of oxygen, but also triggers downstream cascades associated with inflammatory responses, leading to further damage of the oxygen-starved area [25]. Furthermore, due to the limited proliferative ability of the terminally differentiated cardiomyocytes in adult mammalian hearts, the ability of the heart to regenerate is hampered further [26-28]. Cardiac remodeling, post-MI, is primarily fibrotic in nature, leading to the formation of a collagenous scar [25, 29], and eventually ventricular dilatation over time [30-32]. This dilatation process is, more often than not, also associated with an increase in wall stress, further burdening the already traumatized cells in the infarcted region as well as the border-zone region [33, 34]. Further complications, including but not limited to arrhythmias, cardiogenic shock, inflammation of the ventricular wall, cardiac ruptures, or secondary MI's can occur, depending on the size and location of the original MI, enhancing the chances for long-term heart failure (HF) [35-38].

Standard of care and current limitations

One of the major advancements in care used to re-establish blood flow to the infarcted area of the heart was the development of reperfusion therapy. Due to the complex cellular mechanisms induced after reperfusion, this treatment was not readily employed by physicians until the mid-to-late 1970's, even though compelling arguments were made by Fletcher *et al.*[39] in 1958 in favor of its use. Even though reperfusion, relieves or at least greatly reduces ischemia, it also results in a complex group of phenomena, which may initially appear to be deleterious. Some of these phenomena include accelerating necrosis of injured myocytes, cell swelling and bulging, hemorrhagic myocardial infarction,

production of free radicals which induce oxidative stress, as well as electrophysiological changes that could lead to arrhythmias [40-43]. Predictions have been made that, if this technique is utilized properly and in a timely fashion, it could salvage approximately 50% of severely ischemic myocardium [44], while prevention of lethal myocardial reperfusion injury should prevent the necrosis of an additional 40% [45], showing why this method of care is still widely employed.

Additional interventions to re-establish adequate blood flow, include various combinations of pharmacological and/or surgical interventions [46-48]. One of the most readily used surgical approaches is the coronary bypass, where a vascular graft is used as a bridge between the aorta and the area downstream of the ischemic injury, thus bypassing the blockage. This surgery yields optimal results when pharmacological interventions such as antithrombotic agents, antiplatelet therapies and/or lipid management strategies are employed [49]. Another surgical approach that can be considered, if vessel occlusion diagnosis occurs at an early stage, is angioplasty implantation of a vascular stent [50]. Unfortunately, certain patients would not benefit from any intervention aside from a full heart transplant, and as mentioned earlier (see Precision healthcare), there is a massive shortage of these organs available for donation, with donor-recipient matches being even more scarce. While great advances are being made in both the fields of precision health care as well as biomedical engineering, we are simply not yet capable of replacing an entire patient-specific organ. At the moment, the best solution to be offered while a patient waits for a heart transplant match, is supporting their failing heart to effectively buy time until their match becomes available. Presently, left ventricular assist devices (LVADs) are used to aid patients in end-stage HF, yet these systems are riddled with their own set of

complications, including bleeding, thrombosis, strokes and device malfunctions to name a few [51]. The potential to harvest a patient's own cells and/or tissue with the aid of modern technological advances, in addition to pharmacological and optimized tissue engineering approaches have brought us a few steps closer to achieving the ultimate goal of regenerating or even replacing complex failing organs such as the heart.

Tissue engineering approaches to support a failing heart

Over the past few decades, tissue engineers have made great strides in improving the fate of the failing heart, whether done mechanically, electrically, or with the aid of cellular incorporation in attempts to restore function to the damaged tissue.

Use of materials only

Supplying mechanical support to a failing heart suffering from dilatation is vital, whether in cases where high-risk patients are undergoing life-saving surgeries, or in cases where it might be best therapeutic solution for the specific patient [52-54].

Cardiac meshes. The concept of ventricular containment by a synthetic mesh, usually some polyester, came to light between 1999 and 2001 [55-57]. These meshes, also known as Cardiac Support Devices (CSDs), are placed, surgically, around the heart to provide end-diastolic ventricular support. The mesh is intended to reduce wall stress and CM overstretching induced during the end-diastole and periodic volume overload conditions. By reducing these key remodeling stimuli, the remodeling process may be halted or potentially even reversed [58]. More recently, with the incorporation of conductive components like silver nanowire networks into synthetic biocompatible polymers such as sty-

rene-butadiene-styrene rubber, epicardial meshes that are soft, elastic, and highly conductive have been created, supporting the heart on both an electrical as well as a mechanical front [59].

Synthetic and bio-based polymer supports. Of the various myocardium "patching" strategies, many are based on either a synthetic or a bio-based polymer. Both types of materials have their advantages and disadvantages, with the primary design outcome usually dictating the choice between synthetic versus bio-based. Properties to consider during the selection of the scaffold base material of choice, include but are not limited to biocompatibility, biodegradability mechanical properties as well as the ease with which any properties can be tailored [60, 61].

In the 1980's Dacron, also known as polyethylene terephthalate (PETE), was used as an *in vivo* myocardial patch post-MI in four patients [62]. Though this approach initially seemed very promising, the relatively low levels of bioactivity of PETE limits its potential use in regenerative tissue engineering approaches [63]. Another readily used polyester is poly(lactic-co-glycolic acid) or PLGA. Approved by the Food and Drug Administration (FDA) in the 1970s due to its exceptional biodegradation capabilities and biocompatibility, PLGA is arguably the most widely used synthetic polymer in the biomedical industry. Multi-layered adenosine loaded PLGA/gelatin patches have been shown to not only have minimal inflammatory effects when implanted in porcine models, but have also been deemed to have a cardioprotective function [64]. Some of the more readily used bio-based polymers in cardiac tissue engineering approaches include collagen (and its heat-treatment derivative gelatin) as well as fibrin. Both collagen and fibrin occur naturally in the mammalian body and would lead to minimal foreign-body responses if transplanted, with

fibrin having the added benefit of autologous sourcing (see Precision healthcare) [65-68]. Fibrin-associated characteristics, including but not limited to thickness and length of fibers, extent of branching, and pore size, can easily be tailored by modifying the polymerization conditions with different factors such as ionic strength, pH, concentration of fibrin monomer, and hydrophobicity of the polymerization surface [69]. Not only does fibrin have the ability to incorporate both cells and their mediators (e.g. growth factors), but even in the absence of growth factors fibrin has been known to have angiogenic properties [70-72]. Enhancement of patch application methods has also received attention more recently, with innovative approaches such as the idea of a "spray-on" fibrin patch deviating from traditional attachment to the epicardium with sutures [73].

Decellularized scaffolds. Xenogeneic ECMs have been used successfully to replace and/or repair various tissues and organs in both preclinical animal studies and human clinical applications for more than the past three decades [74-77]. Decellularization of rat hearts via coronary perfusion with ionic surfactants was first described in 2008 by Ott *et al*. [78]. This groundbreaking study laid the groundwork for more than 20 years' worth of work by specialists in the field, like Dr. Doris Taylor, in the hopes of retaining the ideal cardiac and vascular architecture of a cadaveric or donor heart, while having the ability to replace the damaged or dead cells with those from the recipient host [79].

Incorporating cells

Since the late 1990s, research in the cardiac tissue engineering field has mainly involved the use of neonatal or embryonic CMs to create three-dimensional (3D) heart tissue surrogates for use in *in vitro* experimental studies [80-84] and, more recently, for the treatment of MI in animal models [85-88]. For maximal regenerative capabilities, healthy,

functional cells need to be supplied to the damaged myocardium for remuscularization and to aid in revascularization [78, 89-91]. Post-treatment, cell integration and paracrine signaling will allow for remuscularization and revascularization of the myocardium, reducing and even replacing the necrotic cells post-MI (**Figure 2**).

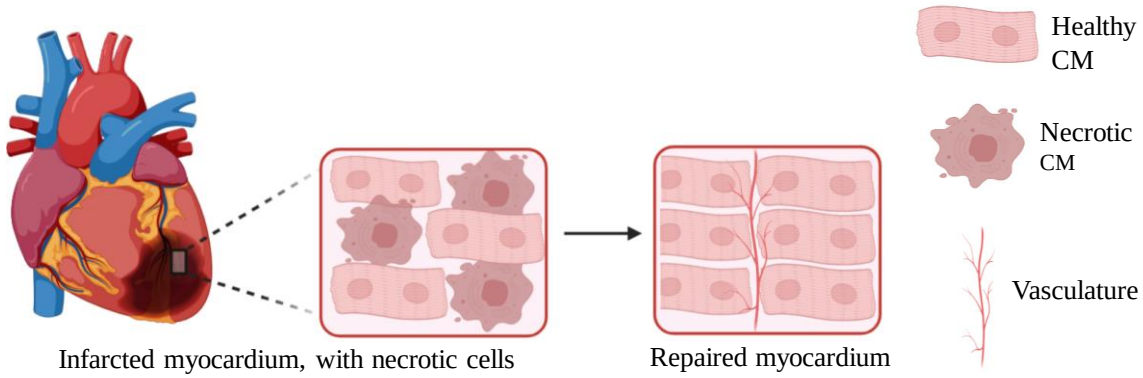

Figure 2: Remuscularization and revascularization of the infarcted myocardium using exogenous cells. Ideally, treatment of the damaged myocardium with cardiac-committed cells (cardiomyocytes), along with specific supportive cells (endothelial, fibroblasts and smooth muscle cells) will result in optimal regeneration, reducing necrosis induced post-MI.

In vivo, ECM composition is represented by a complex mixture of functional and structural molecules that affect a variety of cell fates and activities. Living cells are constantly exposed to mechanical stimuli arising from the surrounding ECM or from neighboring cells. The concept of this "dynamic reciprocity" between the ECM and the resident cells [92] should be kept in mind when designing a therapeutic system, especially one as complex as the heart. An ideal and versatile cell candidate would be one that can proliferate or regenerate as needed while also yielding the heterogeneous cell phenotypes required to form a functional and complex organ or piece of tissue. Except in isolated cases where organ-specific cell types can be isolated, derived, expanded *in vitro*, and utilized, the most likely candidate to fulfill these demands is either a stem or progenitor cell [93-96].

Although slight, the difference between stem cells and progenitor cells, in theory, mostly arises from the most basic definition of a stem cell, i.e. a cell which possesses unlimited self-renewal capabilities, can clone itself, and can developmentally give rise to tri-lineage cells (pluripotency). Progenitor cells, on the other hand, have already committed to a specific germ lineage and can proliferate and mature into precursors within this lineage, which for cardiac cells include, cardiomyocytes (CMs), vascular smooth muscle (SMCs) or endothelial cells (ECs), depending on the characteristics of the starting progenitor cell [97, 98]. Due to their diverse nature and potential applications, the remainder of the section will focus on stem cells.

Stem cells. Defining what, exactly, constitutes a true stem cell has been the focus of numerous controversies in literature over the past two decades. Arguably, stem cells can be classified into three main categories – adult stem cells, embryonic stem cells and induced stem cells. Adult stem cells not only rare, but seemingly more specialized than other real stem cells [99]. Their primary functions are to maintain homeostasis and, in very specialized environments, replace diseased or damaged cells. An example of this includes hematopoietic stem (HSCs), which have the ability to regenerate a functional hematopoietic system (blood-forming cells or mature blood cells) [99, 100]. Embryonic stem cells (ESCs), the other naturally occurring stem cells, derived from the undifferentiated inner mass cells of a blastocyst or early stage embryo, were originally identified in mice in 1981 [101], and in humans in 1998 [102]. ESCs differ from adult stem cells in that they fulfil all the requirements of a stem cell, though their culturing *in vitro* requires very strict monitoring for potential clustering which would result in phenotypic aberrations and spontaneous differentiation [103]. The use of ESCs has been steeped in ethical questions, as

their harvest and subsequent differentiation comes at the cost of a fertilized embryo. The questions raised regarding the ethical use of ESCs, led to the development of the third type of stem cell, the induced pluripotent stem cell (iPSC). These cells were isolated from mice in 2006 [104], humans in 2007 [105] and allowed scientists to induce stem cell properties in somatic cells. The successful induction relies on the transfer of transcriptional factors, associated with the pluripotency of ESCs, into the desired donor cells [106], effectively re-programming the somatic donor cell. This discovery and the development of these scientific methods have made many previous precision medicine approaches, specifically in the patient-specific domain of tissue and organ replacement, more realistic.

Following their respective discoveries and development, all three types of stem cells (adult, embryonic and induced) have been readily employed in attempts to regenerate the damaged and failing heart. Unfortunately, HSCs which were some of the first stem cells studied for cardiac regeneration, have limited transdifferentiation capabilities, and are not capable of differentiating into CMs for remuscularization when implanted post-MI [107, 108]. HSCs do, however, possess the ability to function as supportive cells post-MI, by way of their potential to stimulate angiogenesis and neovascularization via paracrine signaling [109] and have subsequently shown improvement in cardiac function in early clinical studies [110, 111]. Due to their limited transdifferentiation capabilities, the tissue engineering field focused more effort on developing approaches for myocardial regeneration from ESCs and later iPSCs. Cardiogenic stem cells, such as ESCs and iPSCs, have been catapulted into the forefront of the regenerative cardiac tissue engineering industry with their abilities of generating large numbers of contractile CMs that are thought to enhance cardiac function through direct electromechanical coupling with host cells, not

only potential paracrine signaling [112, 113]. Potential therapeutic benefits are primarily associated with substantial remuscularization of the infarct or peri-infarct area as opposed to revascularization alone [114]. Aside from potential ethical questions raised in the use of ESCs, these cells and their derivatives are generally classified as allogeneic, and disposed to immune rejection [115]. iPSCs on the other hand have the potential for autologous transplantation when utilizing cells harvested from a patient directly [116, 117].

iPSCs in cardiac tissue engineering. iPSCs are known sources of various cardiac cell types, including CMs, ECs, SMCs as well as cardiac fibroblasts (FBs) [118-121]. iPSC-derived cells have been used in various tissue-based approaches to mimic the native myocardium [15, 122-125], but also as therapeutic aids to attenuate damage caused during MI, ranging from seeding decellularized scaffolds [126] to numerous cardiac patches laden with cells [118, 127-129]. These tissue-based approaches afford the opportunity to study mechanistic interactions between the cells as well as the relationship between the cells and the ECM in a more representative 3D environment compared to 2D culture.

Engineered tissues, furthermore, not only provide a stable, protective method of cell delivery, but also the additional benefit of supplying mechanical support to a weakened heart wall. Whether the therapeutic value in a cardiac engineered tissue patch is mostly due to paracrine signaling from the implanted cardiogenic cells, or active mechanical forces that support cardiac function by enhancing contractile capabilities, or perhaps some combination of these actions remains to be seen. What has been shown, however, is that even when non-CM-containing patches were implanted in rats post-MI, improvements in infarct sizes were noted, though these improvements did not accompany subsequent improvements in LV ejection fraction [128]. These results were in stark contrast with

rats from the same study, where CM-containing patches were implanted, and cardiac output as a function of ejection fraction, was similar to those noted in sham-operated animals. Human induced pluripotent stem cell-derived CMs (hiPSC-CMs) and their supporting cells, hiPSC-ECs and hiPSC-SMCs, were transplanted via an *in situ* fibrin patch over the infarction site in swine hearts, resulting in reduced in myocardial wall stress, improved metabolic turnover, enhanced contractile performance, enhanced vascularization, and importantly a lack in ventricular arrhythmias [130]. Incorporation of hiPSC-CMs, -ECs, and –SMCs into a gelatin matrix, via 3D bioprinting allowed for the incorporation of high-resolution features into human cardiac muscle patch (hCMP), prior to its implantation into a murine MI-model [131]. Implantation of the 3D printed hCMP structures resulted in enhanced cardiac function, reduced infarct sizes, increased vasculogenesis, as well as reduced apoptosis when compared with control animals that had a cell-free scaffold implanted.

Limitations of hiPSC-CM use

In vitro culture. Though the development and understanding of hiPSC-CMs have made major advances since the late 2000s, the field still faces hurdles that hamper the optimal use of these cell. One such hurdle, relates to the generation of hiPSC-CMs *in vitro*. The majority of production and optimization protocols yield heterogonous populations of hiPSC-CMs, which are not chamber-specific, unlike the CMs found in the native heart [132-135]. This cellular heterogeneity may significantly hamper the use of the hiPSC-CMs for many of the applications, due to differences in metabolism, conduction potential as well as mechanical contractile capabilities.

In vivo engraftment and survival. Despite the vast regenerative and therapeutic potential that hiPSC-CMs and their resulting tissues hold, *in vivo* applications have been hampered due to cellular engraftment and cell survival due to limited vasculature in and around the ischemic, infarcted region [89, 90, 130, 131, 136, 137]. Following an infarction, the region experiences an inflammatory response, followed by ECM remodeling and further inflammatory responses to the subsequent ECM remodeling finally resulting in fibrous scar formation [138]. After four weeks *in vivo*, few studies show engraftment rates surpassing 10%, with some of the most promising studies (those yielding 10-12% engraftment rates) being those with cardiac patch structures that contain at least one supporting cell type in addition to hiPSC-CMs, i.e. hiPSC-ECs or hiPSC-SMCs [118, 130, 131].

hiPSC-CM structural maturity and associated gene expression levels. Following differentiation, hiPSC-CMs resemble human fetal CMs in terms of gene expression levels [139] and morphology [140-143]. Similar to fetal CMs, hiPSC-CMs possess a round morphology, a single nucleus and take up around one tenth the surface area that mature, adult CMs do [143, 144]. Mature, adult CMs on the other hand possess an elongated rod-like shape, with up to 30% of the cells being binucleated [145]. Ultrastructure disorganization, associated with sarcomeric length, alignment, organization and abundance, is also common in hiPSC-CMs, becoming more organized during CM maturation, which is vital in generating physiologically relevant contractions. Average sarcomere lengths in adult CMs range between 2.0-2.2 μm [146], and around 1.8 μm in fetal human CMs [147]. hiPSC-CM-associated sarcomeres are up to 25-30% shorter than adult CMs and up to 6-11% shorter (measured at 1.6-1.7 μm) and less wide than fetal CMs [148]. Further structural deficits include cellular junctions such as the intercalated discs which can be found at the Z-lines of the

sarcomeres, gap junctions including connexin 43 (Cx43) as well as adherens including N-caderin (N-Cad), all of which function by enhancing communication as well as mechanical and/or electrical function throughout the contractile apparatus as a whole [144, 149]. Despite the lack in structural machinery, certain genes and proteins associated with cardiac contractile capabilities, such as alpha- and beta-myosin heavy chains (α-MHC and β-MHC) as well as chamber-specific myosin light chain 2 (MLC2v and MLC2a) are present in both hiPSC-CMs and mature CMs, but in different ratios [13, 15, 150, 151]. Unfortunately, many of the inadequacies related to cellular maturity greatly affect the functional performance, as measured by conduction velocity (CV), metabolic turnover, mechanical contractility, as well as cellular integration capabilities *in vivo* [152-155].

hiPSC-CM functional maturity and associated gene expression levels. One of the key indicators of CM functional maturity at the tissue level is the ability to support fast action potential conduction. Fast CVs are indicative of well-aligned and highly stratified tissue constructs that possess polarized gap junctions. Conduction velocities (CVs) of genetically purified hiPSC-CMs cultured and tested in 2D format have been reported as high as ~21 cm/s [156], while more complex hiPSC-CM-based 3D systems still lag behind with CVs around 14 cm/s [118], with the potential of reaching up to 25 cm/s when highly organized [131]. However promising, the CVs reported for hiPSC-derived tissue still fall short of those observed in native adult LV tissue (~30-100 cm/s [141, 157]), indicating the lack of junction development and alignment required for optimal signal transfer between cells. In addition to the reduced CV, hiPSC-CM contractions tend to be spontaneous and asynchronous, a behavior that has been noted in fetal CMs as well [158]. These spontaneous contractions are associated with the deficient calcium handling machinery, including but

not limited transverse tubules (T-tubules), sarcoplasmic reticulum (SR), and transmembrane proteins such as L-type calcium channels [159]. In 3D cultures, active contraction forces generated by hiPSC-CMs are roughly 1% of those generated by adult CMs, i.e. they differ by two orders of magnitude, and more closely resemble fetal CMs [147, 160]. Metabolically, hiPSC-CMs also resemble fetal CMs, as their primary energy is acquired via glycolysis, whereas mature CMs acquire energy via fatty acid β-oxidation [161, 162].

The modular tissue fabrication approach

The ventricular wall is thickest near the cardiac base (> 10 mm) and thins to 1-2 mm at the apex [163, 164]. Cardiac tissue intended for regenerative purposes or even as replacement tissue, especially those intended to not only function as a temporary cellular delivery vehicle but also as a mechanical support structure should arguably be at least as thick as the LV wall. Considering the low engraftment rates expected post-MI, the structures should also be able to deliver a large number of viable and functional cells to allow for optimal potential outcomes [89].

The layer-by-layer concept. The layer-by-layer (LbL) fabrication (LbL) approach, is a method in which sequential layers of a material of interest are deposited individually in a bottom-up fashion. Over the past five decades, many LbL fabrication techniques have been developed, including but not limited to dipping, spin-coating, spray-coating and electromagnetic processes [165-167]. These processes have made notable contributions to various fields, such as the pharmaceutical and cosmetic industries as well as optics, energy and separations technologies [168, 169]. This unique fabrication method allows for a high degree of control over and tailoring of physicochemical properties, including construct architecture, permeability, and Young's (elastic) modulus [170-174].

LbL fabrication in cardiac tissue engineering. Cardiac tissue engineering utilizing modular fabrication such as the LbL approach surfaced in the early 2000s, with studies where CMs were seeded in confluent sheets on temperature-responsive (poly(N-isopropylacrylamide)) PIPAAm-coated dishes [175]. This technique exploits the lower critical solution temperature (LCST) of PIPAAm, 32 °C, above which a conformational phase transition from swollen hydrated state (hydrophilic) to a shrunken dehydrated state (hydrophobic) occurs within the polymeric matrix [176, 177]. Cells are seeded and cultured at 37 °C, then cooled to 32 °C, upon which allowing for confluent sheets of cells to be released without the digestion of their ECM or the disruption of cellular alignment, and accompanying intercellular connections, including gap junctions required for electronic signal transduction between neighboring CMs (**Figure 3**).

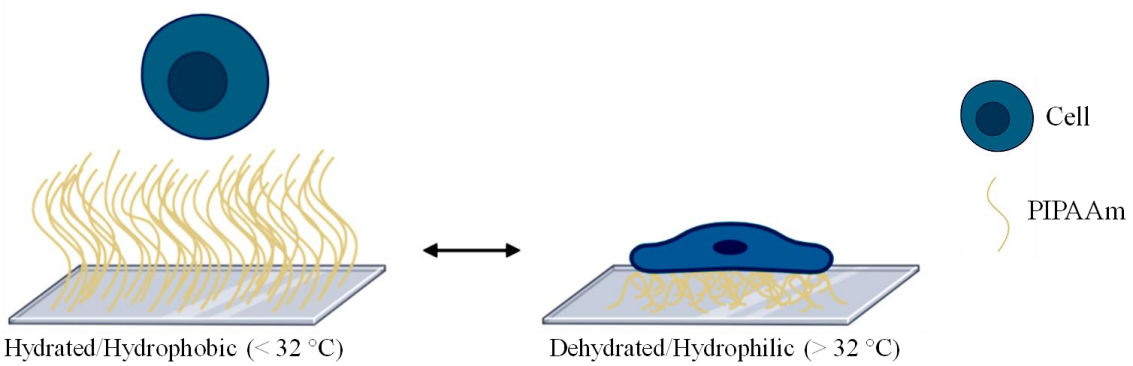

Figure 3: Exploitation of PIPAAm LSCT to create cell sheets. Confluent cell sheets can be released from petri dishes coated with PIPAAm by reducing the temperature from 37 °C to around or below the LCST of PIPAAm, which is 32 °C.

These early studies showed the layers were not only capable of being detached from their 2D culturing environment and fusing, but sheets layered or stacked together are able to fuse into a more representative 3D structure, and subsequently conduct electrical signals synchronously [175, 178, 179]. *In vivo* utilization of cell sheets fabricated from

hiPSC-CMs in a porcine MI-model showed significant improvements in cardiac function as well as LV remodeling, yet still low engraftment rates were noted [180]. Incorporation of supportive cells, such as ECs and SMCs, have allowed for the creation of the necessary vasculature in these thick structures, preventing hypoxia and subsequent necrosis when stacking more than three or four layers of muscle cells on each other. It has been demonstrated that incorporation of these supportive cells, in combination with gelatin beads as a separation layer to allow for fluid penetration, resulted in viable tissue exceeding 40 stacked cell layers with a total thickness of around 800 µm, which survived *in vivo* for up to 12 weeks [181].

With the degree of control over high-resolution aspects of designs, computer-aided 3D bioprinting has become of great interest to the field of cardiac tissue engineering [182]. Layering of cell-laden scaffolds and the use of scaffold-free designs have become more prevalent over the past five years, especially in the cardiac field [183-187]. Utilizing a 3D printing approach provides a large degree of control over cellular and ECM alignment, or in the case of scaffold-free printing, the opportunity to have the cellular fusion and ECM production without the prerequisite matrix remodeling associated when using a bio-ink. The most readily used scaffold-free design at present requires the preparation of cells in spheroid format for later deposition onto an array of needles, which will allow for spheroid fusion and subsequent tissue generation.

Modular cardiac tissue fabrication limitations

Aside from a few method-specific hurdles [188-191], modular cardiac tissue fabrication methods are hampered by many of the same issues that limit the functional scale-up of all cardiac engineered tissues.

Vascularization and nutrient-limitations. Current production of engineered tissue is hampered due to 3D tissues lacking adequate vascularization become necrotic within 100-200 μm of the boundary regions [192-196]. Supplying the tissue constructs with the required supportive cells allow for neovascularization *in vitro* and angiogenesis *in vivo*, yet due to oxygen- and nutrient-limitations brought on by deficient vascular density, engineered cardiac tissue constructs surpassing 250 μm in thickness are rarely seen without substantial degrees of necrosis, especially in long-term cultures lacking perfusion systems [80, 195, 197-200].

Host coupling. Depending on the time lapse that occurs post-MI and therapeutic interventions such as engineered cardiac tissue application, ECM remodeling and potential fibrotic scar formation can occur. This remodeling can severely impact the efficacy of the cell therapy, reduce electromechanical coupling between the engineered cardiac tissue and the host and potentially lead to arrhythmias caused by conduction blocks [201-204].

Summary and Objectives

Herein we aimed to generate a viable 3D engineered cardiac tissue model of the human LV myocardium in both form and function, fabricated from multi-lineage hiPSC-derived cells. These cells are of particular interest and value in the biomedical engineering and clinical fields due to their diverse differentiation capabilities and autologous nature. The LbL fabrication process will yield a tissue model that demonstrates various characteristics associated with the form and function of thick, viable LV myocardial tissue, including, but not limited to ECM composition, cellular representation (hiPSC-CM, -ECs, and -FBs), viscoelastic properties, vascularization, ultrastructure development, as well as the development of physiologically relevant conduction velocities.

Although various *in vitro* fabrication and culturing processes have been developed for engineered cardiac tissues, few have been able to generate viable constructs in excess of 1 mm in thickness, with the thickest recorded tissue measuring in at 1.25 mm after one week in culture [118]. Through the utilization of a fabrication process that allows for the sequential deposition of specialized cells as opposed to depositing large volumes of co-cultured cells, LbL fabrication has the ability to yield more organized, stratified tissue constructs that are more representative of the native myocardium, without becoming nutrient-limited and necrotic.

FABRICATION AND CHARACTERIZATION OF A THICK, VIABLE BI-LAYERED STEM CELL-DERIVED SURROGATE FOR FUTURE MYOCARDIAL TISSUE REGENERATION

by

DANIELLE PRETORIUS, ASHER M. KAHN-KRELL, WESLEY C. LABARGE, XI LOU, RAMASWAMY KANNAPPAN, ANDREW E. POLLARD, VLADIMIR G. FAST, JOEL L. BERRY, ALAN W. EBERHARDT, JIANYI ZHANG

Biomedical Materials

Danielle Pretorius, Asher M. Kahn-Krell, Wesley C. LaBarge, Xi Lou, Ramaswamy Kannappan, Andrew E. Pollard, Vladimir G. Fast, Joel L. Berry, Alan W. Eberhardt, Jianyi Zhang, (2020); doi.org/10.1088/1748-605X/abc107

ABSTRACT

Cardiac tissue surrogates show promise for restoring mechanical and electrical function in infarcted left ventricular (LV) myocardium. For these cardiac surrogates to be useful *in vivo*, they are required to support synchronous and forceful contraction over the infarcted region. These design requirements necessitate a thickness sufficient to produce a useful contractile force, an area large enough to cover an infarcted region, and prevascularization to overcome diffusion limitations. Attempts to meet these requirements have been hampered by diffusion limits of oxygen and nutrients (100-200 μm) leading to necrotic regions. This study demonstrates a novel layer-by-layer (LbL) fabrication method used to produce tissue surrogates that meet these requirements and mimic normal myocardium in form and function. Thick (1.5-2 mm) LbL cardiac tissues created from human induced pluripotent stem cell-derived cardiomyocytes and endothelial cells were assessed, *in vitro*, over a four week period for viability (< 5.6 ± 1.4 % necrotic cells), cell morphology, viscoelastic properties and functionality. Viscoelastic properties of the cardiac surrogates were determined via stress relaxation response modeling and compared to native murine LV tissue. Viscoelastic characterization showed that the generalized Maxwell model of order 4 described the samples well ($0.7 < R^2 < 0.98$). Functional performance assessment showed enhanced T-tubule network development, gap junction communication as well as conduction velocity (16.9 ± 2.3 cm/s). These results demonstrate that LbL fabrication can be utilized successfully in creating complex, functional cardiac surrogates for potential therapeutic applications.

Keywords: layer-by-layer, tissue engineering, stem cell, viscoelasticity, vascularization, cardiac regeneration

INTRODUCTION

Cardiac tissue engineering strategies focusing on recellularization and functional restoration after acute myocardial infarction (AMI) have shown promise to improve the clinical outcomes for patients [1-3]. Clinically, AMI is associated with contractile cell-loss, particularly in the left ventricle (LV), resulting in increased risks of arrhythmia and post-infarction LV remodeling. Cell therapies using the products of human induced pluripotent stem cells (hiPSCs) have been examined, pre-clinically [4], as a viable therapeutic option with their ability to produce patient-specific cardiac cells [5, 6]. In light of these results, the search continues for an effective method of restoring function of the AMI damaged heart, which is necessary for a successful therapeutic application. Furthermore, mechanical stabilization of the damaged region is also required to prevent excessive ventricular dilatation [7, 8].

A healthy myocardium maintains its structure and function under billions of pumping cycles. Much is known about the mechanics of myocardium as a hyperviscoelastic tissue undergoing large deformations during filling and pumping [9-11] but the mechanics of tissue surrogates is highly understudied. At present, there is a gap in knowledge related to how tissue surrogates function in both the short- as well as the long-term as true functional support structures to infarcted hearts. In addition, passive mechanical mismatch in compliance has the potential to induce further damage via maladaptive remodeling. Wang *et al.* [12] found that scaffolds with mismatched stiffness, compared to

the native myocardium, were unable to reduce infarcted myocardial wall stress. Furthermore, mismatched scaffold flexibility adversely affected active mechanical properties, specifically failing to mimic active myocardial contraction and expansion. Engineered surrogates that closely capture the mechanical properties of the host myocardium have been shown to support the direction and propagation of progenitor cells associated with tissue regeneration [13, 14]. In addition, viscoelastic parameters, like creep and stress relaxation, that describe the time and rate dependency of the mechanical response to deformation have been shown to be vital for a tissue-engineered replacements to be successful [15].

One promising fabrication method is the layer-by-layer (LbL) approach, in which sequential layers of material are deposited individually. Many LbL fabrication methods have been developed over the past five decades [16-18], making notable contributions to various fields, including the pharmaceutical and cosmetic industries [19, 20]. In a functional myocardium CMs are typically found adjacent to one another as opposed next to the smooth muscle cells (SMCs), fibroblasts (FBs) or endothelial cells (ECs). The mixing of cardiac cells in engineered cardiac tissue, likely prevents the hiPSC-CMs from coalescing into a fully interconnected contractile apparatus and may partially explain why force-generation measurements in these co-cultured tissues remained lower than in native heart tissue [21]. LbL fabrication allows for a high degree of control over physicochemical properties, including construct architecture, permeability, and Young's (elastic) modulus [22-26]. When engineering tissue like the myocardium, this technique has the potential to enhance construct performance, as it allows for the sequential deposition of specialized cells as opposed to depositing large volumes of co-cultured cells. This is especially important for

functional aspects such as contractile function and electromechanical connectivity for example [27]. Unfortunately, current production of thick implantable engineered tissue is hampered by the fact that 3D structures lacking adequate vascularization generally become necrotic within 100-200 μm of the boundary regions [28-30]. EC presence in the myocardium is not limited to providing vascularization but is vital to adult cardiomyocyte (CM) function, including CM organization and contractile force generation [31-37]. Numerous strategies have aimed to optimize vascularization in engineered tissue using variations of LbL techniques [38-41], yet due to oxygen- and nutrient limitations [42, 43] cardiac surrogates thicker than 250 μm are rarely seen without significant degrees of necrosis. These previous LbL approaches have, however, allowed for the production of, albeit thin, native tissue-like metabolically active structures that possessed blood vessels. Studies on temperature-responsive (poly(N-isopropylacrylamide)) PIPAAm-sheets seeded with CMs showed that the layers were not only capable of being detached from their 2D culturing environment and fusing, but post-fusion, were able to conduct electrical signals synchronously [44]. These synchronous conduction capabilities can be attributed to factors like cellular alignment and coupling, along with the maturation of calcium-handling machinery like T-tubule networks as expressed by markers for junctophilin-2 (JP2) and ryanodine receptor (RyR) [45, 46]. In total, the current LbL techniques for fabricating cardiac surrogates have not yielded a clinically viable alternative.

In the present study, we aimed at developing a thick, viable cardiac tissue surrogate from hiPSC-derived cells. The cardiac surrogates were characterized at various time points in order to inform future decisions, including optimal implantation time post-fabri-

cation as well as material composition. Characterization included 1) histology and immunostaining to analyze the cellular and structural morphology, 2) immunostaining to quantify viability, 3) immunostaining of 2D and 3D structures to analyze cell migration and vascularization, 4) stress relaxation tests and subsequent model fitting of the responses to determine the viscoelastic properties, 5) immunostaining and quantification of ECM remodeling and how it's related to the viscoelastic properties of the cardiac surrogates, 6) electron microscopy to examine the ultrastructure of the tissue and 7) optical mapping to determine the action potential and conduction velocity spectra to assess functionality. It was hypothesized that utilizing a modular fabrication approach, such as LbL deposition, would not only allow for the production of thicker tissues but also increase their robustness in terms of long-term culturability.

Materials and methods

Cell culture and characterization

Human induced pluripotent stem cells (hiPSCs) were reprogrammed from human cardiac fibroblasts, and subsequently differentiated into iCMs, as previously reported [4, 47, 48]. Generally, spontaneous contractions were observed in the iCM cultures between days 7 and 10 after the differentiation protocol commenced, with beating numbers increasing up to day 12. Metabolic purification of iCMs via glucose deprivation (RPMI 1640 without glucose, supplemented with sodium DL-lactate and B27^{+}, Gibco) for 3-6 days, initiated at day 11, allowed for a population of iCMs that was at least 95% cTnT positive. hiPSCs were maintained at optimal conditions, as previously described [49], on 6-well plates coated with Matrigel (Corning), using mTeSR 1 maintenance media (STEMCell Technologies, Canada). hiPSC-endothelial cells (iECs) were differentiated as described

previously [21, 50, 51]. Briefly, undifferentiated hiPSCs were seeded into a 0.5 mL fibrin scaffold and treated with CHIR99021 and U46619 in EBM2 medium (Lonza, USA) supplemented with $B27^-$ for 24 h. The medium was replaced with EBM2 supplemented with $B27^-$, vascular endothelial growth factor (VEGF), erythropoietin (EPO), and transforming growth factor β1 (TGFβ1), and then cultured for 96 hours with a media change halfway through. Finally, the scaffold was released and cultured in EGM2-MV medium (Lonza, USA) supplemented with $B27^+$, VEGF, SB-431542, with media changes every two days. hiPSC-ECs were purified and enriched by collecting cells positive for CD31 using fluorescence-activated cell sorting device (FACSAria II). Antibodies used for selection along with dilutions are listed Supplemental Table S1. See Supplemental Figure S1 for cell characterization and Supplemental Figure S2 for the proliferation assay performed in to prove the lack of tumorigenic properties of the iCMs utilized.

Fibrin matrix composition

The supporting fibrin matrix (per milliliter) used for each alternating layer of the cardiac tissue fabrication consisted of the following components as was defined previously [21]: 0.12 mL fibrinogen (25 mg/mL, Sigma-Aldrich, CAS# 9001-32-5), 0.02 mL Matrigel (Corning, # 356235), 0.56 mL of HEPES (20 mM, pH 7.4, Corning), 0.001 mL $CaCl_2$ (2 M), 0.3 mL DMEM (Gibco, High glucose, #11965-118), 0.006 mL thrombin (80 U/mL, MP Biomedicals).

Polydimethylsiloxane (PDMS) stilts

PDMS stilts were fabricated by mixing PDMS (Dow Corning Sylgard 184 Silicone, Product # 2065622) in a 10:1 elastomer:curing agent ratio and poured into a 100 mm diameter Pyrex Petri dish (Corning, # 3160102). These were cured at 75 °C for 2

hours in an oven, after which custom stilts of 10 mm x 5 mm (2.5 mm thick) were cut. All PDMS structures were autoclaved prior to use in tissue fabrication.

Optimized tissue surrogate fabrication

Following cell differentiation, cardiac tissue fabrication commenced (**Figure 1**). Petri dishes (BioLite Cell Culture Treated Dishes, Thermo Scientific) were coated with a 5 % pluronic F-68 solution (Gibco, # 24040032) and incubated at 4 °C overnight. The pluronic solution was removed, and a sterile polycarbonate frame (internal area: 1 x 2 cm^2) was attached with a 2 % agarose solution. Note that the frames were modified with channels to allow for maximal media contact following tissue fabrication. iCMs were dissociated (STEMdiff Cardiomyocyte Dissociation Medium, STEMCell) and mixed with the fibrin matrix at a concentration of $10x10^6$ cells/mL. Note that the deposition of the iCM layer denotes "D0" for the remainder of the fabrication process. 400 µL of this solution was quickly deposited into each mold to produce the first layer. Following complete polymerization, the culture medium was added (STEMdiff Cardiomyocyte Support Medium, 2 mg/mL Ɛ-aminocaproic acid) and incubated at 37 °C (5 % CO_2) for 2 days. The next layer, comprised of iECs, was made in a similar fashion, with the following exceptions: iECs were dissociated using trypsin (0.25 % trypsin, 0.1 % EDTA, Corning, # 25053CI) and then mixed with the fibrin matrix at a concentration of $10x10^6$ cells/mL. 200 µL of this solution was quickly deposited into each mold, yielding a 2:1 ratio of iCMs:iECs [21]. Fresh culture medium (10 % fetal bovine serum, 2 % $B27^+$, and 2 mg/mL Ɛ-aminocaproic acid, 10 µM ROCK inhibitor in DMEM) was added, following layer polymerization. After 24 h, the frame containing the cardiac tissue surrogate was lifted

off of the dish surface and placed on top of custom-cut PDMS stilts, allowing for the tissue to be fully suspended in fresh culture media (2 % fetal bovine serum, 2 % B27^{+}, and 2 mg/mL Ɛ-aminocaproic acid in DMEM). Incubation continued for the desired period of time (1-4 weeks in total), with media replacement once per week.

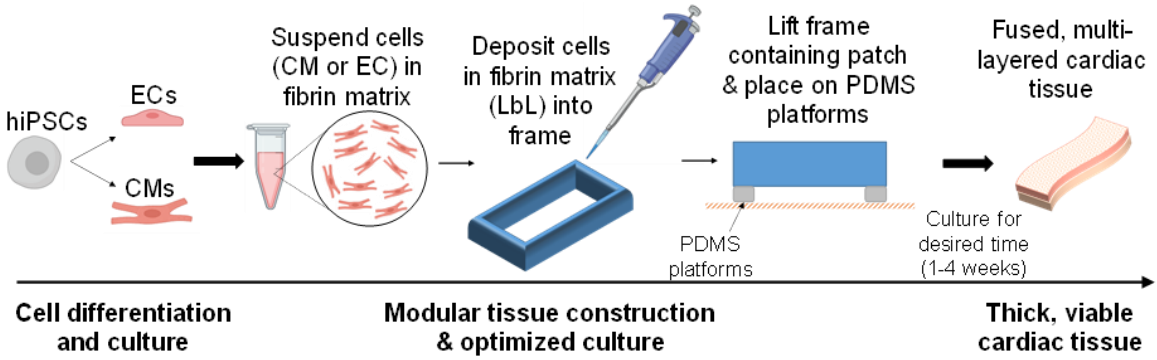

Figure 1: Basic description of optimized cardiac tissue surrogate fabrication process, allowing for extended culturing of thick tissue structures. The first layer of cells is deposited and cultured for 48 hours, after which the second layer is deposited using LbL approach. The second layer of cells is deposited, allowed to polymerize, and the entire structure contained in its frame is then lifted off of the dish surface and placed ontop of PDMS platforms. Thick, viable, multi-layered tissue can be cultured for the desired amount of time (1-4 weeks)

Tissue preservation

Samples were fixed in 4 % formaldehyde (Pierce, Thermo Scientific, # 28906) for 1 hour prior to embedding in either optimal cutting temperature compound (OCT compound, Fisher Health Care, USA) or paraffin for histological analysis (10 µm sections). Whole-mount samples were stored in PBS until staining.

Histochemistry

Deparaffinized and rehydrated sections were stained in hematoxylin solution (Mayer's, Merck, 3 min) then working eosin Y solution (2 min). Following dehydration

sampled were mounted in Permount and imaged with a bright field microscope (Olympus IX83 epifluorescent microscope).

Immunohistochemistry

OCT embedded sections were blocked and permeabilized for 30 min in 10 % donkey serum, 3 % BSA, and 0.05 % Triton-X. Primary antibodies were incubated for 1 h at room temperature (Supplementary Table S1). Following PBS wash (3 x 5 min), secondary antibodies labeled with fluorescent tags and 4′, 6-diamidino-2-phenylindole (DAPI, 100 ng/ml) were added for 1 h at room temperature (Supplementary Table S1). Sections were mounted in VECTASHIELD Antifade Mounting Medium and visualized by confocal laser scanning (Olympus FV3000 confocal microscope).

Whole-mount staining

Fixed whole-mount samples were blocked and permeabilized in 10 % donkey serum, 10 % Tween-20, 3 % BSA, 0.05 % Triton-X, and 0.02 % sodium azide in PBS overnight at 4 °C. Primary antibodies were incubated overnight at 4 °C (Supplementary Table S1). Samples were washed in PBST (3 x 10 min) then fluorescently labeled secondary antibodies were added overnight at 4 °C with the addition of DAPI. Following washing, tissue was cleared according to the previously described protocol [52] with a 3 hour incubation in Ce3D clearing agent. Whole-mount constructs were transferred to an Ibidi µ-Slide (# 80286), covered with VECTASHIELD Antifade Mounting Medium, and visualized by confocal laser scanning.

Determination of structure viscoelastic properties

All sample specimens, including PDMS, fresh murine heart tissue and cardiac tissue surrogates were treated with the same procedure described here. Specimen size measurements (surface area, *A*) used in the determination of the stress from the forces measured ($\sigma = F/A$) were determined with a digital caliper (Mitutoyo 500-196-30, Digimatic). Stress relaxation responses, stress (σ) vs. time (t), were characterized using a generalized Maxwell model [53] of order 4 (**Figure 2** c) in MATLAB (MathWorks, R2018, see Supplemental Information for the code). All specimens were transported from the incubator or sacrificed animal in chilled PBS and tested immediately. Stress relaxation testing in compression [54] was done using a Low Force Testbench (TA Instruments, New Castle, DE), where a 10 % strain (ε) was applied and held for 4 minutes on each sample. Samples were strained (ε) at 10 % by varying the applied deformation with thickness. Force (F) was measured with a 250 g load cell (**Figure 2** a, b).

The generalized Maxwell model was defined using the following equations, where E_i and η_i represent the modulus and viscosity of the i^{th} elements, and σ the measured stress:

$$\boldsymbol{Model}:\ \boldsymbol{\sigma(t) = \varepsilon E_0 + \varepsilon E_1\left(e^{-\frac{E_1}{\eta_1}t}\right) + \varepsilon E_2\left(e^{-\frac{E_2}{\eta_2}t}\right) + \varepsilon E_3\left(e^{-\frac{E_3}{\eta_3}t}\right) + \varepsilon E_4\left(e^{-\frac{E_4}{\eta_4}t}\right)} \quad \text{Eq. 1}$$

For each curve fit, the instantaneous modulus could be determined by the summation of each elastic modulus term (t=0), whereas the equilibrium modulus was determined at $t\rightarrow\infty$ where $E_0=\sigma/\varepsilon$. Viscosity was determined as the summation of each viscosity element (η_i).

$$\boldsymbol{Instantaneous\ Young's\ modulus\ (Pa)} = \boldsymbol{E_0 + E_1 + E_2 + E_3 + E_4} \quad \text{Eq. 2}$$

$$\boldsymbol{Equilibrium\ Young's\ modulus\ (Pa)} = \boldsymbol{E_0} \quad \text{Eq. 3}$$

$$\boldsymbol{Viscosity\ (Pa \cdot s)} = \boldsymbol{\eta_1 + \eta_2 + \eta_3 + \eta_4} \quad \text{Eq. 4}$$

Prior to performing tests on the engineered tissue samples, the validity of this method was tested using PDMS of different crosslinking densities. Moduli and viscosity obtained from these validation experiments were used to confirm the goodness-of-fit for the Maxwell model of order 4 (**Figure 2** d). The generalized Maxwell model of order 4 allowed for a good fit to the experimentally obtained data ($R^2 > 0.98$).

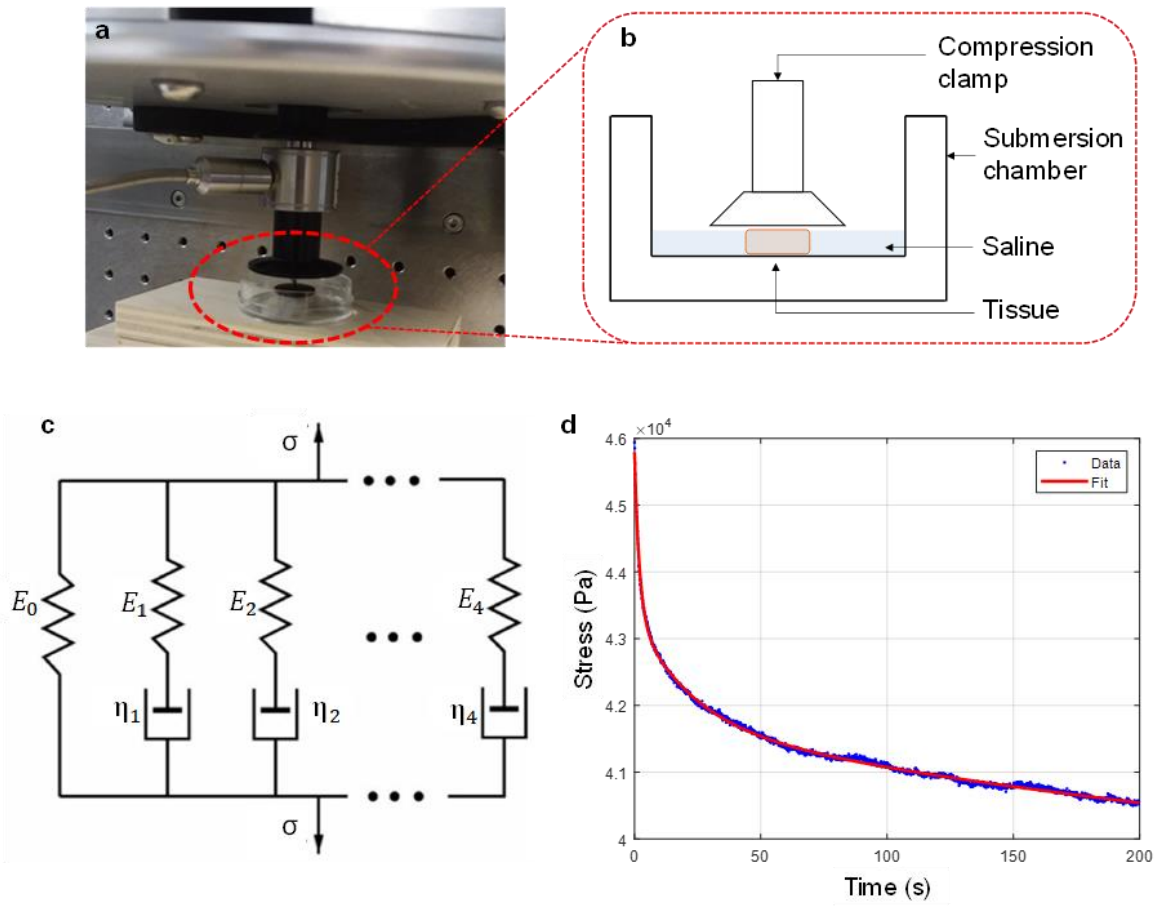

Figure 2: The experimental setup used to quantify the viscoelastic properties of the engineered cardiac tissue. (a) Shows an image of the compression clamp and the submersion chamber, whereas (b) shows a schematic of the experimental setup. (c) Generalized Maxwell model of order 4 schematic. E_i and η_i represent the modulus and viscosity of the i^{th} elements, and σ is the measured stress, with (d) showing the stress relaxation response ("Data") and modeling ("Fit") of PDMS crosslinked at an elastomer:curing agent ratio of 34:1, showing the goodness-of-fit for the generalized Maxwell model of order 4 (R^2>0.98)

Animal studies: murine heart samples

Studies were performed using healthy murine hearts as a control sample in viscoelastic testing for cardiac tissue surrogates that were generated during this study. All animal procedures were performed in accordance with the guidelines for animal experimentation set forth and approved by Institutional Animal Care and Use Committee (IACUC,

APN 20216), School of Engineering, University of Alabama at Birmingham; and conformed to the Guidelines for the Care and Use of Laboratory Animals published by the US National Institutes of Health (2011). Control tissue samples from SCID mouse left ventricles were obtained after perfusion with saline and arrested in diastole by injection with 25 mM potassium chloride (KCl). Animals were gender-randomized.

Transmission electron microscope (TEM) imaging

Ultrastructural analysis of the thick cardiac tissue surrogates was done via TEM imaging. After culturing for the required amount of time (1-4 weeks), the tissue surrogates were fixed in a 2.5 % glutaraldehyde solution for 1 h at 4 °C prior to being delivered to the UAB High-Resolution Imaging Facility for further processing. Sample blocks were sectioned using a diamond knife for clean and even sections. Samples were mounted and viewed using a Tecnai Spirit T12 Transmission Electron Microscope. Images were collected for analysis at each time point of interest (1 week, 2 weeks, and 4 weeks of tissue culture).

Four-electrode micro-impedance spectra (4EMS)

To assess intercellular coupling in the tissue surrogates, we used systems of very small and closely spaced electrical sensors custom-fabricated into linear arrays that are integrated with adjacent instrumentation to provide low-amplitude stimulation current to the interstitial compartment of 15 preparations. Within each array, alternating current stimuli were delivered between the outer pair of electrodes at frequencies of 10 Hz to 4000 Hz as described previously [21, 55, 56]. Each stimulus established a three-dimensional interstitial potential field that was then sensed as a voltage difference between sensors

that formed an inner pair of electrodes that in turn allowed the identification of a microscopic composite impedance (μCI) that included both real (tissue resistivity) and imaginary (tissue reactivity) components. At relatively low frequencies, supplied current remains primarily interstitial, and as a consequence, the current-to-voltage ratio provides information regarding the strength of interstitial electrical coupling. As frequency increases, supplied current shunts to the intracellular compartment via membrane capacitance and intracellular coupling strength becomes essential in assessing the response. Tissue resistivity and reactivity were identified during four sequential acquisition intervals in each preparation.

Optical mapping

To assess action potential duration, conduction velocity, and minimum pacing cycle length, LbL tissue surrogates were stained with a voltage-sensitive dye RH-237 (2.5 μM) for 10 minutes, transferred to a perfusion chamber mounted on an inverted microscope. Samples were perfused with Hank's balanced salt solution (HBSS) at approximately 37 ˚C. Sample pacing/stimulation was done with a bipolar electrode consisting of a glass pipette filled with HBSS and a silver wire coiled around its tip. The electrode tip was positioned at the sample's edge using a micromanipulator. Rectangular stimulation pulses were used, with a duration of 2 ms and current strength 1.5-times the excitation threshold. Fluorescence was excited with a 200-W Hg/Xe arc lamp and recorded with a 16×16 photodiode array (Hamamatsu) at a spatial resolution of 110 μm per diode as previously described 57. Excitation light was filtered at 532–587 nm, and emitted fluorescent light was filtered at > 650 nm. To eliminate motion artifacts caused by the sample's

spontaneous contractions, the perfusion solution was supplemented with 5 μM of blebbistatin. Isochronal maps of the activation spread were constructed from activation times measured at 50 % of the maximum action potential amplitude. Conduction velocity was calculated at each recording site from local activation times and averaged across the whole mapping area. Action potential duration was measured at 50 % and 80 % of signal recovery (APD_{50}) and (APD_{80}), respectively.

Image analyses

All image quantification analyses were performed with ImageJ. Where indicated, arbitrary units (A.U) are representative of a pixel count and intensity for each sample.

Statistical analyses

For statistical analysis, data are shown in the form mean ± SEM. Significance was chosen as $p < 0.05$. This was determined using either Student's t-test or ANOVA where applicable. One sample Wilcoxon tests ($\alpha = 0.05$) were used in the viscoelastic statistical analyses of between cardiac tissue surrogates ($n = 3$) and native murine LV tissue ($n = 5$). These analyses were performed utilizing GraphPad Prism8 data analysis software package.

Results

LbL fabrication produces thick, synchronously beating, fused tissue surrogates

Tissue surrogates produced with the optimized method described in **Figure 1** yielded structures of 1.73 ± 0.075 mm in thickness after one week in culture (**Figure 3** a). Following the first 24 h post-iCM layer deposition (on D1), the beating-rate (per min) of each tissue surrogate was determined (**Figure 3** b). This yielded a rate of 74 ± 8.4 beats/min (bpm). On the second day, the beat-rate lowered significantly ($p = 0.01$) to 63 ± 5.8 bpm. After iEC layer addition on D3 and an additional three days of culture (D6), the beating-rate on the sixth day had decreased further to 29 ± 4.1 bpm ($p = 0.0008$). Whether this significant decrease in bpm is due to paracrine signaling from the iECs or whether the internal cardiac pacemaker system become somewhat quiescent, remains to be seen.

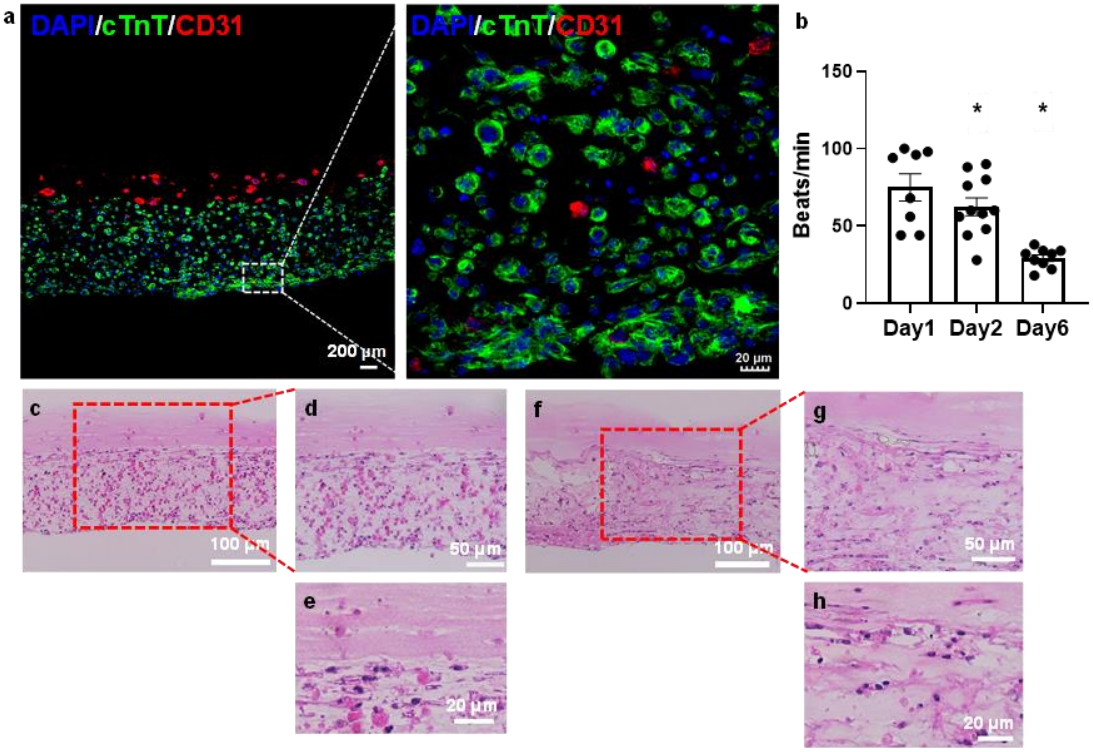

Figure 3: LbL production yields thick, synchronously beating, fused tissue surrogates. (a) Confocal micrograph of fabricated LbL cardiac tissue surrogates showing cell distribution and tissue surrogates thickness after 1 week in culture (n = 4). (b) LBL tissue surrogates beat-rate over the first 6 days during culture, $p < 0.05$, (n = 11). H&E staining of LbL tissue surrogates at Day 7 (c-e), and Day 28 (f-h) of culturing

Alterations in ECM composition between weeks one and four were observed via H&E staining (**Figure 3** c-h). Histology suggests increases in structural ECM components such as collagen (increased intensity as well as the distribution of eosinophilic staining, **Figure 3** c-h). With increased culture time, compaction of the structures became more apparent (**Figure** 3 f), and structures, although initially somewhat disorganized, resembled *in vivo* muscle. Structure coupling was confirmed by not only the synchronous macroscopic beating of the tissue surrogates (**Figure 3** b) but also through the fusion of the two layers as visualized on H&E sections. Another observation was the iEC migration out of their originally deposited layer into the resident iCM layer as is clear from the somewhat acellular appearance of the top layer of the tissue surrogate (**Figure 3** c-h),

Cell migration from the iEC later into the iCM resulted in a localized elevated concentration of iECs near the layer-fusion site, and was primarily evident during the initial culture stages (after 1 week, **Figure 3** c-e) as opposed to later culture stages (week 4, **Figure 3** f-h). Due to the difficulty in distinguishing between the different cells and their distribution throughout the structure based on H&E alone, further specific immunofluorescent staining was completed and quantified (**Figure 5**). The effect of this migration on the viability of the cardiac surrogates was determined via immunofluorescent staining and subsequently quantified. It should be noted that structures visualized here via H&E staining appear thinner than those preserved in OCT. This difference in overall tissue thickness is attributed to the multiple dehydration-related steps required during the H&E processing of the hydrogel structures leading to decreased preservation of the original architecture.

LbL fabrication yields highly viable tissue

The viability of the tissue was determined with pMLKL staining (**Figure 4**), which specifically stains for cell necroptosis [58] and is associated with inflammatory markers [59]. The pMLKL-positive cells were quantified as a percentage (%) of the total number of cells present (i.e., normalized to the DAPI staining). No significant differences were found in the degree of necrotic staining for any of the time points analyzed. The necrotic staining was quantified (**Figure 4** c) as 4.5 ± 2.3 % after one week, 4.3 ± 1.1 % after two weeks, and 5.6 ± 1.4 % after four weeks in culture (see Supplemental Figure S3 for staining at week 4). These values were comparable with the ~4 % pMLKL positive staining obtained by Gao *et al*. previously for their large tri-lineage iPSC-derived thick (1.25 mm) cardiac muscle patches after 1 week in culture [21].

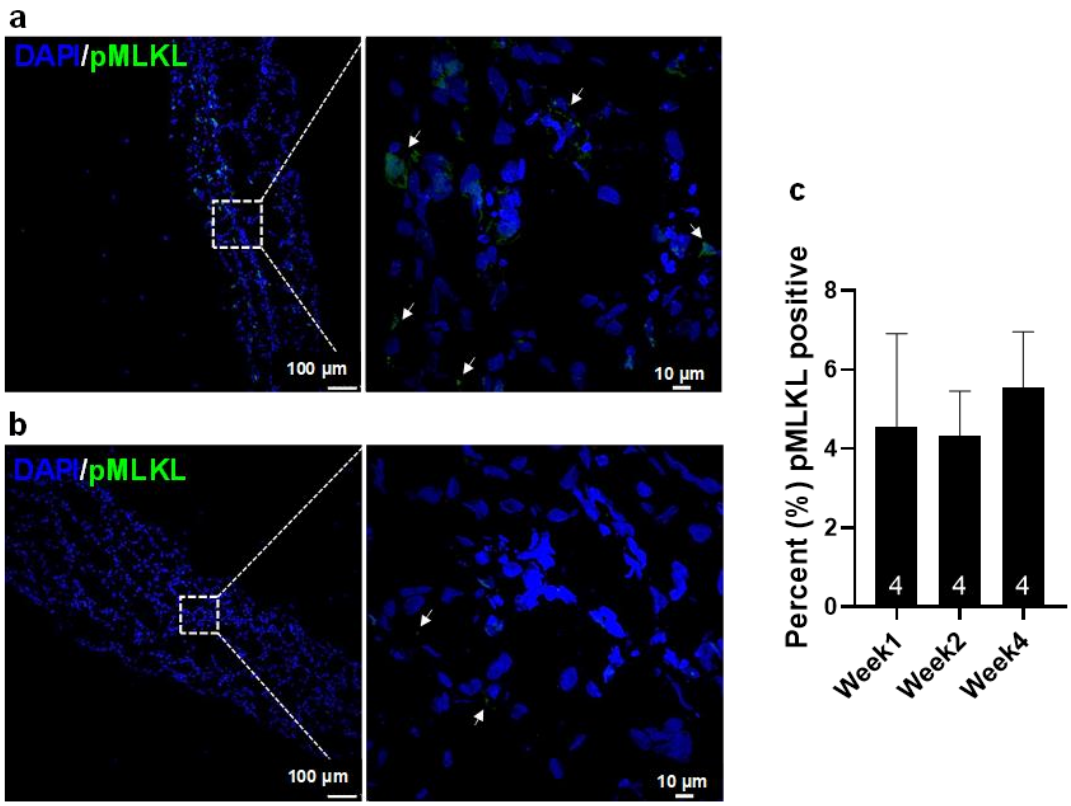

Figure 4: Degree of necrosis identified in cardiac tissue surrogates via pMLKL marker. Confocal micrograph of LbL tissue surrogates displaying necrotic cells identified by the necrosis marker phosphorylated MLKL (Ser358, pMLKL) at week 1 (a) and week 2 (b) of culture. (c) Percentage of necrotic cells in LbL tissue surrogates, (n = 4)

Cell migration and tissue vascularization

Imaging of the fluorescently stained sections (**Figure 5**) showed iEC migration into the iCM region of the dual-layered tissue surrogates. Evidence of migration was initially seen after day five and continued throughout the culture period. This migration process continued over the four weeks of culture, with clear integration into the iCM layer observed from the 2D sections by the 4th week (**Figure 5** a). In order to confirm vasculature formation as well as establish a timeline for the formation process, whole-mount staining was employed. Staining of samples after two weeks of culture (**Figure 5** c)

showed branching vascular networks. Whole-mount staining further confirmed the observations regarding iEC integration and elucidated that iCM orientation was random and did not yet present with the degree of cell alignment seen in native myocardial tissue (**Figure 5** c). Clear delineation of cell distribution can be seen in Supplemental Figure S4. Quantification of each cell type at weeks one, two and four, respectively, showed that the amount of CD31 expression relative to cTnT expression remained stable over the 4 week period with no statistically significant differences between the expression ratios at each time point (n = 3, Supplemental Figure S4 c). Furthermore, no statistically significant differences between the cTnT expression relative to the DAPI expression was noted either (n = 3, Supplemental Figure S4 d).

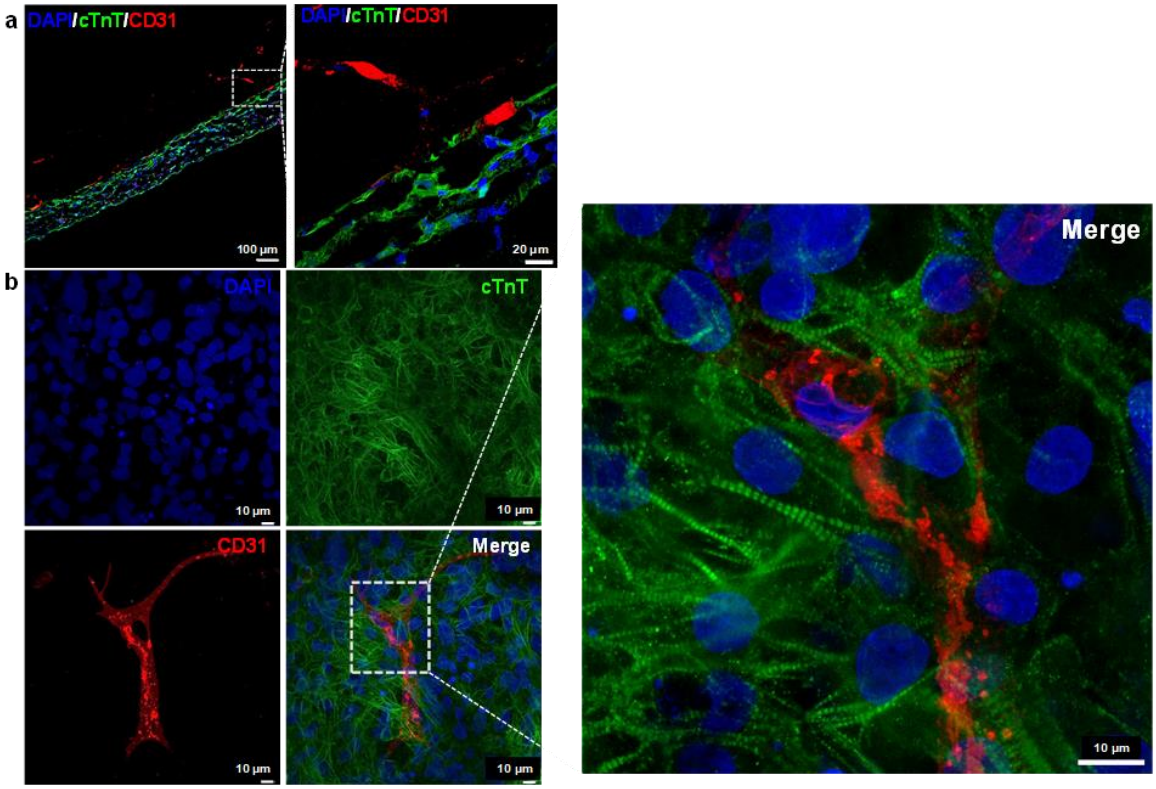

Figure 5: Temporal cellular migration and vascularization. Fluorescent staining with cTnT and CD31 showing developing vasculature in tissue cultured for (a) 4 weeks, along with (b) whole-mount staining of a 2-week tissue surrogate. Scale bars for the zoomed-in images are 20 µm and 10 µm for (a) and (b) respectively.

Use of the viscoelastic model in compression mode

Engineered tissue modeling over the four weeks yielded excellent fits to the experimentally obtained results, as $R^2 > 0.7$ for all samples from weeks 1 and 2 respectively, while $R^2 > 0.88$ for samples from week 4 (**Figure 6** a). Instantaneous moduli of 4.72 ± 0.84 kPa, 5.82 ± 0.47 kPa, and 4.85 ± 0.16 kPa were measured for week 1, week two, and week four samples, respectively (**Figure 6** b). The standard deviation in the samples decreased as the culture time increased from 1 week to 2 weeks to 4 weeks. Viscosity modeling yielded values of 8.03x104 ± 2.42x103 Pa•s, 3.35x104 ± 6.31x103 Pa•s, and 6.70x104 ± 2.14x104 Pa•s respectively. Tissue surrogate viscoelastic properties (n = 3 for each group) were compared to those of healthy LV tissue from SCID mice (n = 5). Mouse LV tissue instantaneous modulus was measured at 6.43 ± 1.13 kPa, while viscosity was 2.00x105 ± 8.32x104 Pa•s. Equilibrium moduli of 1.08 ± 0.31 kPa, 1.31 ± 0.37 kPa, and 0.40 ± 0.10 kPa were obtained for week 1, week two, and week four samples, respectively (**Figure 6** c). The equilibrium modulus for the control mouse LV samples was observed at 2.81 ± 0.48 kPa. Non-parametric tests (one sample Wilcoxon) showed that there were no statistically significant differences between the viscoelastic properties of the cardiac tissue surrogate and the healthy murine LV tissue ($\alpha = 0.05$), even with the differences in properties noted for the tissue surrogates at different time points.

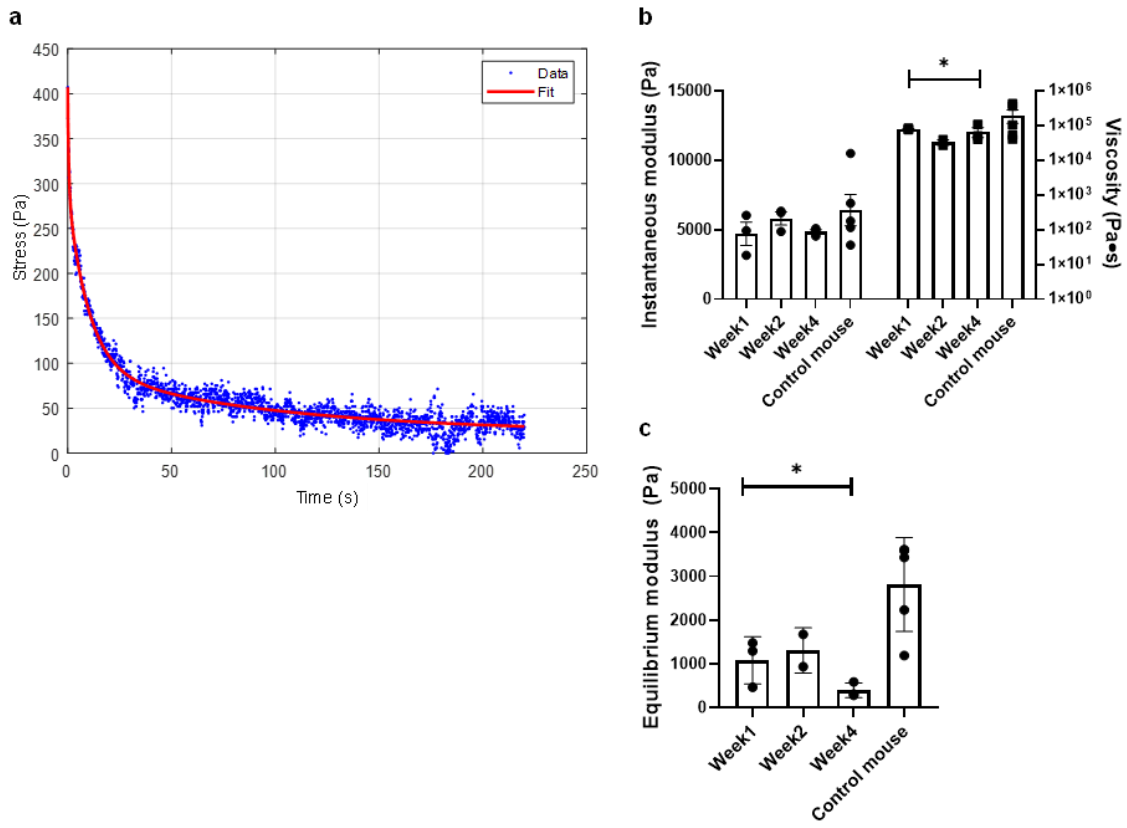

Figure 6: Viscoelastic characterization of native mouse tissue and engineered cardiac tissue surrogates. (a) Stress relaxation response ("Data") and modeling ("Fit") of a 4-week tissue surrogate as well as (b, c) the quantification of the modeling results for all samples over 4 weeks (n = 3 for all groups of tissue surrogates; n = 5 for control mice; *$p < 0.05$).

Dynamic ECM evolution

During the 4-week culturing period, the ECM underwent multiple phases of remodeling. The degree to which this very dynamic process occurs was monitored and quantified *in vitro* through analysis of individual matrix component degradation and deposition. For ECM analyses, 3 samples were analyzed at each time point, with at least five images per matrix component. Since the fibrin used in the matrix fabrication consisted of both bovine thrombin and fibrinogen, an antibody targeting a bovine specific epitope was

used in its analysis. An antibody with a fibrinogen β-chain that matched the β-chain section of the fibrinogen used to fabricate the fibrin matrix was used to stain and analyze the evolution of fibrin over four weeks in culture (**Figure 7** a). Analysis showed discernable degradation of the fibrin matrix over this period. Since the engineered tissue remained structurally intact and previous research has shown that ECM remodeling occurs during iCM culturing [60, 61], samples were analyzed for additional ECM components, including collagen 1 (Col1), collagen 3 (Col3), collagen 4 (Col4), laminin (Lam) and fibronectin (FN) (**Figure 7** b). Quantification showed a nearly 3-fold increase in collagen one production from weeks 1 to 4. A general trend was observed in basal membrane component production, i.e., the relative amounts of both collagen four, as well as laminin, decreased from week 1 to week 2, to week 4. The variations in structural ECM components, like collagen 1, affect the overall stiffness of the tissue surrogates, whereas dense basement membrane components, including laminin and collagen 4, play more of a role in viscous properties [62-64]. The decreasing viscosity of the tissue surrogates (**Figure 6** b) is likely linked to the reduction in basement membrane ECM components. Furthermore, week 2 saw a notable increase for fibronectin, which is highly expressed in the heart during early stages of embryogenesis and has also been shown to be vital in the vasculogenesis process [65]. The enhanced expression of fibronectin noted after two weeks in culture may be linked to the formation of the branched vessel-like structures noted in **Figure 5** c. In addition to altering viscosity properties of the structure, collagen 4 likely has another functional role, specifically that of an anti-angiogenic signaling cue [66, 67]. The statistically significant increase in collagen 4 in week 2 coincides with an even more notable statistically significant increase in fibronectin expression (**Figure 7** b). This phenomenon can most

likely be attributed to an “on-off” switch regulating the vessel formation process occurring in the tissue surrogate.

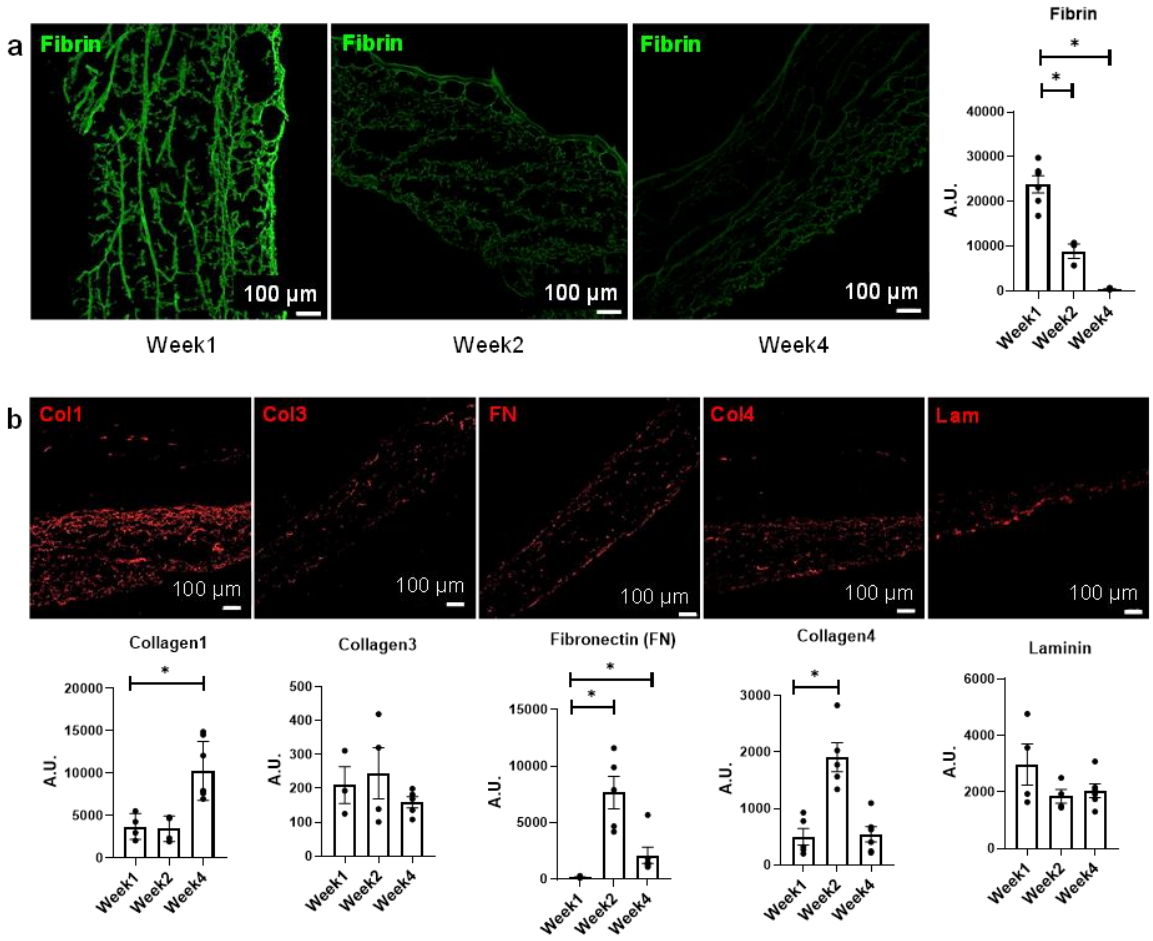

Figure 7: Representative images and subsequent quantification of ECM evolution over a 4-week period, with (a) showing the degradation of fibrin and (b) showing the deposition of Collagen 1, Collagen 3, Fibronectin (FN), Collagen 4 and Laminin at week 4. Scale bars = 100 µm, n = 5, *p < 0.05

Ultrastructure development is suggestive of tissue maturation

Alterations noted in the ECM via H&E and immuno-fluorescent staining (**Figure 3** c-h) were also confirmed via TEM (**Figure 8**). As culture-time increased from one to four weeks (**Figure 8** a vs. **Figure 8** c vs. **Figure 8** e), there was an increase in the num-

ber of gap junctions (GJ) observed between the cells (**Figure 8** d). Increases in the number of GJ (see Supplemental Figure S5 for immunofluorescent staining of connexin 43 as well as its quantification), along with the statistically significant increase in sarcomere length (distance between z-bands) from 1.53 ± 0.02 to 1.68 ± 0.12 μm between week one and two, with a further increase to 1.70 ± 0.02 μm at week four (**Figure 8** g) suggest that the fabrication method along with the extended culturing promote a degree of functional maturation [68]. These sarcomere lengths are physiologically relevant and compare with those observed in both neonatal rats and sheep (1.5 – 1.9 μm) [69, 70].

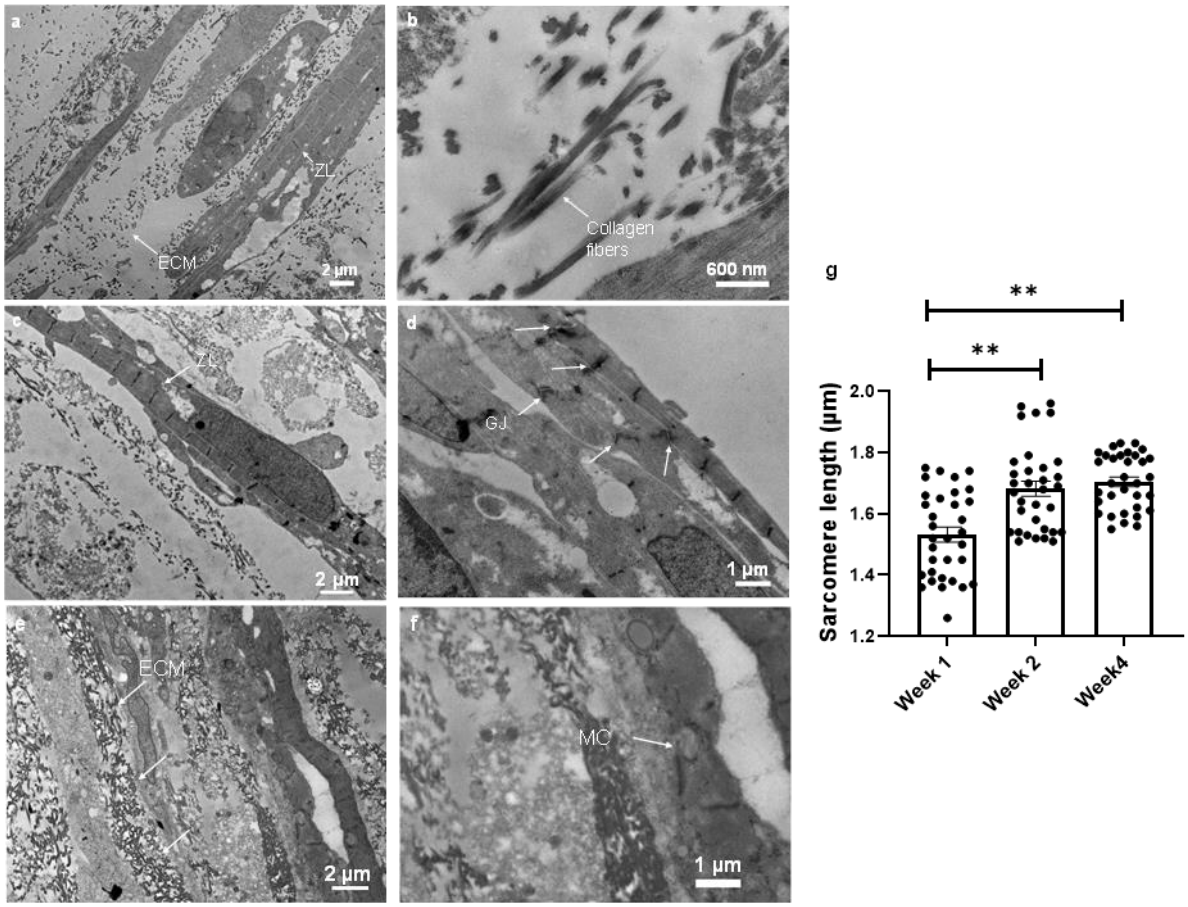

Figure 8: TEM of bi-layered tissue surrogates (a) 1 week after fabrication, showing alterations in ECM composition as well as cardiomyocyte Z-lines (ZL); (b) higher magnification with collagen fibers clearly distinguishable from other ECM components; (c) 2 weeks after fabrication, showing more distinct Z-lines as well as (d) higher magnification with gap junctions (GJ) between cells; (e) 4 weeks after fabrication, showing further alterations in ECM deposition, as well as (f) higher magnification with mitochondria (MC) starting to arrange along the contractile elements. (g) Sarcomere length comparison (n = 33) between structures cultured for 1 week, 2 weeks and 4 weeks; **$p < 0.0001$.

Functional performance of bi-layered tissue surrogates

Functional performance was assessed by t-tubule formation, intracellular gap junction formation (4EMS) as well as optical mapping to determine conduction velocities through the tissue. All mapping of surrogates was performed after 1 week in culture. Staining and subsequent quantification of the tissue surrogates for both junctophilin (JP2,

Figure 9 a, Supplemental Figure S6) and ryanodine receptor (RyR, **Figure 9** b, Supplemental Figure S6) expression suggested that there was a significant increase in the number of t-tubules formed between the first and fourth week of tissue culture. Resistivity-reactivity spectra (**Figure 9** c) compared favorably with spectra from our earlier report with rabbit left ventricular myocardium [55], supporting gap junction intracellular communication (GJIC) developed in these cardiac tissue surrogates to an extent similar to that in native myocardium. The heatmap generated from optical mapping (**Figure 9** d) shows a lack of arrhythmogenicity in the bi-layered structures. Furthermore, structures showed conduction velocities of 16.9 ± 2.3 cm/s, with the ability to be paced to 300 ms (3.33 Hz) from 800 ms (1.25 Hz), before being recovered to 800 ms pacing. ADP_{50} and ADP_{80} were noted as 128 ± 12.0 and 186 ± 17.7 ms, respectively.

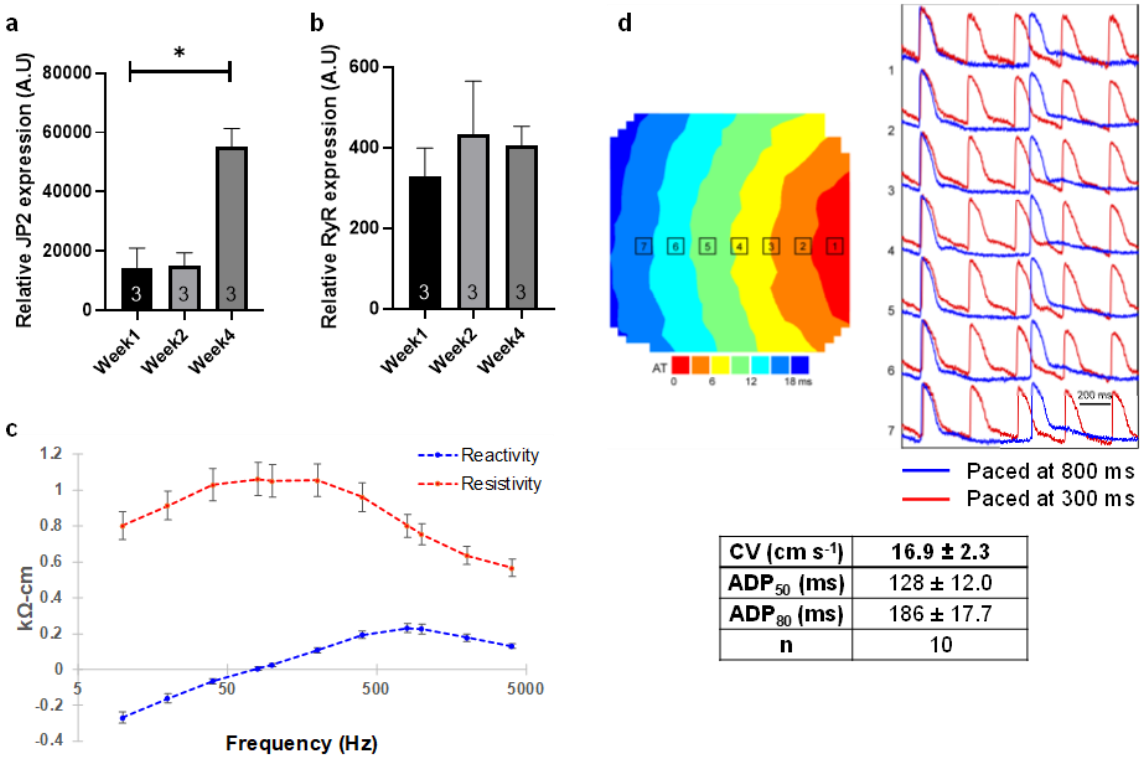

Figure 9: Functional analyses of bi-layered cardiac tissue surrogates. Expression of (a) JP2 and (b) RyR in the cardiac tissue surrogate structures over the different culture periods, *p < 0.05 (n = 3). (c) Tissue reactivity and resistivity shown as a function of stimulation frequency, (n = 15). (d) Summary of tissue optical mapping, with representative signal propagation heatmap as well as pacing at both 300 ms (red) and 800 ms (blue) (n = 10).

Discussion

Mimicking the myocardium in both form and function has been a goal for researchers in the cardiovascular field for decades. Not only is the heart a cellularly complex organ, but a structurally sophisticated one at that, and mimicking it as a living, electrical, mechanical structure is no easy feat. In this study, a new fabrication method using hiPSC derived cardiac cells for producing engineered cardiac tissue was developed and characterized. This method was based on a bottom-up LbL concept, to allow for enhanced viability and robustness over a 4-week period, as well as the development of

physiologically relevant structures on a cellular and microstructure level. This study is the first to our knowledge to show large and easily scalable (1 x 2 cm2) hiPSC-derived cardiac tissue surrogates that are thick (~1.73 mm), viable and prevascularized without significant necrosis/apoptosis during 4-weeks following up assessments. Not only have we demonstrated that these structures show minimal necrosis (< 5.4%) over a 4 week period, but also that they develop enhanced myocyte maturation as evidenced by characteristics in subcellular structure , electrophysiology, and calcium-handling capabilities. Quantification of the temporal stability of the relative expression of CD31 to cTnT as well as the relative expression of cTnT to DAPI further supported the findings showing minimal necrosis throughout the structures (Supplemental Figure S4). Additionally, this study quantified the temporal changes that occur during ECM remodeling in the engineered tissue surrogates via immunofluorescent staining, as well as modeling of viscoelastic properties.

Increases in the elastic modulus of engineered cardiac tissue surrogates cultured over four weeks were noted, but not as significant as was expected. Significant changes in the viscosity of the engineered tissue surrogates were noted after two weeks in culture. Due to the dynamic nature of ECM remodeling, it is difficult to discern which ECM component was mostly responsible for the reduction in viscosity noted in week 2, but general trends suggested reduced laminin could be responsible. Furthermore, the increase in fibronectin expression observed in week two coincided with the notable formation of branched vessel-like structures in the cardiac tissue surrogates. As fibronectin is highly expressed in the heart during early stages of embryogenesis and has been shown to be vital in the vasculogenesis process [65] these observations are likely linked. Regulation of

vessel formation via an "on-off" switch was likely achieved via the expression of Col4 at week 2 [66, 67].

The temporal viscoelastic properties of the engineered tissue surrogates were compared to those of healthy mouse LV tissue. The elasticity moduli reported in this study ranged between ~4.7-5.8 kPa, while the control mouse samples were 6.4 kPa, suggesting that the engineered tissue designed in this study had viscoelastic properties comparable to healthy LV tissue. Comparable elasticity values can be difficult to obtain in the literature due to variations in testing methods; however, healthy rat heart tissue elasticity has been reported to be 18 ± 2 kPa [71], while embryonic mouse epicardial tissue has been reported to have an elastic modulus of 12 ± 4 kPa [72]. Equilibrium moduli values for the bi-layered engineered tissue fell short when compared to healthy mouse LV tissue, though not by a statistically significant amount. This could, in part, be because primary structural ECM deposition was dependent on iCMs alone, whereas native cardiac tissue consists of known structural ECM-producing cells specifically, fibroblasts.

Cardiac cells are under constant, self-generated cyclic mechanical stress, which can affect their differentiation, development as well as maturation. Additional loading of CMs has shown to be an effective tool in advancing certain maturation markers, like the upregulation of connexin 43, in these cells. Stretching has been demonstrated to directly affect the activity of ion channels and increase gap junction-mediated cell coupling [73-76]. The bi-layered tissue surrogate developed during this study did not undergo any additional mechanical or electrical loading, yet was still able to develop physiologically relevant ultrastructural attributes like increased sarcomere length and mitochondrial alignment along the contractile elements. The mechanical forces, however faint, that the iCMs

cyclically generate, are also a source of constant fluidic motion and convection within the culture environment and may contribute to the system's ability to remain viable for weeks with minimal cell necrosis. Normal functions of cardiomyocytes require the endothelial cells in the microenvironment, which likely contribute to the novel fabricated thicker and functional cardiac tissue surrogates in the present study. In addition to the natural motion of the tissue surrogate, the formation of branched vessel-like structures may enhance the oxygen and nutrients delivery to the center of the thicker engineered cardiac tissue.

Cardiac transverse tubules (T-tubules) (**Figure 9** a & b) are highly branched invaginations of cardiomyocyte sarcolemma that are rich in ion channels essential for excitation-contraction coupling, maintenance of resting membrane potential, action potential initiation and regulation, and signaling transduction. Mature T-tubule networks are present in mammalian ventricular cardiomyocytes, with the transverse components of t-tubules occurring near sarcomeric z-discs. Cardiac T-tubules contain membrane micro-domains, enriched with ion channels and signaling molecules, and as such, are vital signaling hubs in the regulation of cardiomyocyte function. Dyads formed at the junctions between the T-tubule membrane and neighboring sarcoplasmic reticulum (SR) are vital in calcium signaling and EC coupling necessary for beat-to-beat cardiac contraction. The juxtaposition of the L-type Ca channel (LTCC) located in the T-tubule membrane with the ryanodine receptor (RyR2), the major cardiac SR Ca^{2+} release channel, is necessary for the initiation of the proper calcium transients required following each beat-to-beat action potential. These systems are thought to promote the synchronous activation of the

whole depth of the cell despite the fact that the signal to contract is relayed across the external membrane. The importance of the T-tubule network should not be underestimated, as it is responsible for one-third of the capacitance of the membrane, along with most of the influx of Ca^{2+} that triggers the release of intracellular SR Ca^{2+} enters across the T-tubular fraction [77]. Increases in the expression of T-tubule markers like JP2 are indicative of improved calcium handling abilities [78, 79]. Conduction velocities that approach those seen in native LV tissue (30-100 cm/s [80]) have rarely been achieved in 3D structures with hiPSC-CMs. Structures consisting of cells from neonatal rats have, however, been shown to reach velocities of up to ~32 cm/s [81]. The LbL cardiac tissue surrogate produced in the current study (**Figure 1**) does, however, outcompete its predecessors with its 16.9 ± 2.3 cm/s, compared to 14.1 ± 1.0 cm/s [21]. The ability of the bi-layered structures to be paced to 300 ms without becoming arrhythmogenic was a further indication of their robustness and capability to perform under high-stress conditions [82].

It should be noted that, even though this 3D *in vitro* study was performed over an extended period (4 weeks), it only represents a brief moment in time in terms of the characteristics of a larger ensemble. In order to better understand the system and continue optimization, longer-term culture studies, along with implantation success, have to be assessed. Furthermore, incorporating directional tissue maturation techniques, using a perfusion system as opposed to static culture [83], including electrical or mechanical stimulation [68, 82, 84, 85], could further enhance tissue performance and allow for viscoelastic engineered tissue surrogates that further resembles the native myocardium.

Conclusions

Here we have shown how modular fabrication methods, like LbL, can be utilized and optimized to yield thick (~1.73 mm), viable, easy-to-scale-to clinically relevant sized cardiac tissue surrogates. *In vitro* characterization showed tissue structures resembling those of native cardiac tissue, both structurally and functionally. Well-developed calcium-handling machinery, minimal arrhythmogenic potential, and promising conduction velocities were observed. Viscoelastic characterization and comparison with native mouse LV tissue showed that the Generalized Maxwell model of order 4 described the samples very well. The viscoelastic characterization also suggested that the addition of structural ECM producing cells, specifically fibroblasts, may allow for production of cardiac tissue equivalents that further mimic native myocardial tissue.

Future work will focus on the incorporation of additional cells like fibroblasts, yielding further biomimetic structures and allowing for the expansion of potential theranostic applications. *In vivo* studies in a large animal model will also commence in order to assess the potential clinical application of these larger, thicker, cardiac tissue equivalents. Assessment of improvement will include the engraftment rate of transplanted cells, LV dilatation, LV wall stress, infarct size, and arrhythmogenic potential.

Acknowledgments

This study was supported in part by the National Institutes of Health (NIH) through grants NHLBI grants RO1 HL95077, HL114120, HL131017, and HL149137. The authors would like to thank Dr. Chengming Fan for surgical assistance, Dr. Yanwen

Liu for their excellent technical assistance, Dr. Silvio Litovsky for cardiac pathology assistance and the UAB High-Resolution Imaging Facility as well as the UAB Pathology Core Lab for their assistance with sample preparation. All mechanical experiments were performed in the UAB Experimental Biomechanics Core (EBC).

REFERENCES

1. Lucas DT and Szweda LI. Declines in mitochondrial respiration during cardiac reperfusion: Age-dependent inactivation of α-ketoglutarate dehydrogenase. 1999;96:6689-6693.

2. Lake CL, Sellers TD, Crosby IK, Wellons HA and Crampton RS. Effects of coronary grafting technique upon reperfusion cardiac rhythm, ventricular function, and other variables. Am Surg. 1985;51:497-503.

3. Murphy E and Steenbergen C. Mechanisms Underlying Acute Protection From Cardiac Ischemia-Reperfusion Injury. 2008;88:581-609.

4. Ye L, Chang Y-H, Xiong Q, Zhang P, Zhang L, Somasundaram P, Lepley M, Swingen C, Su L, Wendel Jacqueline S, Guo J, Jang A, Rosenbush D, Greder L, Dutton James R, Zhang J, Kamp Timothy J, Kaufman Dan S, Ge Y and Zhang J. Cardiac Repair in a Porcine Model of Acute Myocardial Infarction with Human Induced Pluripotent Stem Cell-Derived Cardiovascular Cells. Cell Stem Cell. 2014;15:750-761.

5. Xiaojun L, Cheston H, Gisela W, Kexian Z, Laurie BH, Samira MA, Kunil KR, Jianhua Z, Timothy JK and Sean PP. Robust cardiomyocyte differentiation from human pluripotent stem cells via temporal modulation of canonical Wnt signaling. Proceedings of the National Academy of Sciences of the United States of America. 2012;109:E1848-57.

6. Xiaojun L, Xiaoping B, Abraham A-A, Jialu L, Yue W, Wentao D, Kaitlin KD, Eric VS and Sean PP. Efficient differentiation of human pluripotent stem cells to endothelial progenitors via small-molecule activation of WNT signaling. Stem cell reports. 2014;3:804-16.

7. Chapter 4 Challenges in Tissue Engineering. In: Y. Ikada, ed. Interface Science and Technology: Elsevier; 2006(8): 423-462.

8. Rumberger JA. Ventricular dilatation and remodeling after myocardial infarction. Mayo Clinic proceedings. 1994;69:664-74.

9. Holmes JW, Borg TK and Covell JW. Structure and Mechanics of Healing Myocardial Infarcts. 2005;7:223-253.

10. Fung YC. Biomechanics: Mechanical Properties of Living Tissues. New York: Springer-Verlag; 1993.

11. Sacks MS. Biaxial Mechanical Evaluation of Planar Biological Materials. In: S. C. Cowin and J. D. Humphrey, eds. Cardiovascular Soft Tissue Mechanics Dordrecht: Springer Netherlands; 2001: 199-246.

12. Wang B, Borazjani A, Tahai M, Curry AL, Simionescu DT, Guan J, To F, Elder SH and Liao J. Fabrication of cardiac patch with decellularized porcine myocardial scaffold and bone marrow mononuclear cells. Journal of biomedical materials research Part A. 2010;94:1100-10.

13. Engler AJ, Sen S, Sweeney HL and Discher DE. Matrix Elasticity Directs Stem Cell Lineage Specification. Cell. 2006;126:677-689.

14. Reilly GC and Engler AJ. Intrinsic extracellular matrix properties regulate stem cell differentiation. Journal of Biomechanics. 2010;43:55-62.

15. Advanced Tools for Tissue Engineering: Scaffolds, Bioreactors, and Signaling. 2006;12:3285-3305.

16. Richardson JJ, Björnmalm M and Caruso F. Technology-driven layer-by-layer assembly of nanofilms. 2015;348:aaa2491.

17. Zhang X, Chen H and Zhang H. Layer-by-layer assembly: from conventional to unconventional methods. Chemical Communications. 2007:1395-1405.

18. Kirkland JJ. Porous Thin-Layer Modified Glass Bead Supports for Gas Liquid Chromatography. Analytical Chemistry. 1965;37:1458-1461.

19. Jin W, Toutianoush A and Tieke B. Use of Polyelectrolyte Layer-by-Layer Assemblies as Nanofiltration and Reverse Osmosis Membranes. Langmuir. 2003;19:2550-2553.

20. Siepmann J and Peppas NA. Hydrophilic Matrices for Controlled Drug Delivery: An Improved Mathematical Model to Predict the Resulting Drug Release Kinetics (the “sequential Layer” Model). Pharmaceutical Research. 2000;17:1290-1298.

21. Gao L, Gregorich ZR, Zhu W, Mattapally S, Oduk Y, Lou X, Kannappan R, Borovjagin AV, Walcott GP, Pollard AE, Fast VG, Hu X, Lloyd SG, Ge Y and Zhang J. Large Cardiac Muscle Patches Engineered From Human Induced-Pluripotent Stem Cell-Derived Cardiac Cells Improve Recovery From Myocardial Infarction in Swine. Circulation. 2018;137:1712-1730.

22. Donath E, Sukhorukov GB, Caruso F, Davis SA and Möhwald H. Novel Hollow Polymer Shells by Colloid-Templated Assembly of Polyelectrolytes. Angewandte Chemie International Edition. 1998;37:2201-2205.

23. Dreaden EC, Morton SW, Shopsowitz KE, Choi J-H, Deng ZJ, Cho N-J and Hammond PT. Bimodal Tumor-Targeting from Microenvironment Responsive Hyaluronan Layer-by-Layer (LbL) Nanoparticles. ACS Nano. 2014;8:8374-8382.

24. Cui J, Liu Y and Hao J. Multiwalled Carbon-Nanotube-Embedded Microcapsules and Their Electrochemical Behavior. The Journal of Physical Chemistry C. 2009;113:3967-3972.

25. Lulevich VV, Andrienko D and Vinogradova OI. Elasticity of polyelectrolyte multilayer microcapsules. The Journal of Chemical Physics. 2004;120:3822-3826.

26. Best JP, Neubauer MP, Javed S, Dam HH, Fery A and Caruso F. Mechanics of pH-Responsive Hydrogel Capsules. Langmuir. 2013;29:9814-9823.

27. Rother J, Richter C, Turco L, Knoch F, Mey I, Luther S, Janshoff A, Bodenschatz E and Tarantola M. Crosstalk of cardiomyocytes and fibroblasts in co-cultures. Open biology. 2015;5:150038.

28. Oliver Cassell CS, Stefan Hofer OP, Morrison WA and Knight KR. Vascularisation of tissue-engineered grafts: the regulation of angiogenesis in reconstructive surgery and in disease states. British Journal of Plastic Surgery. 2002;55:603-610.

29. Risau W. Mechanisms of angiogenesis. Nature. 1997;386:671-674.

30. Ishaug-Riley SL, Crane-Kruger GM, Yaszemski MJ and Mikos AG. Three-dimensional culture of rat calvarial osteoblasts in porous biodegradable polymers. Biomaterials. 1998;19:1405-1412.

31. Marchionni MA. neu tack on neuregulin. Nature. 1995;378:334-335.

32. Lee K-F, Simon H, Chen H, Bates B, Hung M-C and Hauser C. Requirement for neuregulin receptor erbB2 in neural and cardiac development. Nature. 1995;378:394-398.

33. Bjarnegård M, Enge M, Norlin J, Gustafsdottir S, Fredriksson S, Abramsson A, Takemoto M, Gustafsson E, Fässler R and Betsholtz C. Endothelium-specific ablation of PDGFB leads to pericyte loss and glomerular, cardiac and placental abnormalities. Development. 2004;131:1847-1857.

34. Gödecke A, Heinicke T, Kamkin A, Kiseleva I, Strasser RH, Decking UKM, Stumpe T, Isenberg G and Schrader J. Inotropic response to β-adrenergic receptor stimulation and anti-adrenergic effect of ACh in endothelial NO synthase-deficient mouse hearts. The Journal of Physiology. 2001;532:195-204.

35. Champion HC, Georgakopoulos D, Takimoto E, Isoda T, Wang Y and Kass DA. Modulation of In Vivo Cardiac Function by Myocyte-Specific Nitric Oxide Synthase-3. Circulation research. 2004;94:657-663.

36. Barouch LA, Harrison RW, Skaf MW, Rosas GO, Cappola TP, Kobeissi ZA, Hobai IA, Lemmon CA, Burnett AL, O'Rourke B, Rodriguez ER, Huang PL, Lima JAC, Berkowitz DE and Hare JM. Nitric oxide regulates the heart by spatial confinement of nitric oxide synthase isoforms. Nature. 2002;416:337-339.

37. Dunn KK, Reichardt IM, Simmons AD, Jin G, Floy ME, Hoon KM and Palecek SP. Coculture of Endothelial Cells with Human Pluripotent Stem Cell-Derived Cardiac Progenitors Reveals a Differentiation Stage-Specific Enhancement of Cardiomyocyte Maturation. Biotechnology Journal. 2019;14:1800725.

38. Khademhosseini A, Suh KY, Yang JM, Eng G, Yeh J, Levenberg S and Langer R. Layer-by-layer deposition of hyaluronic acid and poly-l-lysine for patterned cell co-cultures. Biomaterials. 2004;25:3583-3592.

39. Ware BR, Durham MJ, Monckton CP and Khetani SR. A Cell Culture Platform to Maintain Long-term Phenotype of Primary Human Hepatocytes and Endothelial Cells. Cellular and Molecular Gastroenterology and Hepatology. 2018;5:187-207.

40. Sasaki K, Akagi T, Asaoka T, Eguchi H, Fukuda Y, Iwagami Y, Yamada D, Noda T, Wada H, Gotoh K, Kawamoto K, Doki Y, Mori M and Akashi M. Construction of three-dimensional vascularized functional human liver tissue using a layer-by-layer cell coating technique. Biomaterials. 2017;133:263-274.

41. Norotte C, Marga FS, Niklason LE and Forgacs G. Scaffold-free vascular tissue engineering using bioprinting. Biomaterials. 2009;30:5910-5917.

42. Bursac N, Papadaki M, Cohen RJ, Schoen FJ, Eisenberg SR, Carrier R, Vunjak-Novakovic G and Freed LE. Cardiac muscle tissue engineering: toward an in vitro model for electrophysiological studies. American Journal of Physiology-Heart and Circulatory Physiology. 1999;277:H433-H444.

43. Shadrin IY, Allen BW, Qian Y, Jackman CP, Carlson AL, Juhas ME and Bursac N. Cardiopatch platform enables maturation and scale-up of human pluripotent stem cell-derived engineered heart tissues. Nat Commun. 2017;8:1825.

44. Shimizu T, Yamato M, Kikuchi A and Okano T. Two-Dimensional Manipulation of Cardiac Myocyte Sheets Utilizing Temperature-Responsive Culture Dishes Augments the Pulsatile Amplitude. Tissue Engineering. 2001;7:141-151.

45. Munro ML, Jayasinghe ID, Wang Q, Quick A, Wang W, Baddeley D, Wehrens XHT and Soeller C. Junctophilin-2 in the nanoscale organisation and functional signalling of ryanodine receptor clusters in cardiomyocytes. 2016;129:4388-4398.

46. Landstrom AP, Kellen CA, Dixit SS, Oort RJv, Garbino A, Weisleder N, Ma J, Wehrens XHT and Ackerman MJ. Junctophilin-2 Expression Silencing Causes Cardiocyte Hypertrophy and Abnormal Intracellular Calcium-Handling. 2011;4:214-223.

47. Burridge PW, Matsa E, Shukla P, Lin ZC, Churko JM, Ebert AD, Lan F, Diecke S, Huber B, Mordwinkin NM, Plews JR, Abilez OJ, Cui B, Gold JD and Wu JC. Chemically defined generation of human cardiomyocytes. 2014;11:855-60.

48. Lian X, Zhang J, Azarin SM, Zhu K, Hazeltine LB, Bao X, Hsiao C, Kamp TJ and Palecek SP. Directed cardiomyocyte differentiation from human pluripotent

stem cells by modulating Wnt/β-catenin signaling under fully defined conditions. Nature Protocols. 2012;8:162.

49. Zhu W, Gao L and Zhang J. Pluripotent Stem Cell Derived Cardiac Cells for Myocardial Repair. JoVE. 2017:e55142.

50. Su L, Kong X, Lim S, Loo S, Tan S, Poh K, Dutton J, Stewart C, Cook S, Su X, Ma J, Zhang J and Ye L. The prostaglandin H2 analog U-46619 improves the differentiation efficiency of human induced pluripotent stem cells into endothelial cells by activating both p38MAPK and ERK1/2 signaling pathways. Stem Cell Res Ther. 2018;9:313.

51. Zhang S, Dutton JR, Su L, Zhang J and Ye L. The influence of a spatiotemporal 3D environment on endothelial cell differentiation of human induced pluripotent stem cells. Biomaterials. 2014;35:3786-93.

52. Li W, Germain RN and Gerner MY. High-dimensional cell-level analysis of tissues with Ce3D multiplex volume imaging. Nature Protocols. 2019;14:1708-1733.

53. Pollack GH. Maximum Velocity as an Index of Contractility in Cardiac Muscle. 1970;26:111-127.

54. Ramadan S, Paul N and Naguib HE. Standardized static and dynamic evaluation of myocardial tissue properties. Biomedical materials (Bristol, England). 2017;12:025013.

55. Pollard AE and Barr RC. A new approach for resolution of complex tissue impedance spectra in hearts. IEEE transactions on bio-medical engineering. 2013;60:2494-503.

56. Waits CMK, Barr RC and Pollard AE. Sensor spacing affects the tissue impedance spectra of rabbit ventricular epicardium. Am J Physiol Heart Circ Physiol. 2014;306:H1660-H1668.

57. Sowell B and Fast VG. Ionic mechanism of shock-induced arrhythmias: role of intracellular calcium. Heart Rhythm. 2012;9:96-104.

58. Linkermann A, Kunzendorf U and Krautwald S. Phosphorylated MLKL causes plasma membrane rupture. Mol Cell Oncol. 2014;1:e29915-e29915.

59. Negroni A, Colantoni E, Pierdomenico M, Palone F, Costanzo M, Oliva S, Tiberti A, Cucchiara S and Stronati L. RIP3 AND pMLKL promote necroptosis-induced inflammation and alter membrane permeability in intestinal epithelial cells. Digestive and Liver Disease. 2017;49:1201-1210.

60. Wendel JS, Ye L, Tao R, Zhang J, Zhang J, Kamp TJ and Tranquillo RT. Functional Effects of a Tissue-Engineered Cardiac Patch From Human Induced Pluripotent Stem Cell-Derived Cardiomyocytes in a Rat Infarct Model. Stem Cells Transl Med. 2015;4:1324-1332.

61. Bax NAM, van Marion MH, Shah B, Goumans M-J, Bouten CVC and van der Schaft DWJ. Matrix production and remodeling capacity of cardiomyocyte progenitor cells during in vitro differentiation. Journal of molecular and cellular cardiology. 2012;53:497-508.

62. Lu P, Takai K, Weaver VM and Werb Z. Extracellular matrix degradation and remodeling in development and disease. Cold Spring Harb Perspect Biol. 2011;3:a005058.

63. Ford AJ and Rajagopalan P. Extracellular matrix remodeling in 3D: implications in tissue homeostasis and disease progression. 2018;10:e1503.

64. Cox TR and Erler JT. Remodeling and homeostasis of the extracellular matrix: implications for fibrotic diseases and cancer. Dis Model Mech. 2011;4:165-178.

65. George EL, Georges-Labouesse EN, Patel-King RS, Rayburn H and Hynes RO. Defects in mesoderm, neural tube and vascular development in mouse embryos lacking fibronectin. Development (Cambridge, England). 1993;119:1079-91.

66. Carmeliet P. Angiogenesis in health and disease. Nature Medicine. 2003;9:653-660.

67. Colorado PC, Torre A, Kamphaus G, Maeshima Y, Hopfer H, Takahashi K, Volk R, Zamborsky ED, Herman S, Sarkar PK, Ericksen MB, Dhanabal M, Simons M, Post M, Kufe DW, Weichselbaum RR, Sukhatme VP and Kalluri R. Anti-angiogenic Cues from Vascular Basement Membrane Collagen. 2000;60:2520-2526.

68. Ronaldson-Bouchard K, Ma SP, Yeager K, Chen T, Song L, Sirabella D, Morikawa K, Teles D, Yazawa M and Vunjak-Novakovic G. Advanced maturation of human cardiac tissue grown from pluripotent stem cells. Nature. 2018;556:239-243.

69. Sheldon CA, Friedman WF and Sybers HD. Scanning electron microscopy of fetal and neonatal lamb cardiac cells. Journal of molecular and cellular cardiology. 1976;8:853-862.

70. Anversa P, Olivetti G and Loud AV. Morphometric study of early postnatal development in the left and right ventricular myocardium of the rat. I. Hypertrophy, hyperplasia, and binucleation of myocytes. 1980;46:495-502.

71. Berry MF, Engler AJ, Woo YJ, Pirolli TJ, Bish LT, Jayasankar V, Morine KJ, Gardner TJ, Discher DE and Sweeney HL. Mesenchymal stem cell injection after myocardial infarction improves myocardial compliance. 2006;290:H2196-H2203.

72. Jacot JG, Martin JC and Hunt DL. Mechanobiology of cardiomyocyte development. Journal of Biomechanics. 2010;43:93-98.

73. Kaushik G and Engler AJ. From stem cells to cardiomyocytes: the role of forces in cardiac maturation, aging, and disease. Prog Mol Biol Transl Sci. 2014;126:219-242.

74. Zhuang J, Yamada KA, Saffitz JE and Kléber AG. Pulsatile Stretch Remodels Cell-to-Cell Communication in Cultured Myocytes. 2000;87:316-322.

75. Yamada K, Green KG, Samarel AM and Saffitz JE. Distinct pathways regulate expression of cardiac electrical and mechanical junction proteins in response to stretch. Circ Res. 2005;97:346-53.

76. Wang TL, Tseng YZ and Chang H. Regulation of connexin 43 gene expression by cyclical mechanical stretch in neonatal rat cardiomyocytes. Biochemical and biophysical research communications. 2000;267:551-7.

77. Scriven DRL, Dan P and Moore EDW. Distribution of Proteins Implicated in Excitation-Contraction Coupling in Rat Ventricular Myocytes. Biophysical journal. 2000;79:2682-2691.

78. Parikh SS, Blackwell DJ, Gomez-Hurtado N, Frisk M, Wang L, Kim K, Dahl CP, Fiane A, Tonnessen T, Kryshtal DO, Louch WE and Knollmann BC. Thyroid and Glucocorticoid Hormones Promote Functional T-Tubule Development in Human-Induced Pluripotent Stem Cell-Derived Cardiomyocytes. Circ Res. 2017;121:1323-1330.

79. Li S, Chen G and Li RA. Calcium signalling of human pluripotent stem cell-derived cardiomyocytes. 2013;591:5279-5290.

80. Yang X, Pabon L and Murry CE. Engineering Adolescence. 2014;114:511-523.

81. Jackman CP, Ganapathi AM, Asfour H, Qian Y, Allen BW, Li Y and Bursac N. Engineered cardiac tissue patch maintains structural and electrical properties after epicardial implantation. Biomaterials. 2018;159:48-58.

82. LaBarge W, Mattappally S, Kannappan R, Fast VG, Pretorius D, Berry JL and Zhang J. Maturation of three-dimensional, hiPSC-derived cardiomyocyte spheroids utilizing cyclic, uniaxial stretch and electrical stimulation. PloS one. 2019;14:e0219442-e0219442.

83. Zhao F, Pathi P, Grayson W, Xing Q, Locke BR and Ma T. Effects of Oxygen Transport on 3-D Human Mesenchymal Stem Cell Metabolic Activity in Perfusion and Static Cultures: Experiments and Mathematical Model. 2005;21:1269-1280.

84. Radisic M, Park H, Shing H, Consi T, Schoen FJ, Langer R, Freed LE and Vunjak-Novakovic G. Functional assembly of engineered myocardium by electrical stimulation of cardiac myocytes cultured on scaffolds. 2004;101:18129-18134.

85. Ruan JL, Tulloch NL, Razumova MV, Saiget M, Muskheli V, Pabon L, Reinecke H, Regnier M and Murry CE. Mechanical Stress Conditioning and Electrical Stimulation Promote Contractility and Force Maturation of Induced Pluripotent Stem Cell-Derived Human Cardiac Tissue. Circulation. 2016;134:1557-1567.

Supplemental Material and Methods

Flow cytometry analysis

Flow cytometry analysis was performed as described previously [50-52]. Briefly, cells were dissociated using 0.25 % trypsin and resuspended as single cells, permeabilized in 0.1 % Triton X-100 at 4 °C for 10 min, then incubated with primary and secondary antibodies for 30 min at 4 °C with 3 x 5 min wash in between. Finally, cells were resuspended in 2 % fetal bovine serum/phosphate-buffered saline (FBS/PBS) containing 5 μL of propidium iodide (10 μg/mL) and evaluated with a FACS Aria instrument (BD Biosciences, USA). Antibodies used, along with dilutions, are listed Supplemental Table S1.

Cardiomyocyte proliferation assay

Cardiomyocyte proliferation was tested using a proliferation assay from CyQUANT Direct Cell Proliferation Assay Kit (Invitrogen, Cat# C35011). Briefly, CM proliferation was determined via green fluorescent nucleic acid staining of the nucleus, after which the fluorescence intensity of the readout was obtained 120 min after reagent addition via microplate reader. Based on the results, there was no significant difference between the proliferation of 28-day-old and 42-day-old hiPSC-CMs (see Supplemental Figure S2). Student t-test was performed, $p = 0.6565$ ($n = 6$).

Table S1: Antibodies used for flow cytometry, FACS, and immunofluorescent staining.

Antibody Name	**Application**	**Company**	**Catalog Number**
Alexa Fluor® 647 Mouse Anti-Human CD31	FACS	BD Bio sciences	561654
Cardiac Troponin T Monoclonal Antibody (13-11)	Flow Analysis	Invitrogen	MA5-12960
Rabbit Anti-Cardiac Troponin T antibody [EPR3695]	Immunofluorescent Staining	Abcam	91605
Mouse Anti-Cardiac Troponin T antibody [1F11]	Immunofluorescent Staining	Abcam	10214
Goat anti-Mouse IgG Secondary Antibody, Alexa Fluor 555	Immunofluorescent Staining	Invitrogen	A32727
Donkey anti-Mouse IgG Secondary Antibody, Alexa Fluor 488	Immunofluorescent Staining	Invitrogen	A21202
Donkey anti-Rabbit IgG Secondary Antibody, Alexa Fluor 488	Immunofluorescent Staining	Invitrogen	A21206
Donkey anti-Rabbit IgG Secondary Antibody, Alexa Fluor 555	Immunofluorescent Staining	Invitrogen	A31572
Rabbit Anti-Collagen I antibody	Immunofluorescent Staining	Abcam	34710
Mouse Anti-CD31 antibody [JC/70A]	Immunofluorescent Staining	Abcam	9498
Rabbit Anti-Fibrinogen beta chain antibody	Immunofluorescent Staining	Abcam	137830
Rabbit Anti-Collagen III antibody	Immunofluorescent Staining	Abcam	7778
Rabbit Anti-Fibronectin antibody	Immunofluorescent Staining	Abcam	2413
Rabbit Anti-Collagen IV antibody	Immunofluorescent Staining	Abcam	6586
Rabbit Anti-Laminin antibody	Immunofluorescent Staining	Abcam	11575
Rabbit Anti-VE Cadherin	Immunofluorescent Staining	Abcam	33168
Mouse Anti-VWF Antibody (F8/86)	Immunofluorescent Staining	Santa Cruz Biotech	53466
Rabbit Anti-N-Cadherin	Immunofluorescent Staining	Abcam	18203
Anti-Alpha Actinin	Immunofluorescent Staining	Sigma	A7811
Anti-Connexin 43 / GJA1 antibody - Intercellular Junction Marker	Immunofluorescent Staining	Abcam	11370
Mouse Anti-Ryanodine Receptor antibody [C3-33]	Immunofluorescent Staining	Abcam	2827
JPH2 Polyclonal Antibody	Immunofluorescent Staining	Thermo Fisher	40-5300

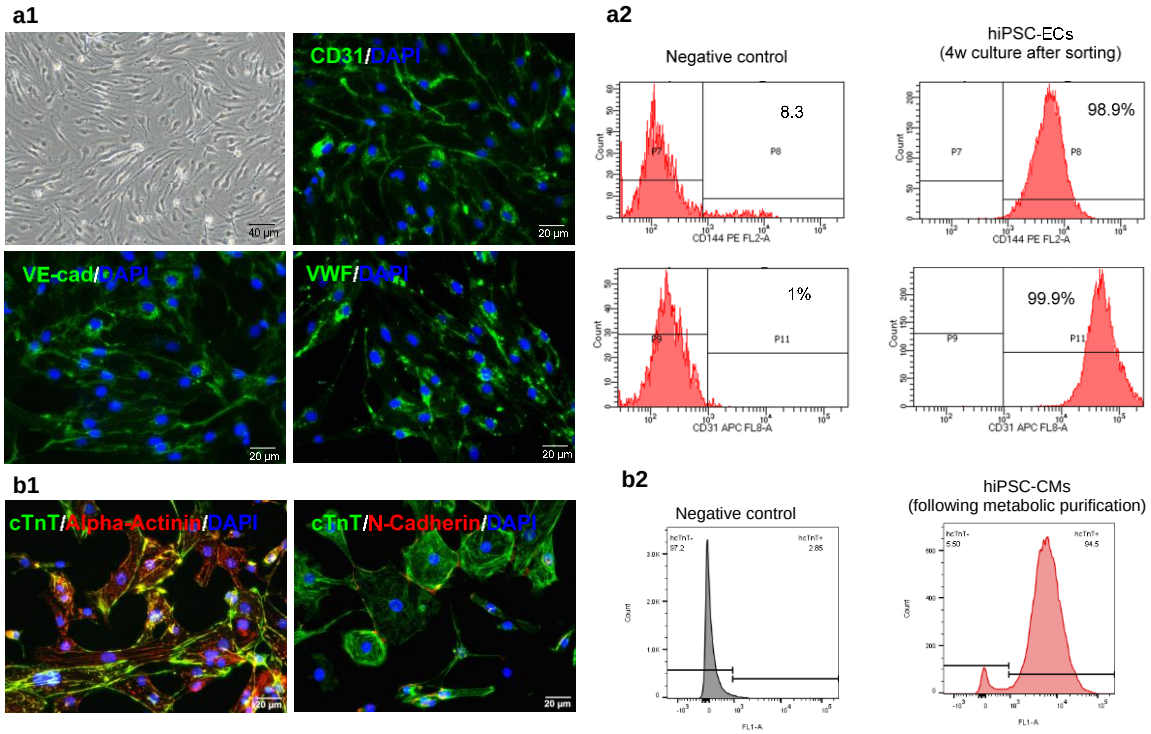

Figure S1: **Characterization of hiPSC-derived cells.** Characterization data confirming differentiation and purification for iECs (a) and iCMs (b) using immunofluorescent staining (1) and flow cytometry (2) analysis.

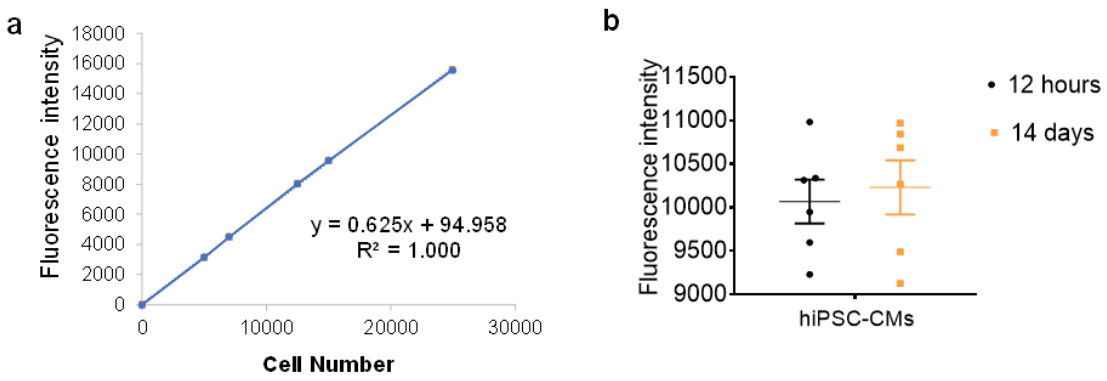

Figure S2: **Fluorescence-based cell proliferation assay**. (a) Standard curve and (b) the resulting measurements at Day 28 (12 hours) of hiPSC-CMs culture in 96-well plate (15,000 cells/well) as well as measurements at Day 42 (14 days). p = 0.6565 (n = 6)

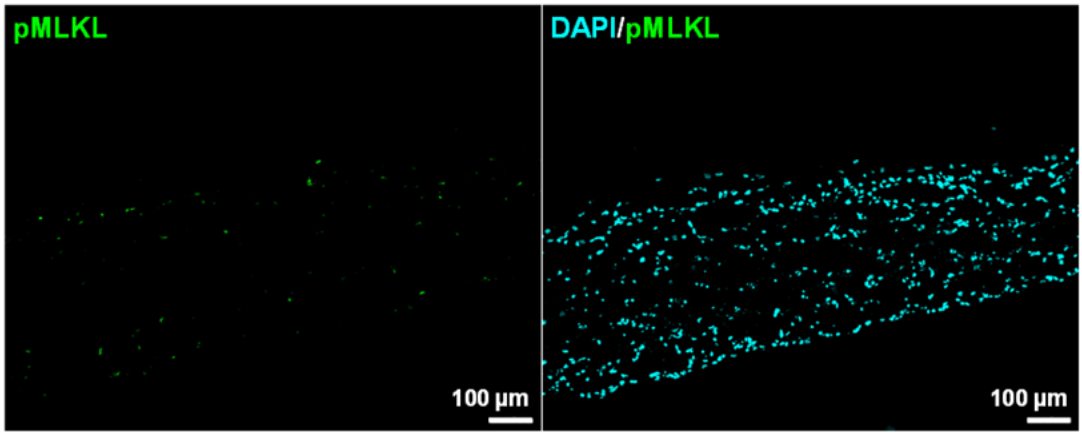

Figure S3: **Cardiac surrogate viability**. Immunofluorescent staining showing presence of DAPI and phosphorylated MLKL (Ser358, pMLKL) after 4 weeks in culture.

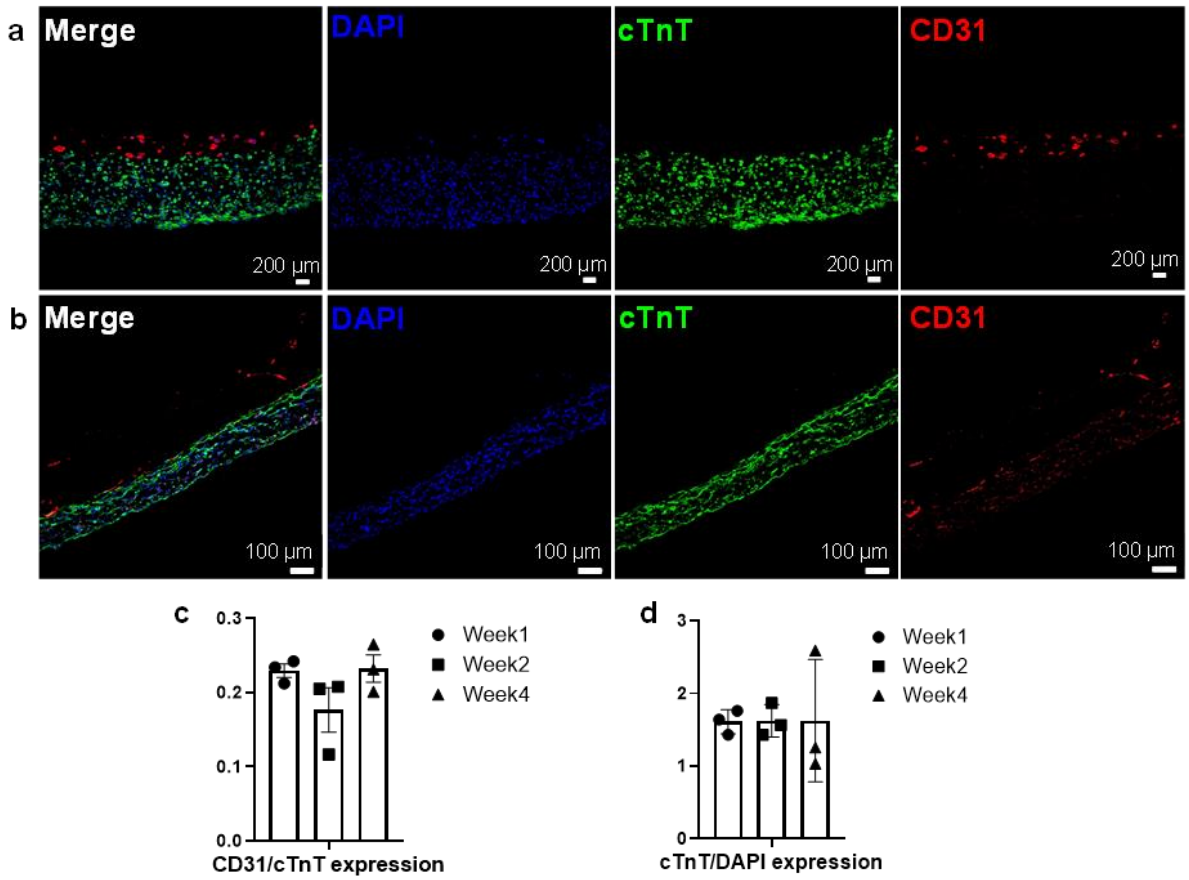

Figure S4: **Cell fate during culture process**. Immunofluorescent staining showing presence of DAPI, cTnT and CD31 after (a) 1 week in culture and (b) 4 weeks in culture. Quantification of expression intensity and subsequent expression ratios for all 4 weeks for (c) CD31/cTnT expression as well as (d) cTnT/DAPI. No statistically significant difference noted between groups for (c) or for (d), n = 3.

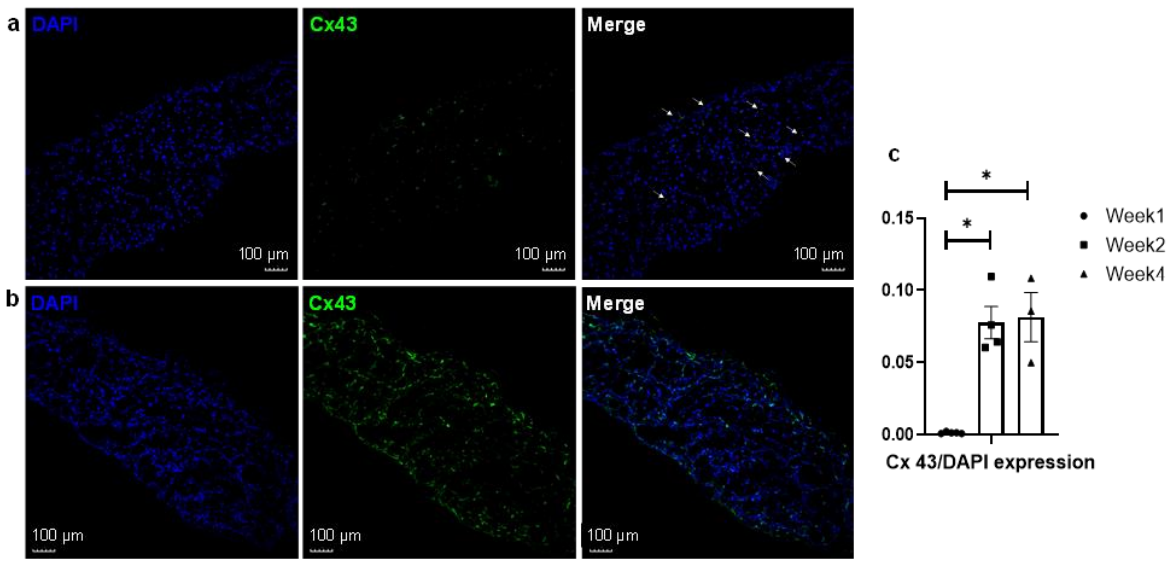

Figure S5: **Gap junction development**. Immunofluorescent staining showing connexin 43 (Cx43) gap junction presence after (a) 1 week in culture and (b) 2 weeks in culture, along with the (c) quantification of the ratio of Cx43/DAPI fluorescence expression. *$p < 0.05$, with $n = 4$

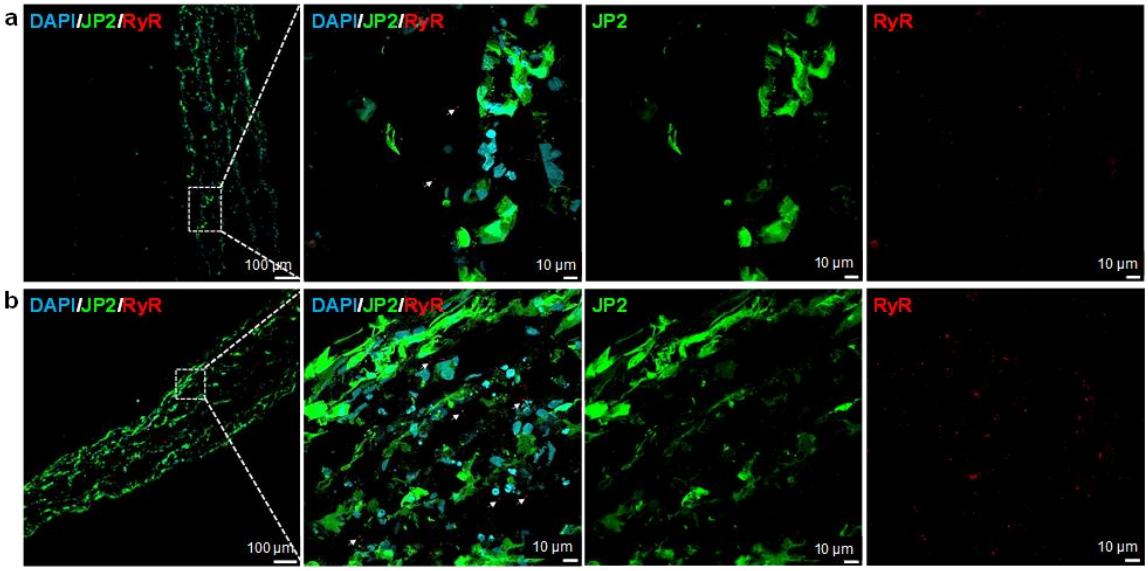

Figure S6: **T-tubule network development**. Confocal micrograph of junctophilin (JP2) and ryanodine receptor (RyR) expression levels in cardiac tissue surrogates after (a) 7 days, and (b) 28 days in culture, respectively.

All videos associated with this work, clips 1-5, are available online at: https://iop-science.iop.org/article/10.1088/1748-605X/abc107

Supplemental Matlab code: Generalized Maxwell model of order four

```
%% Load datasets
% Raw data sheets used in this file/program should only consist of numbers
% Delete the graphs and the titles in all the columns or MatLab won't
% recognize the file
% convert the Excel file to a .csv if necessary
% Ensure that all the files are in the same folder
% Ensure the directory is set (left click the tab at the top to
% set directory)
%%

load('PDMS6edit.csv') % loads the Raw data file generated with Low Force Testbench into MatLab
Do = 2.830*10^-3;          % Sample thickness - sample-dependent (meters)
PlotOn = 1; % 1 = plot, 0 = don't plot
%FileName = 'DataSet02';     % creates a new destination to store results

%%
%   Section converts the load obtained from instrument to Stress measurements,
%   and identifies point were sample strain was introduced

Force = PDMS6edit(:,7); % Load value in gram-force

Force = Force/101.971621;   %Gram-force to Newton

Area = 4.165*10^-5; % Area of sample (in m2)

Stress = Force / Area; % Y-Values in Graph (Stress)

Time = PDMS6edit(:,2); % Elapsed Time (s) (temporarily uses entire Time column before selecting for the
desired range)

%plot (Time, Stress)

Ep = 0.1;    % 10 percent sample strain

[StressVal, StressPos] = max(Stress(:));   %find max Y-value

%%
%create new matrix - only consider data points relevant to 10 percent
%strain

NewMat = [Time, Stress];    %assign Time to column1 and Stress to column2 of NewMatrix
k = 1;

for i = StressPos:size(NewMat, 1)
    maxT(k) = Time(i) - Time(StressPos);
    maxS(k) = Stress(i);

    k = k+1;
end

max_mat = [maxT', maxS'];    %this is the new matrix containing only the experimental data relevant to the
strain experiment

%plot (maxT, maxS)

%%
opts = fitoptions( 'Method', 'NonlinearLeastSquares' );
ft = fittype( 'a + b0*exp(-c0*x) + b1*exp(-c1*x) + b2*exp(-c2*x) + b3*exp(-c3*x)', 'independent', 'x', 'dependent',
'y');         %model fitting
```

```
opts.DiffMaxChange = 100000;      %how much the coefficients of each a, b0, c0 etc. changes with ongoing
iterations
opts.DiffMinChange = 1e-10;
opts.Display = 'Off';
opts.Lower = [0 0 0 0 0 0 0 0 0];  %lower limits of exponents should be zero at minimum
opts.MaxFunEvals = 10000;
opts.MaxIter = 100000;        %number of iterations
opts.Robust = 'LAR';        %LAR refers to least absolute residuals - ensures more robust fit of model
opts.StartPoint = [36000 3500 4500 4500 1800 0.002 1e-04 1e-05 1e-06];
opts.Upper = [100000 10000 10000 10000 10000 10000 10000 10000 10000];     %ceiling of a, b0, c0 etc

[fitresult, gof] = fit(maxT', maxS', ft, opts);

% Plot fit with data.
Name = 'Result %d';

%figure( 'Name', sprintf(Name));
h = plot( fitresult,  maxT', maxS' );

set(h,'LineWidth',2)

legend( h, 'Data', 'Fit', 'Location', 'NorthEast' );
% Label axes
xlabel Time
ylabel Stress
grid on

%% This is using the fit parameters
for i = 1 : 4
        a(i) = fitresult.a;
        b0(i) = fitresult.b0;
        c0(i) = fitresult.c0;

        b1(i) = fitresult.b1;
        c1(i) = fitresult.c1;
        b2(i) = fitresult.b2;
        c2(i) = fitresult.c2;
        b3(i) = fitresult.b3;
        c3(i) = fitresult.c3;

        R2_Value(i) = gof.rsquare;     %gof -goodness of fit
end

for i = 1:4
    E0(i) = a(i)/Ep;
    E1(i) = b0(i)/Ep;
    n1(i) = E1(i)/c0(i);

    E2(i) = b1(i)/Ep;
    n2(i) = E2(i)/c1(i);

    E3(i) = b2(i)/Ep;
    n3(i) = E3(i)/c2(i);

    E4(i) = b3(i)/Ep;
    n4(i) = E4(i)/c3(i);

end

%%
```

LAYER-BY-LAYER FABRICATION OF LARGE AND THICK HUMAN CARDIAC MUSCLE PATCH CONSTRUCTS WITH SUPERIOR ELECTROPHYSIOLOGICAL PROPERTIES

by

DANIELLE PRETORIUS, ASHER M. KAHN-KRELL, XI LOU, VLADIMIR G. FAST, JOEL L. BERRY, TIMOTHY J. KAMP, JIANYI ZHANG

Frontiers in Cell and Developmental Biology

Danielle Pretorius, Asher Kahn-Krell, Xi Lou, Vladimir Fast, Joel Berry, Timothy Kamp, Jianyi Zhang, (2021), doi: 10.3389/fcell.2021.670504

ABSTRACT

Engineered cardiac tissues fabricated from human induced pluripotent stem cells (hiPSCs) show promise for ameliorating damage from myocardial infarction, while also restoring function to the damaged left ventricular (LV) myocardium. For these constructs to reach their clinical potential, they need to be of a clinically relevant volume and thickness, and capable of generating synchronous and forceful contraction to assist the pumping action of the recipient heart. Design prerequisites include a structure thickness sufficient to produce a beneficial contractile force, prevascularization to overcome diffusion limitations and sufficient structural development to allow for maximal cell communication. Previous attempts to meet these prerequisites have been hindered by lack of oxygen and nutrient transport due to diffusion limits (100-200 μm) resulting in necrosis. This study employs a layer-by-layer (LbL) fabrication method to produce cardiac tissue constructs that meet these design prerequisites and mimic normal myocardium in form and function. Thick (> 2 mm) cardiac tissues created from hiPSC-derived cardiomyocytes, -endothelial cells and -fibroblasts were assessed, in vitro, over a 4-week period for viability (< 6 % necrotic cells), cell morphology and functionality. Functional performance assessment showed enhanced t-tubule network development, gap junction communication as well as previously unseen, physiologically relevant conduction velocities (> 30 cm/s). These results demonstrate that LbL fabrication can be utilized successfully to create prevascularized, functional cardiac tissue constructs from hiPSCs for potential therapeutic applications.

Keywords: hearts, tissue engineering, layer-by-layer fabrication, stem cell, electrophysiology

INTRODUCTION

The use of engineered cardiac muscle patch constructs focusing on repair and functional restoration following an acute myocardial infarction (AMI), have shown promise in improving clinical outcomes for patients [1-3]. Clinically, AMI is associated with postinfarction LV remodeling and heart failure [4, 5]. Cell therapy approaches utilizing products associated with human induced pluripotent stem cells (hiPSCs) have been examined pre-clinically as a viable therapeutic option [6-8]. Despite these promising results, the search continues for an effective method of restoring both mechanical and electrical function to the AMI damaged region of the heart, which is necessary for a successful therapeutic application. Furthermore, electrical function is largely dependent upon the electrical excitability of the cells and subsequently the engineered tissue. Unfortunately, due to their immature phenotype, hiPSC-derived cardiomyocytes (iCMs) tend to have reduced electrical excitability compared to mature, adult CMs found in the native myocardium [9, 10].

One of the key indicators for CM functional maturity at the tissue level is the capacity to support fast action potential (AP) conduction. In cardiac tissue, AP represents the time-dependent changes in the transmembrane electrical potential in CMs, which occur during each heartbeat, and are functions of highly coordinated, time- and voltage-dependent changes in activity of various ion channels and transporters [11]. Conduction velocities (CVs) of genetically purified iCMs in monolayer format have been reported as high

as ~21 cm/s [12], with more complex 3D systems still lagging behind at reported CVs around 14 to 17 cm/s [13, 14] with the potential of reaching up to 25 cm/s when highly organized [15]. However promising, the CVs reported for hiPSC-derived tissue still fall short of those observed in native adult LV tissue (~30 – 100 cm/s [16, 17]). Some of the highest CVs reported for engineered cardiac tissue have been obtained with neonatal rat CMs, and was recorded at 32.3 ± 1.8 cm/s, yet at their thickest, these structures were recorded to only be 100 μm [18].

Utilization of promising fabrication strategies which yield highly organized structures, such as the layer-by-layer (LbL) approach, allow for superior control over a range of physicochemical properties. In a previous study, we demonstrated that our LbL fabrication method yields thick, vascularized engineered cardiac tissue, with CVs ranging between 17 – 19 cm/s, as well as viscoelastic properties that were similar to native murine myocardial tissue [14], yet this study only utilized CMs and endothelial cells (ECs). It is known, however, that fibroblasts (FBs) play key roles in the healthy native adult mammalian heart. FBs contribute to general heart function, homeostasis, and structure, most notably during the production and remodeling of extracellular matrix (ECM). Culturing CMs in the presence of FBs has also been shown to affect the electrophysiological properties of the CMs [19].

In the present study, we aimed at developing a LbL approach to engineer large and thick tri-lineage (CM, EC and FB) cardiac tissue constructs. The engineered cardiac tissue was characterized at various time points, over a 4 week period, in order to qualify and quantify the changes that occur in the structures in vitro, which ultimately lead to a better potential understanding of the remodeling that these structures undergo in vivo. We

hypothesized that by mimicking the cellular composition of the native myocardium, i.e. utilizing CMs, ECs and FBs, with a LbL fabrication process would not only allow for the production of thicker tissues but also increase their ability to mimic the native myocardium more closely in terms of form and function. Characterization included 1) histology and immunostaining to analyze the cellular and structural morphology, 2) immunostaining to quantify viability, 3) immunostaining of 2D cryosections and 3D structures to analyze cell migration, potential vascularization and final cellular fate, 4) immunostaining and quantification of ECM remodeling, 5) RNA analysis to quantify and corroborate the results obtained from immunostaining and 6) optical mapping to determine the action potential and conduction velocity to assess functionality.

Materials and Methods

Cell culture and characterization

Human cardiac fibroblast induced pluripotent stem cells (hiPSCs) were reprogrammed from human cardiac fibroblasts, and subsequently differentiated into hiPSC-cardiomyocytes (iCMs), as previously reported [8, 20, 21]. Generally, spontaneous iCM contractions were observed between days 7 and 10 after commencement of the differentiation protocol, with beating numbers increasing up to day 12. Metabolic purification of iCMs was achieved via glucose deprivation (RPMI 1640 without glucose, supplemented with sodium DL-lactate and B27^{+}, Gibco) for 3-6 days, initiated at day 9, allowed for a population of iCMs that yielded a minimum of 95% cTnT positive. hiPSCs were maintained at optimal conditions, as previously described [22], on 6-well plates coated with Matrigel (Corning), using mTeSR 1 maintenance media (STEMCell Technologies, Canada).

hiPSC-endothelial cells (iECs) were differentiated as described previously [13, 23, 24]. Briefly, undifferentiated hiPSCs were seeded into 0.5 mL fibrin scaffolds and treated with CHIR99021 and U46619 in EBM2 medium (Lonza, USA) supplemented with $B27^-$ for 24 hrs. The medium was then replaced with EBM2 which was supplemented with $B27^-$, vascular endothelial growth factor (VEGF), erythropoietin (EPO), and transforming growth factor β1 (TGFβ1), and then cultured for an additional 96 hours with a media change midway through. Finally, the scaffolds were released and cultured in EGM2-MV medium (Lonza, USA) supplemented with $B27^+$, VEGF, SB-431542, with media changes every two days. hiPSC-ECs were purified and enriched via collection of cells positive for CD31 using fluorescence-activated cell sorting (FACSAria II). Antibodies used for selection and cell characterization are listed Supplementary Table S1. See Supplementary Figure S1 for cell characterization and Supplementary Figure S2 for the proliferation assay showing the lack of tumorigenic properties of the iCMs utilized in this study.

hiPSC-FB (cFB) differentiation commenced using hiPSC-line DF19-9-11T with cells at 100% confluence (day 0) [19]. The hiPSC culture medium was changed to RPMI/$B27^-$ and supplemented with 12 μM CHIR99021, with cells treated in this medium for 24 hrs (day 1). Medium was changed once again to RPMI/$B27^-$ for another 24 hrs (day 2). Within 24 hrs (before day 3), the medium was changed to cardiac fibroblast differentiation basal medium (CFBM, see Supplementary Table S2) supplemented with 75 ng/ml bFGF (WiCell Research Institute). Cells were then cultured with CFBM + 75 ng/ml bFGF every other day up to day 20 when they were utilized for flow cytometry analysis and passaged for subsequent use in tissue fabrication.

Fibrin matrix composition

The fibrin matrix used (per milliliter) used for the differentiation of the iECs as well as for the construction of each alternating layer of the cardiac tissue during the modular fabrication process consisted of the following components as was defined previously [13]: 0.12 mL fibrinogen (25 mg/mL, Sigma-Aldrich, CAS# 9001-32-5), 0.02 mL Matrigel (Corning, # 356235), 0.56 mL of HEPES (20 mM, pH 7.4, Corning), 0.001 mL $CaCl_2$ (2 M), 0.3 mL DMEM (Gibco, High glucose, #11965-118), 0.006 mL thrombin (80 U/mL, MP Biomedicals).

Polydimethylsiloxane (PDMS) platforms

PDMS platforms were fabricated by mixing PDMS (Dow Corning Sylgard 184 Silicone, Product # 2065622) in a 10:1 elastomer:curing agent ratio and poured into a 100 mm diameter Pyrex Petri dish (Corning, # 3160102). These were cured at 75 °C for 2 hours in an oven, after which custom platforms of 10 mm x 5 mm (2.5 mm thick) were cut. Prior to their use in the tissue fabrication and culture process, all PDMS structures were autoclaved.

Optimized LbL engineered tissue fabrication

Following cell differentiation, cardiac tissue fabrication commenced (**Figure 1**). Petri dishes (BioLite Cell Culture Treated Dishes, Thermo Scientific) were coated with a 5 % pluronic F-68 solution (Gibco, # 24040032) and incubated at 4 °C overnight. The pluronic solution was removed, and a sterile polycarbonate frame (internal area: 1 x 2 cm^2) was attached with a 2 % agarose solution. Note that the frames were modified with channels to allow for maximal media contact following tissue fabrication. iCMs were dissociated (STEMdiff Cardiomyocyte Dissociation Medium, STEMCell) and mixed with the

fibrin matrix at a concentration of $10x10^6$ cells/mL. Note that the deposition of the iCM layer denotes "D0" for the remainder of the fabrication process. 400 µL of this solution was quickly deposited into each mold to produce the first layer. Following complete polymerization, the culture medium was added (STEMdiff Cardiomyocyte Support Medium, 2 mg/mL Ɛ-aminocaproic acid) and incubated at 37 °C (5 % CO_2) for 2 days. The next layer, comprised of iECs, was made in a similar fashion, with the following exceptions: iECs were dissociated using trypsin (0.25 % trypsin, 0.1 % EDTA, Corning, # 25053CI) and then mixed with the fibrin matrix at a concentration of $10x10^6$ cells/mL. 200 µL of this solution was quickly deposited into each mold, yielding a 2:1 ratio of iCMs:iECs [13]. Fresh culture medium (10 % fetal bovine serum, 2 % $B27^+$, and 2 mg/mL Ɛ-aminocaproic acid, 10 µM ROCK inhibitor in DMEM) was added, following layer polymerization. After 24 hours, the frame containing the engineered cardiac tissue was lifted off of the dish surface and placed on top of custom-cut PDMS stilts, allowing for the tissue to be fully suspended in fresh culture media (2 % fetal bovine serum, 2 % $B27^+$, and 2 mg/mL Ɛ-aminocaproic acid in DMEM). After a further 48 hours, the next layer, comprised of cFBs, was made in a similar fashion, with the following exceptions: cFBs were dissociated using TrypLE (Gibco, # 12604013) and then mixed with the fibrin matrix at a concentration of $10x10^6$ cells/mL. 100 µL of this solution was quickly deposited into each mold, yielding a 2:1:0.5 ratio of iCMs:iECs:cFBs [13, 25]. Incubation continued for the desired period of time (1-4 weeks in total), with media replacement once per week.

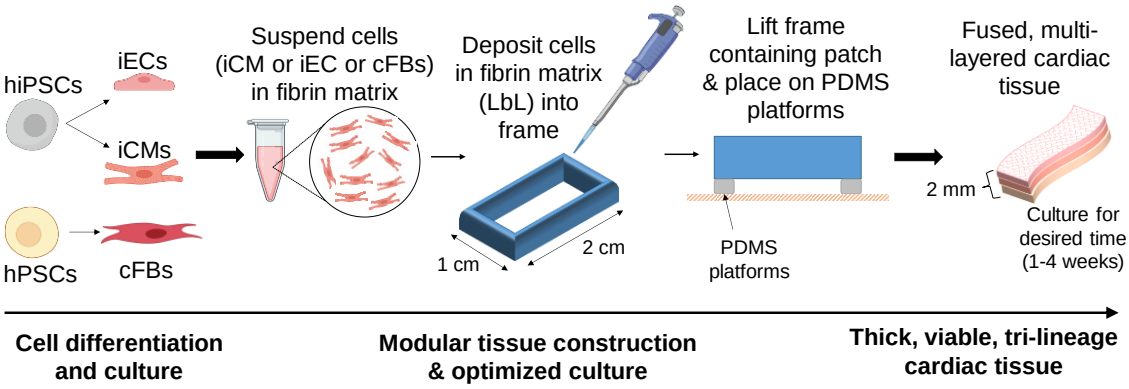

Figure 1: Basic description of optimized cardiac tissue surrogate fabrication process, allowing for extended culturing of thick tissue structures. The first layer of cells is deposited and cultured for 48 hours, after which the second layer is deposited using LbL approach. The second layer of cells is deposited, allowed to polymerize, and the entire structure contained in its frame is then lifted off of the dish surface and placed ontop of PDMS platforms. The third layer of cells is deposited in a similar fashion. Thick, viable, multi-layered tissue can be cultured for the desired amount of time (1-4 weeks)

Tissue preservation

Fabricated tissue samples were fixed in 4 % formaldehyde (Pierce, Thermo Scientific, # 28906) for 1 hour prior to embedding in either optimal cutting temperature compound (OCT compound, Fisher Health Care, USA) or paraffin for histological analysis. Histological analyses were performed on 10 µm sections. Whole-mount samples were stored in PBS until staining.

Histochemistry

Deparaffinized and rehydrated sections were stained with hematoxylin solution (Mayer's, Merck, 3 min) followed by working eosin Y solution (2 min). Following subsequent dehydration, all samples were mounted with Permount and imaged using a bright field microscope (Olympus IX83 epifluorescent microscope).

Immunohistochemistry

Fixed OCT embedded sections were blocked and permeabilized for 30 min in 10 % donkey serum, 3 % BSA, and 0.05 % Triton-X. Following addition of primary antibodies, samples were incubated for 1 h at room temperature (Supplementary Table S1). Samples were washed in PBS (3 x 5 min), and subsequently labeled with secondary antibodies with fluorescent tags and 4′, 6-diamidino-2-phenylindole (DAPI, 100 ng/ml) and incubated for at room temperature for 1 h (Supplementary Table S1). Sections were mounted with VECTASHIELD Antifade Mounting Medium and visualized by confocal laser scanning (Olympus FV3000 confocal microscope).

Whole-mount staining

Fixed whole-mount samples were blocked and permeabilized in 10 % donkey serum, 10 % Tween-20, 3 % BSA, 0.05 % Triton-X, and 0.02 % sodium azide in PBS overnight at 4 °C. Then, primary antibodies were added and samples were incubated overnight at 4 °C (Supplementary Table S1). Samples were washed in PBST (3 x 10 min) and fluorescently labeled secondary antibodies along with DAPI were added followed by another overnight incubation at 4 °C. Following washing, tissue was cleared according to the previously described protocol [26] with 3 hr incubation in Ce3D clearing agent. Whole-mount constructs were transferred to an Ibidi µ-Slide (# 80286), covered with VECTASHIELD Antifade Mounting Medium, and visualized via confocal laser scanning (Olympus FV3000 confocal microscope).

RNA isolation and analyses

Samples for RNA analysis were suspended in TRIZOL (Invitrogen) and homogenized. RNA extraction was completed using Direct-zolRNA MiniPrep Plus (Zymo Research Corporation) according to the manufacturer's protocol. Following concentration measurement on the Nanodrop device, 1 μg of RNA was converted into complementary DNA (cDNA) through the reverse transcription reaction using the SuperScript IV VILO Master Mix (Thermo Fisher Scientific) then diluted to a final concentration of 5 ng/μL. qPCR analysis of each sample was performed on a QuantStudio 3 real-time PCR system using PowerUp SYBR Green Master Mix (Thermo Fisher Scientific). Quantification of relative expression was done by normalizing to sample GAPDH expression. Primers used for RT-qPCR analysis are included in Supplementary Table S3.

Optical mapping

To assess action potential duration (APD), conduction velocity (CV), and minimum pacing cycle length, engineered LbL tissue samples were stained with a voltage-sensitive dye RH-237 (2.5 μM) for 10 minutes and transferred to a perfusion chamber mounted on an inverted microscope. Control samples consisted of iCM:iEC bilayered tissue, while test samples consisted of iCM:iEC:cFBs. Samples were constantly perfused with Hank's balanced salt solution (HBSS) at approximately 37 ˚C. Pacing/stimulation of all samples was done with a bipolar electrode consisting of a glass pipette filled with HBSS and a silver wire coiled around its tip. A micromanipulator was used to position the electrode tip at the sample's edge. Rectangular stimulation pulses, with a duration of 2 ms and current strength 1.5-times the excitation threshold were used. Fluorescence was

excited with a 200-W Hg/Xe arc lamp and recorded with a 16×16 photodiode array (Hamamatsu) at a spatial resolution of 110 μm per diode as previously described [27]. Excitation light was filtered at 532–587 nm, and emitted fluorescent light was filtered at > 650 nm. The perfusion solution was supplemented with 5 μM of blebbistatin to eliminate potential motion artifacts caused by the samples' spontaneous contractions. Isochronal maps of the activation spread were constructed from activation times measured at 50% of the maximum action potential amplitude. Conduction velocity was calculated at each recording site from local activation times and averaged across the whole mapping area. Action potential duration was measured at 50% and 80% of signal recovery (APD_{50}) and (APD_{80}), respectively.

Statistical analyses

All results are reported as mean ± standard error (mean ± SEM). Significant differences between two mean values were determined via the Student's Two-Tailed t-Test; and ANOVA or repeated ANOVA with the Tukey post hoc test were used for multiple (more than 2 groups) comparisons or repeated measurements. p-values of less than 0.05 were considered statistically significant. These analyses were performed utilizing GraphPad Prism8 data analysis software package.

Results

LbL fabrication produces thick, synchronously beating, fused engineered cardiac tissue

Engineered cardiac tissue produced with the optimized method described in **Figure 1** yielded structures of 2.12 ± 0.083 mm and 1.38 ± 0.019 mm in thickness after one week and four weeks in culture, respectively (**Figure 2** a, n = 4). The statistically significant ($p < 0.005$) reduction in tissue thickness between week 1 and week 4 are most likely

due to compaction caused by the contractile forces exerted by both the iCMs as well as the cFBs. Following the deposition of the iCMs, synchronization of the iCM layer in all samples was noted after 48 hours (on Day 2). The resulting beating-rate (per min) of each engineered tissue was determined (**Figure 2** b), yielding a rate of 109 ± 11.5 beats/min (bpm). Following the iEC layer addition on Day 3 and an additional two days of culture (Day 5), the beating-rate on the fifth day of culture, prior to cFB deposition had decreased significantly, to 47 ± 2.0 bpm. Following the deposition of the cFBs, and an additional 24 hours of culture (Day 6), the beating-rate of the tissues was noted at 51 ± 3.9 bpm. After 4 weeks in culture, the beating-rate of the constructs were noted at 55 ± 1.8 bpm.

Modification to the ECM composition between weeks one and four were observed via H&E staining (**Figure** 2 c-d). Histology shows increases in structural ECM components such as collagen (increased intensity as well as the distribution of eosinophilic staining, **Figure 2** c-d). As sample time in culture increased, compaction of the structures the degree of compaction increased (**Figure 2** d), and structures, although initially somewhat disorganized (**Figure 2** c), began resembling *in vivo* muscle. The alterations in the ECM composition, specifically those associated with collagen deposition were attributed to both the culture of iCMs as well as the addition of cFBs, based on the strong eosinophilic staining noted in both the bottom as well as the top layers of the structure at week 4 (**Figure 2** d). Fusion and coupling of the structure layers was confirmed by not only the synchronous macroscopic beating of the engineered tissue (**Figure 2** b) but also via H&E staining. Another observation made via H&E was that of cell migration over the culture period. As with a previous study by this group [14], it was noted that iECs

initiated migration and re-arrangement out of their originally deposited layer into the resident iCM layer within less than 48 hours post-deposition, as is clear from the somewhat acellular appearance of the middle layer of the engineered tissue (**Figure 2** c). The degree of cell migration and potential iEC re-arrangement was confirmed with cell-specific immunofluorescent markers (**Figure 4** a). It should be noted that structures visualized here via H&E staining appear thinner than those preserved in OCT or when measured with a caliper. This difference in overall tissue thickness is attributed to the multiple dehydration-related steps required during the H&E processing of the hydrogel structures leading to decreased preservation of the original architecture.

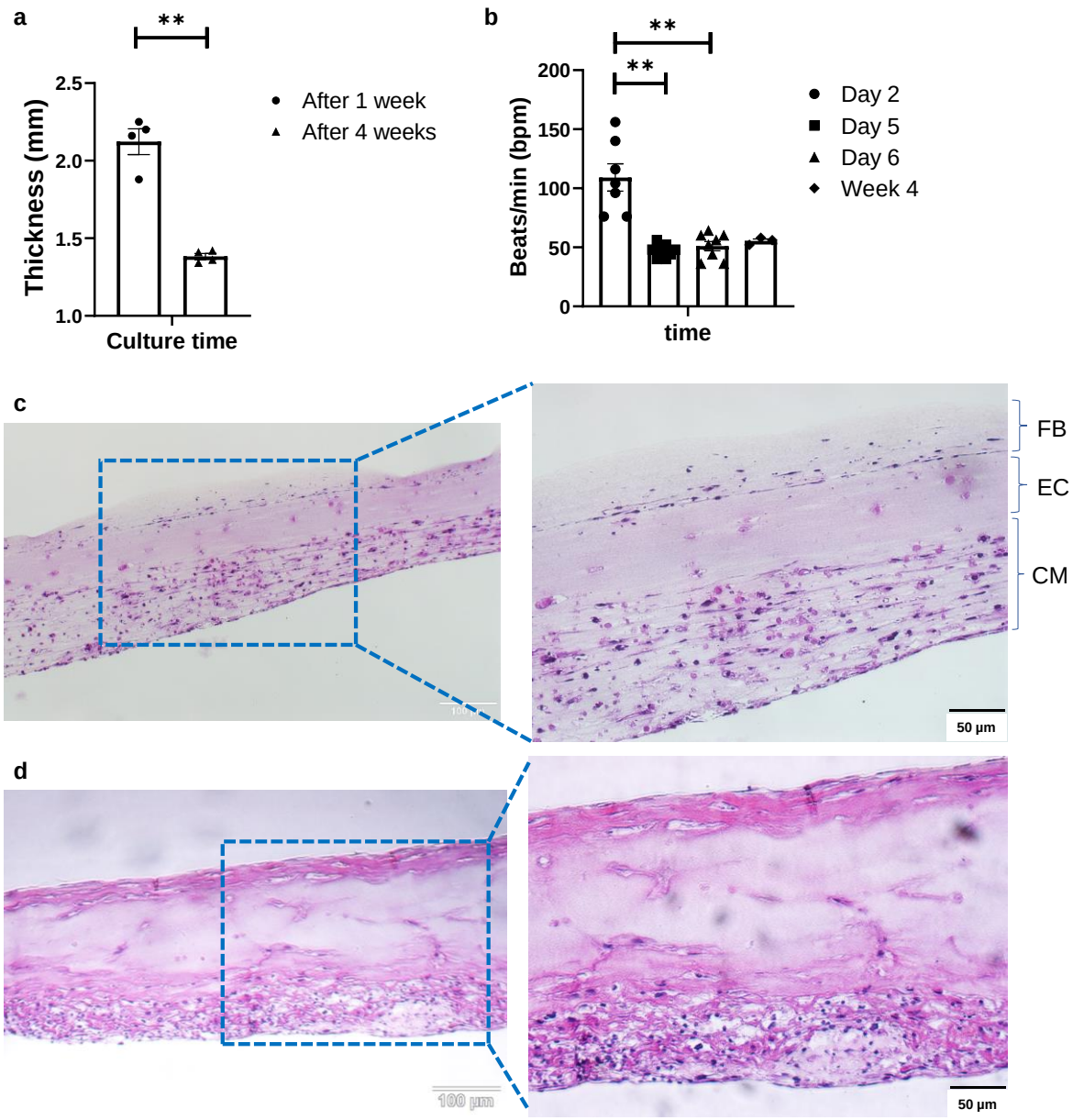

Figure 2: Macroscopic information describing tri-lineage engineered cardiac tissue. (a) Change in tissue thickness between week1 and week4, measured with a caliper (Mitutoyo 500-196-30, Digimatic, n = 4, **p < 0.005). (b) LbL engineered tissue beat-rate over the first 6 days of culture (n = 8) as well as week 4 (n = 3), **p < 0.005. H&E staining of LbL engineered tissue at (c) Day7, and (d) Day28 of culturing

LbL fabrication results in engineered tissue with limited necrosis markers

Tissue viability was determined via pMLKL staining (**Figure 3**), which specifically stains for cell necroptosis [28] and is associated with inflammatory markers [29]. The pMLKL-positive cells were quantified as a percentage (%) of the total number of cells present (i.e., normalized to the DAPI staining, n = 4 with a minimum of 5 images taken per sample). The initial degree of necrosis noted in the engineered tissues was very low, and quantified at 1.17 ± 0.06 %. After an additional week of *in vitro* culture, the degree of necrosis increased to 1.96 ± 0.19 %, while the degree of necrosis after four weeks in culture was observed to be 5.73 ± 0.95 %. Even though the percentage of pMLKL positive cells increased significantly from week 1 to week 2 and week 4, respectively, it still compared well with previously published data from our group, showing 5.6 ± 1.4 % after four weeks in culture of engineered structures that were initially ~1.73 mm thick at week 1 [14].

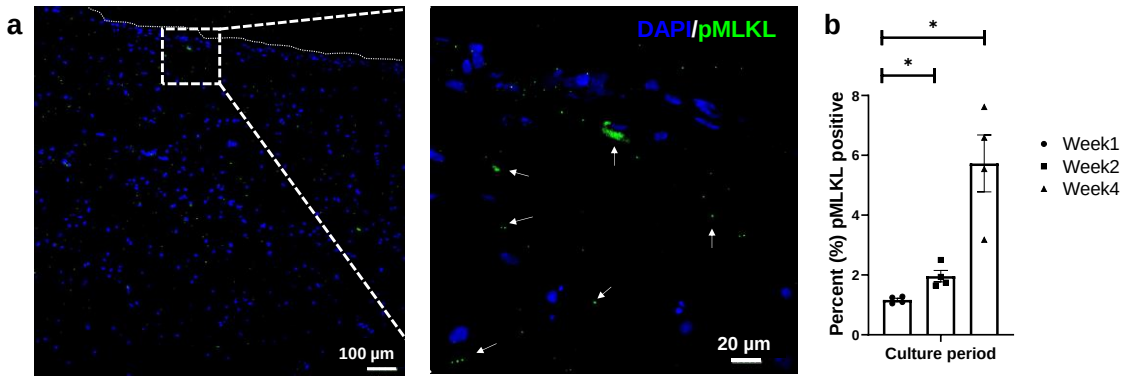

Figure 3: Tri-lineage structure viability. Confocal micrograph of LbL tissue surrogates displaying necrotic cells identified by the necrosis marker phosphorylated MLKL (Ser358, pMLKL) at (a) week 1 of culture, with (b) the percentage of necrotic cells in LbL engineered cardiac tissue, (n = 4, *p < 0.05). Border indicated with short dashed line

Cellular migration and fate

Imaging of the fluorescently stained sections (**Figure 4** a, i) showed migration of the iECs as well as the cFBs towards their iCM counterparts within a number of days after these layers had been deposited. The migration process continued over the four weeks of culture, yet leaving no area of the engineered structure completely acellular (**Figure 4 a**, ii).

Expression levels of various cell markers were monitored over the culture period, i.e. cTnT for iCMs, CD31 for iECs as well as α-SMA (alpha smooth muscle actin), periostin, vimentin and FAP (fibroblast activation protein) for cFBs (**Figure 4** b). At each time point, at least 3 tissue samples were used to determine the respective expression levels. No statistically significant differences were noted in the expression levels of CD31, α-SMA, periostin, vimentin or FAP, suggesting that the expression levels of these factors were stable throughout the culturing period. The slight decrease noted in vimentin expression can potentially be attributed to senescence of the cFB line, which is known to occur in vitro after a specific number of cell divisions and/or passages [19]. The slight increases in factors such as periostin, rather, could potentially be suggestive of an environment that is conducive to cellular motility [30]. The only statistically significant difference was noted in the expression level of cTnT when comparing week 1 to week 4. This increase could more likely than not be attributed to the maturation of the iCMs in the engineered tissue, since iCMs are terminally differentiated cells and minimal proliferation is observed in these cell populations (see Supplementary Figure S2). To further investigate the potential maturation of the iCMs in the engineered tissues, the expression levels of

known maturation markers as well as chamber-specific markers were examined (**Figure 5**).

Developmental and hormonal factors control the expression of alpha- and beta-myosin heavy chain (MHC), two functionally distinct, species-dependent cardiac MHC isoforms [31, 32]. Not only have these isoforms been shown to be correlated with contractile capabilities, but alterations in expression levels are also age-, and species-dependent [33]. Switches in expression from one isoform to another have been highly referenced in literature in developing systems, with increases in β-MHC and more specifically β-MHC:αMHC, being a key indicator of CM maturation [16, 34-37]. During the culturing period, there was a statistically significant decrease in the expression levels of alpha-MHC (α-MHC), noted when comparing the expression levels of week 1 and week 2 as well as week 1 and week 4, respectively. Week 2 also saw an almost 3-fold increase ($p < 0.05$) in the expression level of beta-MHC (β-MHC) when compared to week 1. Analysis of this ratio showed an 8-fold increase from week 1 to week 2 ($p < 0.05$), and a 19-fold increase from week1 to week 4 ($p < 0.005$).

Expression levels for chamber-specific markers, i.e. atrial (MLC2a) and ventricular (MLC2v), were also compared [38]. Analysis showed no statistically significant differences in MLC2a or MLC2v between any of the time points. Interestingly enough, when comparing the expression levels of ventricular:atrial markers, i.e. MLC2v:MLC2a, a 2.7-fold increase ($p < 0.05$) was noted between week 1 and week 2, while a 3.3-fold increase ($p < 0.005$) was observed between week 1 and week 4. With MI affecting the LV more prominently, having cells with a more ventricular-like phenotype present in the engineered tissues is highly advantageous.

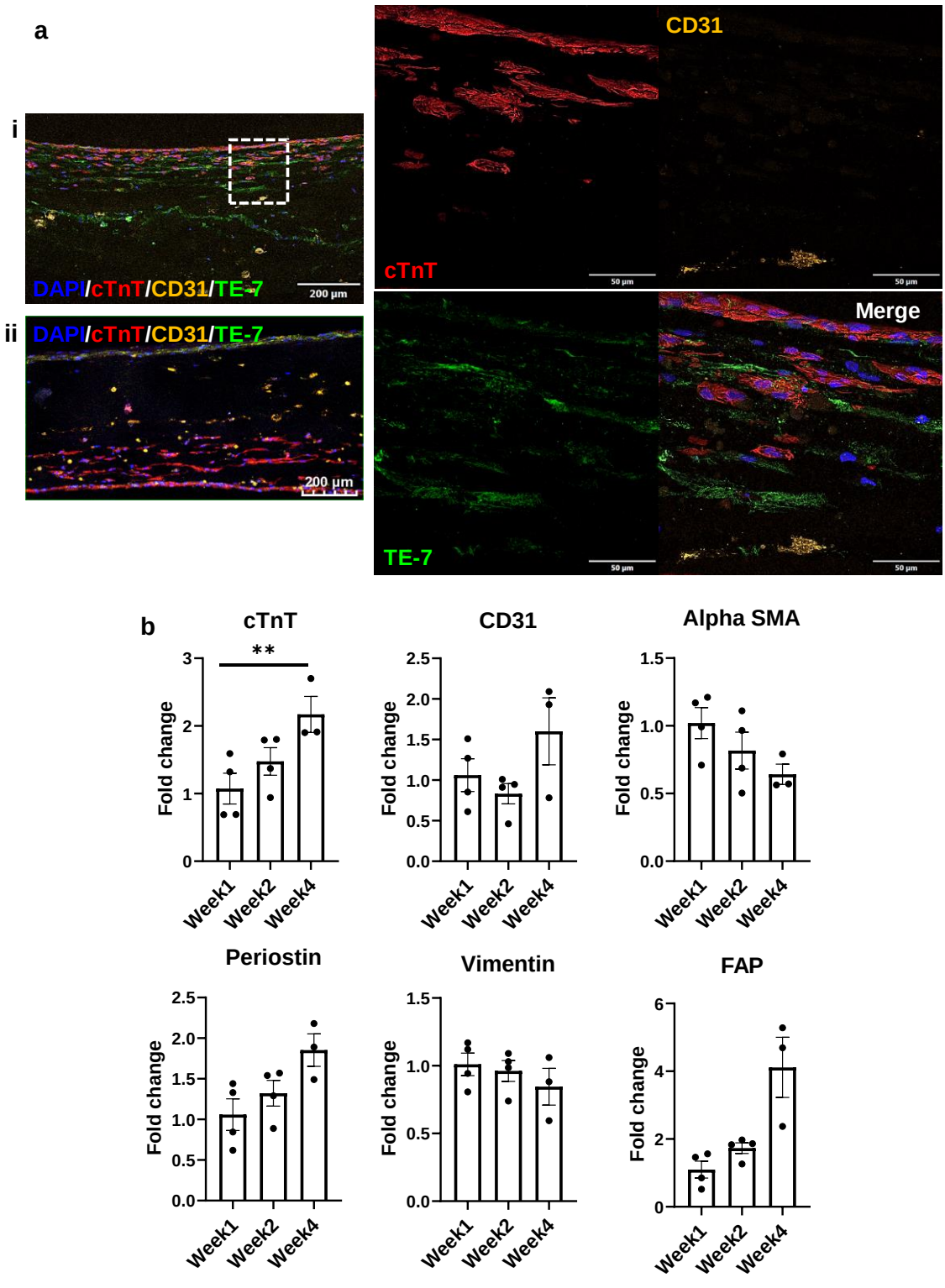

Figure 4: Cellular fate monitoring and quantification. (a) Fluorescent staining with cTnT, CD31 and TE-7 showing tri-lineage engineered tissue after (i) one and (ii) four weeks in culture, respectively, along with (b) expression levels of cell-specific markers at weeks one, two and four, respectively, (n = 4, *p < 0.05, **p < 0.005)

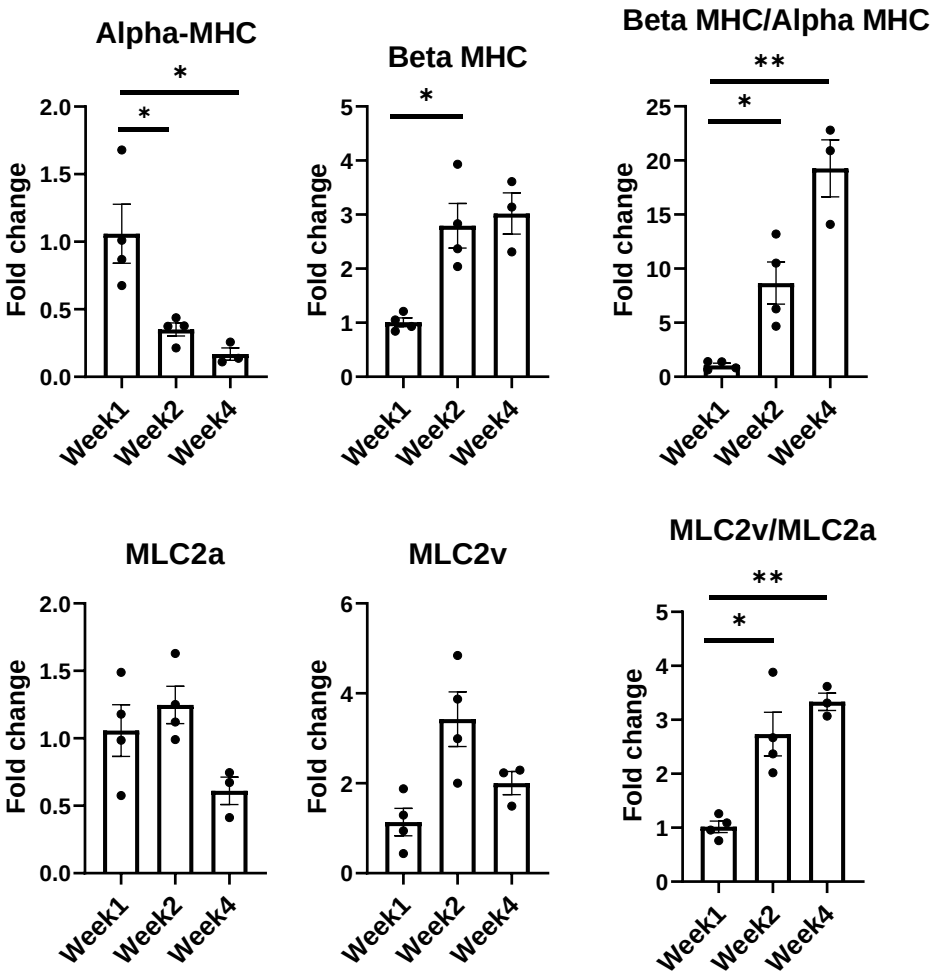

Figure 5: Expression levels of CM-specific maturation and phenotypic markers. Tissue samples taken at weeks one, two and four, respectively, (n = 4 for week1 and week2, n = 3 for week4, *p < 0.05, **p < 0.005).

Dynamic ECM evolution

Throughout the 4-week culturing period, the engineered cardiac tissue structure ECM underwent remodeling to various degrees. As demonstrated in a previous study, due to fibrinolysis, the majority of the fibrin matrix degrades within the first two weeks [14] (see Supplementary Figure S3). For this study, the degree to which the remodeling occurs, and how the addition of the cFBs affected potential matrix deposition compared to our previous study, was monitored and expression levels quantified via RNA analysis.

For this analysis, at least three tissue samples were used per time point. With knowledge obtained from prior studies regarding the ECM remodeling during the culturing of iCMs [14, 36, 37], samples were again analyzed for additional ECM components, including collagen 1 (Col1), collagen 3 (Col3), collagen 4 (Col4), laminin (Lam) and fibronectin (FN) (**Figure 6**). Samples were also analyzed for elastin due to the incorporation of iECs and cFBs as well as the potential for vessel formation [38, 39]. Quantification showed a nearly 5-fold increase in collagen 1 production from weeks 1 to 4. This trend compared well with our previous studies, where bi-layered structures consisting of only iCMs and iECs yielded a 3-fold increase in collagen 1 production [14]. It is known that cFBs are vital in synthesizing ECM proteins, including, but not limited to, fibrillar collagen types 1 and 3, basement membrane type 4 collagen, fibronectin, and laminin [40]. Interestingly enough, the increasing trends in collagen 1 production were also associated with the upregulation trends in periostin (**Figure 4** b), a known proponent of collagen fibrillogenesis and ECM remodeling [41, 42]. Similarly, there was an upregulation trend in the expression levels of FAP. Previous studies have shown that collagen induces FAP expression via binding of $\alpha 3\beta 1$ integrin [43].

Statistically significant increases were observed in the expression levels of collagen 3 when comparing week 1 to week 2 ($p < 0.005$) and week 1 to week 4 ($p < 0.05$), respectively. Expression of collagen 4 levels increased at both week 2 and week 4 compared to week1, though this increase was not statistically significant. An almost 10-fold increase in the expression level of fibronectin was noted when comparing week 1 to week 4. Statistically significant increases in the expression levels of laminin was noted between

week 1 and week 2 ($p < 0.05$). An almost 70-fold increase in the expression level of elastin was observed from week 1 to week 2, followed by a decrease at week 4. One potential cause of this sharp decrease in the elastin expression level could be linked to bFGF production by the iECs in the engineered constructs 47. Previous studies have shown that free bFGF decreases the expression levels of elastin at the transcriptional level in culture 48.Statistically significant increases were observed in the expression levels of collagen 3 when comparing week 1 to week 2 ($p < 0.005$) and week 1 to week 4 ($p < 0.05$), respectively. Expression of collagen 4 levels increased at both week 2 and week 4 compared to week1, though this increase was not statistically significant. An almost 10-fold increase in the expression level of fibronectin was noted when comparing week 1 to week 4. Statistically significant increases in the expression levels of laminin was noted between week 1 and week 2 ($p < 0.05$). An almost 70-fold increase in the expression level of elastin was observed from week 1 to week 2, followed by a decrease at week 4. One potential cause of this sharp decrease in the elastin expression level could be linked to bFGF production by the iECs in the engineered constructs [47]. Previous studies have shown that free bFGF decreases the expression levels of elastin at the transcriptional level in culture [48].

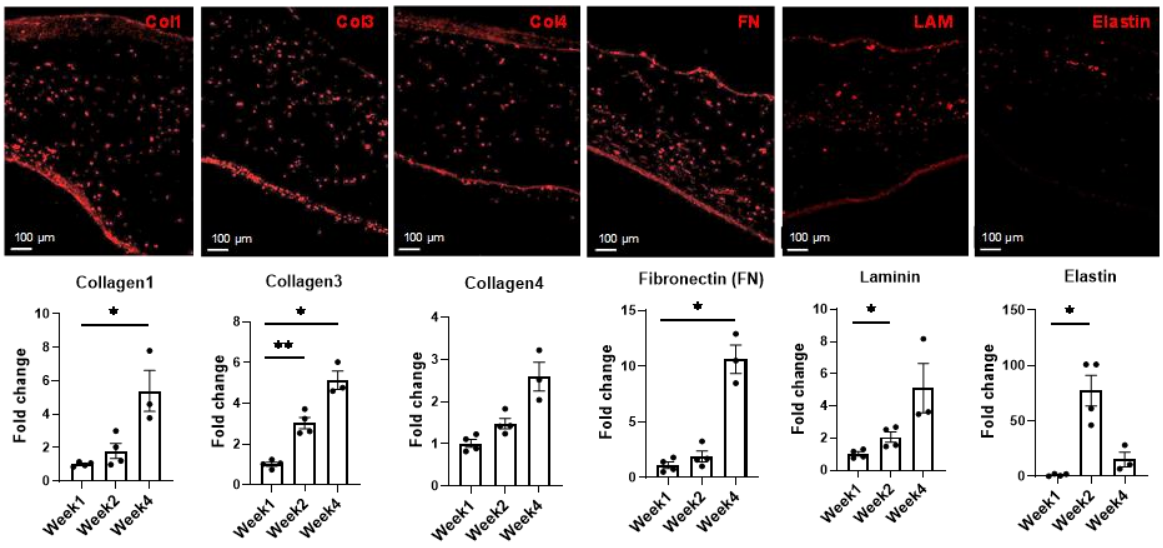

Figure 6: ECM evolution as a result of remodeling over four weeks in culture. Representative images and subsequent quantification of ECM evolution over a 4-week period, showing the deposition of Collagen 1, Collagen 3, Collagen 4, Fibronectin (FN), Laminin (LAM) and Elastin at week 4. Expression levels of each ECM marker was determined via RNA analysis. Scale bars = 100 µm, n = 4 for week 1 and week 2, n = 3 for week 4, *p < 0.05, **p < 0.005

Functional performance of tri-lineage engineered tissue

Expression levels of factors associated with functional performance were assessed by RNA analysis (**Figure 7**) of developmental transcription factor Tbx20, calcium handling machinery (JP2, RyR2, Cx43, SERCA, CACNA1C) and optical mapping (**Figure 8**) to determine conduction velocities through the tissue. All mapping was performed over the four week culture period. From week1 to week2, there was a 2-fold increase in the expression level of RyR2, suggesting that some of the calcium handling machinery, specifically some of the machinery associated with sarcoplasmic reticulum (SR)-associated calcium release, improved [49]. A significant increase in Tbx20 expression was noted, with a 1.7-fold increase and a 2.5-fold increase observed from week1 to week 2 and week 1 to week 4, respectively.

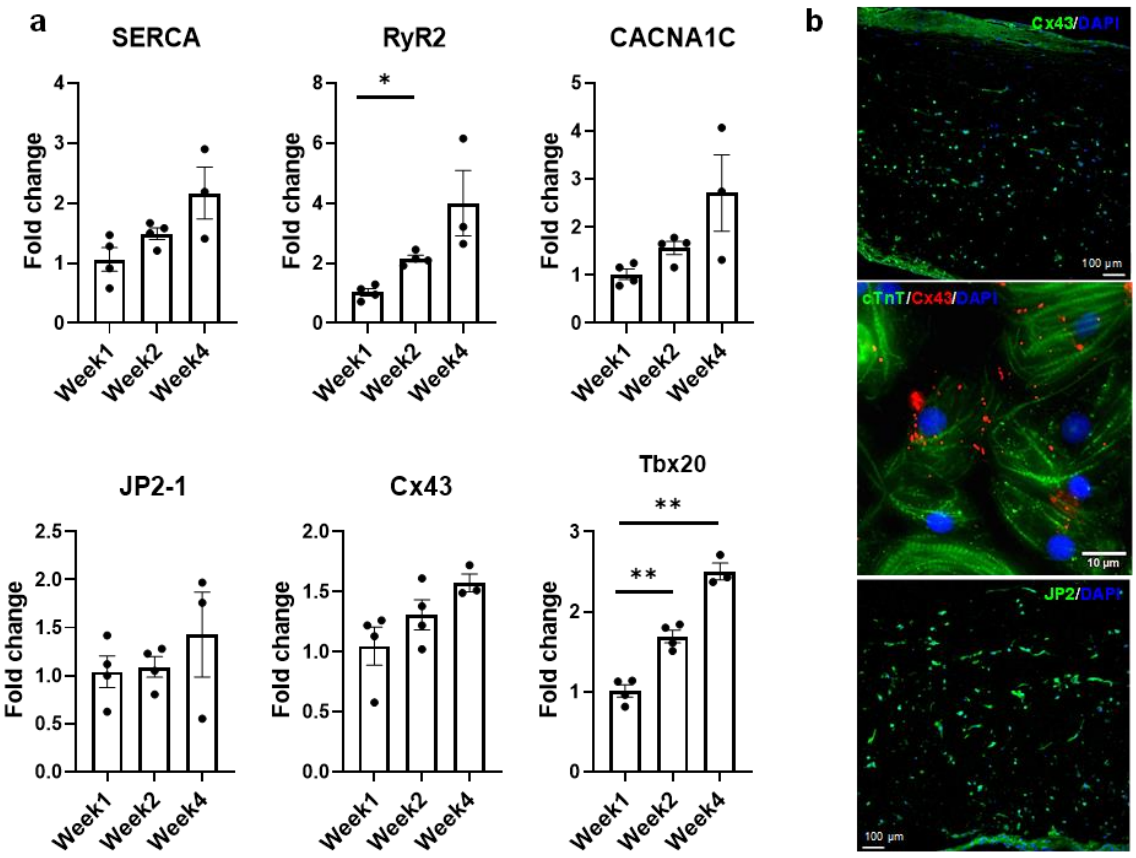

Figure 7: Protein expression of CM-specific markers. (a) Expression levels of CM-specific functional markers at weeks one, two and four, respectively, (n = 4 for week1 and week2, n = 3 for week4, *p < 0.05, **p < 0.005). (B) Representative confocal micrograph of tri-lineage engineered cardiac tissue at week 2 stained for Cx43 and JP2, respectively.

The conduction capabilities of the tri-lineage engineered cardiac tissues were evaluated over the 4 week period and compared to bilayered samples fabricated in a similar fashion, without any fibroblasts (**Figure 8**). Conduction velocities were recorded between pacing cycle lengths of 200 to 800 ms, and average conduction velocities are noted at the respective pacing cycle length in **Figure 8** a. The average conduction velocity trends show that increased time in culture, i.e. 2 weeks vs. 1 week, and 4 weeks vs. 2 weeks, allows for enhanced conduction capabilities. This trend holds true over the entire pacing frequency range, up to 200 ms (5 Hz). Maximum conduction velocities

noted at each time point, regardless of the pacing cycle length it was obtained at, are shown in **Figure 8** b. The maximum conduction velocity noted for each run was 25.6 ± 2.47 cm/s and 21.8 ± 0.97 cm/s for week 1, 37.3 ± 1.65 cm/s and 36.8 ± 2.59 cm/s for week 2, and 39.8 ± 4.35 cm/s and 30.0 ± 1.36 cm/s for week 4, for the tri-lineage and bilayered cardiac tissue structures respectively. Of particular note was that CVs as high as 49 cm/s were obtained after 4 weeks in culture (**Figure 8** b). The tri-lineage structures showed significant increases in conduction velocity from week 1 to week 2, as well as week 1 to week 4, with an overall increasing trend. Bilayered structures also showed a significant increase in the conduction velocity when comparing values obtained at week 1 to week 2, and week 1 to week 4, but overall maximum conduction velocities were obtained after 2 weeks in culture. Tri-lineage engineered tissue structure APD values were obtained as functions of pacing cycle length (**Figure 8** c). Isochronal activation maps show uniform signal propagation across the engineered cardiac tissue after 1 week of culture at pacing cycle lengths of 200 and 800 ms (**Figure 8** d). Isochronal activation maps of engineered tissues paced at weeks two and four also show uniform conduction (Supplementary Figure S4). The lack of observed conduction heterogeneity or conduction blocks suggests low arrhythmic risk of the constructs.

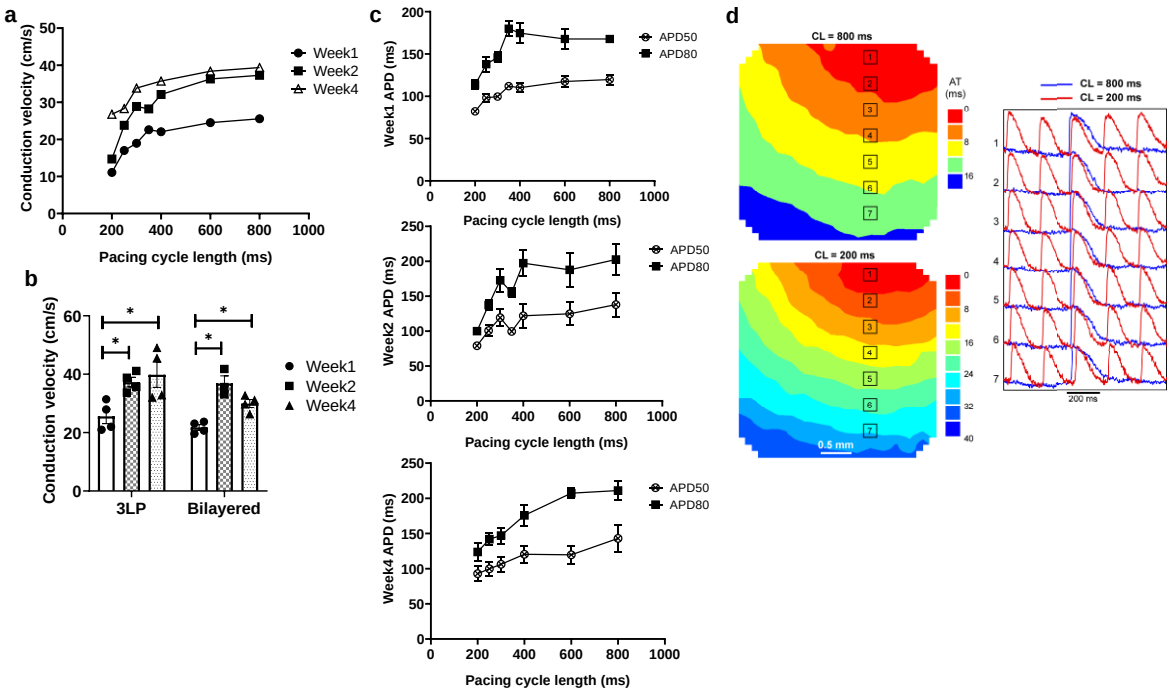

Figure 8: Summary of the electrophysiological results. Optical mapping results showing (a) the average conduction velocity of the tri-lineage engineered cardiac tissue at over the 4-week culture period as a function of pacing cycle length (n = 4), (b) the maximum conduction velocity of the tri-lineage engineered cardiac tissue compared to bilayered control engineered cardiac tissue, at each time point respectively (n = 4 with *p < 0.05), (c) APD_{50} and APD_{80} of the tri-lineage engineered cardiac tissue as a function of pacing cycle length, (n = 4). (d) Representative isochronal electrical activation maps of engineered cardiac tissue, with representative optical action potentials at locations indicated on maps pacing at 200 ms (red) and 800 ms (blue) cycle lengths after 1 week in culture.

Discussion

In this study, a modular LbL fabrication method was developed to fabricate cardiac muscle constructs from three cardiac cell types derived from human pluripotent stem cell lines. Over a 4 week period in culture, it was shown that these large and thick cardiac tissue constructs were functionally superior to previously reported engineered structures from the perspective of their larger, thicker nature, as well as superior action potential duration (APD) conduction velocity. This study is the first to our knowledge to demonstrate

robust (1 x 2 cm^2) hiPSC-derived engineered cardiac tissues that surpass 2 mm in thickness (~2.12 mm), without significant apoptosis/necrosis. The physiologically relevant conduction velocities ranging from around 25 cm/s after 1 week in culture to velocities as high as 49 cm/s after 4 weeks in culture, all lacking arrhythmogenic properties, demonstrate the significant clinical relevance of these cardiac muscle constructs. Previously, the best achievable thickness of engineered cardiac tissue constructs with this level of conduction velocity was only 100 μm [18]. Quantification of the temporal stability of the expression of cTnT, CD31, α-SMA, periostin, vimentin and FAP suggested that all three cell populations (iCM, iEC and cFBs) were stable. Additionally, this study also considered the temporal changes that occur during ECM remodeling in these engineered tissues, via immunofluorescent staining and RNA expression levels.

We have recently reported [13] that a novel dynamically cultured engineered human cardiac muscle patch (hCMPs) demonstrated a significant advancement in the field of myocardial tissue engineering, due to its clinically relevant dimensions (2 cm × 4 cm x 1.2 mm) as well as contractile force generation capabilities were substantially greater than had been previously achieved [45-47]. However, these hCMPs were manufactured by *mixing* hiPSC-CMs, -ECs, and -SMCs into a single layer of cells. In functional myocardium, CMs are typically adjacent to one another as opposed next to the SMCs, fibroblasts (FBs) or ECs, with the mixing of cardiac cells in engineered cardiac tissue likely preventing the hiPSC-CMs from coalescing into a fully interconnected contractile apparatus in the past. This might partially explain why force generation measurements remained lower than in native heart tissue. In the current study with an hCMP composed of layers of hiPSC-CMs, -ECs, -FBs sandwiched in a LbL fashion, compared to a single layer of

hiPSC-CMs, the three-layered patch generated approximately twice the APD conduction velocity compared to the previous study, suggesting a significantly improved physiology using this LbL approach.

Cardiac fibroblasts are known to contribute significantly to the normal extra cellular matrix (ECM) formation. During the four weeks in culture, ECM remodeling occurs. The increases in collagen 3 (**Figure 6**) are likely a precursor to collagen 1 in this case, as it is known to play a vital role in collagen 1 fibrillogenesis and is crucial for normal cardiovascular development [48]. Fibronectin, is highly expressed in the heart during the early stages of embryogenesis and has furthermore been shown to be vital in the vasculogenesis process [49]. It has also been suggested that increases in fibronectin expression, as noted at week 4 could be related to the regulation of vessel formation in similar engineered cardiac tissues [14]. Even though laminin is known to be a basal lamina protein and more closely associated with cellular differentiation, migration and adhesion, it has been suggested that manipulation of the ECM laminin content may be an effective means of inducing structural and functional changes at a cellular level by altering the cardiac titin isoform ratio [50]. Laminins and other proteins are connected to the cell surface by costameres, which are in turn assembled by a combination of integrins and dystroglycans, and serve as a structural and functional bridge. These costameres and their subsequent integrins contribute to signal transduction, transmitting force signals between the contractile apparatus and ECM via interactions with primarily titin and other Z-line associated structures [51]. This process not only supports the mechanical integrity of the sarcolemma, contributes to mechanical signaling but also provides spatial prompts for muscle fiber organization [52]. The upregulation in the levels of laminin observed in the tri-lineage tissues

could, thus, likely be associated with the structural and functional maturation of the iCMs, as well as the enhanced tissue compaction and alignment noted in **Figure 2** c-d. Increases in periostin are associated with significant increases in elastin production by cardiac-specific cell, and more specifically those cells negative for CD31 and CD45 [53]. Furthermore, the increased expression of elastin could likely be attributed to cellular migration and re-arrangement of the endothelial cells into more organized structures as well [54].

Even though the increases in junctophilin (JP2), sarco/endoplasmic reticulum Ca^{2+}-ATPase (SERCA), calcium voltage-gated channel subunit alpha1 C (aka $Ca_{v1.2}$, encoded by CACNA1C) and connexin 43 (Cx43) were not statistically significant, there were clear trends hinting at the development of the calcium handling machinery in the tri-lineage tissues (**Figure 7**). The multi-chambered mammalian heart has its origin from a simple tubual structure via polar elongation, myocardial differentiation and morphogenesis. The large family of T-box (Tbx) transcription factors have been shown to be vital in their role as distinct subprograms during cardiac regionalization [55, 56]. Tbx20 plays a central role in these pathways, and has important activities in both cardiac development and adult function, specifically affecting chamber differentiation and overexpression of Tbx20 has been shown to lead to increased expression of Cx43, and subsequent increases in conduction velocities *in vivo* [57]. The expression of Tbx20 has also been associated with the activation of and maturation-associated genes in iCMs such as those recorded in **Figure 5** [58]. The tri-lineage LbL cardiac engineered tissues fabricated here are the first, to our knowledge, to be fabricated from hiPSC-CMs that have not only generated physiologically relevant conduction velocities in excess of 30 cm/s [16], but generated velocities

close to 50 cm/s with these cells (**Figure 8** b). Whether this increase in structure functionality is a function of cell-cell communication and paracrine signaling, a function of increased culturing time, or a combination of these factors remains to be seen. It has been shown, however, that cFBs do affect the maturation of hiPSC-CMs through secretion of growth-related cytokines when co-cultured [59]. These data suggest that superior electrophysiological function of the current LbL approach may be in part caused by the addition of the cFB layer.

It should be noted that, even though this 3D *in vitro* study enhanced our knowledge-base of thick, engineered cardiac tissue structures and some of their electrophysiological capabilities, further studies are required to better understand the mechanical aspects of the system. In order to better understand, model future system and avoid mechanical mismatch when implanting these structures, their viscoelastic properties need to be determined and related to the dynamic properties of the ECM [60-63].

Conclusions

Here we have shown that a modular fabrication method, like LbL assembly, can be utilized to produce thick (~2.12 mm), viable engineered cardiac tissues from hiPSCs. The incorporation of cardiac FBs into the LbL assembly method allowed for superior, previously unobtainable conduction velocities (> 30 cm/s) along with a lack in arrhythmogenic potential, with tissues having the ability to be paced to 5 Hz (200 ms). *In vitro* characterization showed engineered tissue structures resembling those of native cardiac tissue along with minimal necrosis, even after four weeks in culture. Considering that the tissues engineered for this study have not undergone any form of maturation, nor

have they been exposed to any external stimuli, suggests that their performance capabilities could be enhanced even further.

Future work will include the mechanical testing of the engineered cardiac tissues to determine viscoelastic properties to ultimately prevent mechanical mismatch between the engineered tissues and future host. *In vivo* studies in a large animal model will also commence in order to assess the potential clinical application of these larger, thicker, engineered cardiac tissues in preventing LV dilatation of hearts with postinfarction LV remodeling.

Acknowledgements

This study was supported in part by the National Institutes of Health (NIH) NHLBI grants RO1 HL114120, HL131017, HL149137, UO1 HL134764, and NIH BIB T32 EB023872.

REFERENCES

1. Lucas DT and Szweda LI. Declines in mitochondrial respiration during cardiac reperfusion: Age-dependent inactivation of α-ketoglutarate dehydrogenase. 1999;96:6689-6693.

2. Lake CL, Sellers TD, Crosby IK, Wellons HA and Crampton RS. Effects of coronary grafting technique upon reperfusion cardiac rhythm, ventricular function, and other variables. Am Surg. 1985;51:497-503.

3. Murphy E and Steenbergen C. Mechanisms Underlying Acute Protection From Cardiac Ischemia-Reperfusion Injury. 2008;88:581-609.

4. Henkel DM, Witt BJ, Gersh BJ, Jacobsen SJ, Weston SA, Meverden RA and Roger VL. Ventricular arrhythmias after acute myocardial infarction: A 20-year community study. American heart journal. 2006;151:806-812.

5. Gorenek B, Blomström Lundqvist C, Brugada Terradellas J, Camm AJ, Hindricks G, Huber K, Kirchhof P, Kuck K-H, Kudaiberdieva G, Lin T, Raviele A, Santini M, Tilz RR, Valgimigli M, Vos MA, Vrints C, Zeymer U, Kristiansen SB and Group ESD. Cardiac arrhythmias in acute coronary syndromes: position paper from the joint EHRA, ACCA, and EAPCI task force. EP Europace. 2014;16:1655-1673.

6. Xiaojun L, Cheston H, Gisela W, Kexian Z, Laurie BH, Samira MA, Kunil KR, Jianhua Z, Timothy JK and Sean PP. Robust cardiomyocyte differentiation from human pluripotent stem cells via temporal modulation of canonical Wnt signaling. Proceedings of the National Academy of Sciences of the United States of America. 2012;109:E1848-57.

7. Xiaojun L, Xiaoping B, Abraham A-A, Jialu L, Yue W, Wentao D, Kaitlin KD, Eric VS and Sean PP. Efficient differentiation of human pluripotent stem cells to endothelial progenitors via small-molecule activation of WNT signaling. Stem cell reports. 2014;3:804-16.

8. Ye L, Chang YH, Xiong Q, Zhang P, Zhang L, Somasundaram P, Lepley M, Swingen C, Su L, Wendel JS, Guo J, Jang A, Rosenbush D, Greder L, Dutton JR, Zhang J, Kamp TJ, Kaufman DS, Ge Y and Zhang J. Cardiac repair in a porcine model of acute myocardial infarction with human induced pluripotent stem cell-derived cardiovascular cells. Cell Stem Cell. 2014;15:750-61.

9. Mummery CL, Zhang J, Ng ES, Elliott DA, Elefanty AG and Kamp TJ. Differentiation of Human Embryonic Stem Cells and Induced Pluripotent Stem Cells to Cardiomyocytes. 2012;111:344-358.

10. O'Hara T, Virág L, Varró A and Rudy Y. Simulation of the Undiseased Human Cardiac Ventricular Action Potential: Model Formulation and Experimental Validation. PLOS Computational Biology. 2011;7:e1002061.

11. Liu J, Laksman Z and Backx PH. The electrophysiological development of cardiomyocytes. Advanced drug delivery reviews. 2016;96:253-273.

12. Lee P, Klos M, Bollensdorff C, Hou L, Ewart P, Kamp TJ, Zhang J, Bizy A, Guerrero-Serna G, Kohl P, Jalife J and Herron TJ. Simultaneous Voltage and Calcium Mapping of Genetically Purified Human Induced Pluripotent Stem Cell-Derived Cardiac Myocyte Monolayers. 2012;110:1556-1563.

13. Gao L, Gregorich ZR, Zhu W, Mattapally S, Oduk Y, Lou X, Kannappan R, Borovjagin AV, Walcott GP, Pollard AE, Fast VG, Hu X, Lloyd SG, Ge Y and Zhang J. Large Cardiac Muscle Patches Engineered From Human Induced-Pluripotent Stem Cell-Derived Cardiac Cells Improve Recovery From Myocardial Infarction in Swine. Circulation. 2018;137:1712-1730.

14. Pretorius D, Kahn-Krell A, M. , LaBarge W, C. , Lou X, Kannappan R, Pollard A, E. , Fast V, G. , Berry J, L. , Eberhardt A, W. and Zhang J. Fabrication and characterization of a thick, viable bi-layered stem cell-derived surrogate for future myocardial tissue regeneration. Biomedical Materials. 2020.

15. Gao L, Kupfer ME, Jung JP, Yang L, Zhang P, Sie YD, Tran Q, Ajeti V, Freeman BT, Fast VG, Campagnola PJ, Ogle BM and Zhang J. Myocardial Tissue Engineering With Cells Derived From Human-Induced Pluripotent Stem Cells and a Native-Like, High-Resolution, 3-Dimensionally Printed Scaffold. 2017;120:1318-1325.

16. Yang X, Pabon L and Murry CE. Engineering Adolescence. 2014;114:511-523.

17. Valderrábano M. Influence of anisotropic conduction properties in the propagation of the cardiac action potential. Progress in Biophysics and Molecular Biology. 2007;94:144-168.

18. Jackman CP, Ganapathi AM, Asfour H, Qian Y, Allen BW, Li Y and Bursac N. Engineered cardiac tissue patch maintains structural and electrical properties after epicardial implantation. Biomaterials. 2018;159:48-58.

19. Zhang J, Tao R, Campbell KF, Carvalho JL, Ruiz EC, Kim GC, Schmuck EG, Raval AN, da Rocha AM, Herron TJ, Jalife J, Thomson JA and Kamp TJ. Functional cardiac fibroblasts derived from human pluripotent stem cells via second heart field progenitors. Nature Communications. 2019;10:2238.

20. Burridge PW, Matsa E, Shukla P, Lin ZC, Churko JM, Ebert AD, Lan F, Diecke S, Huber B, Mordwinkin NM, Plews JR, Abilez OJ, Cui B, Gold JD and Wu JC. Chemically defined generation of human cardiomyocytes. 2014;11:855-60.

21. Lian X, Zhang J, Azarin SM, Zhu K, Hazeltine LB, Bao X, Hsiao C, Kamp TJ and Palecek SP. Directed cardiomyocyte differentiation from human pluripotent stem cells by modulating Wnt/β-catenin signaling under fully defined conditions. Nature Protocols. 2012;8:162.

22. Zhu W, Gao L and Zhang J. Pluripotent Stem Cell Derived Cardiac Cells for Myocardial Repair. JoVE. 2017:e55142.

23. Su L, Kong X, Lim S, Loo S, Tan S, Poh K, Dutton J, Stewart C, Cook S, Su X, Ma J, Zhang J and Ye L. The prostaglandin H2 analog U-46619 improves the differentiation efficiency of human induced pluripotent stem cells into endothelial cells by activating both p38MAPK and ERK1/2 signaling pathways. Stem Cell Res Ther. 2018;9:313.

24. Zhang S, Dutton JR, Su L, Zhang J and Ye L. The influence of a spatiotemporal 3D environment on endothelial cell differentiation of human induced pluripotent stem cells. Biomaterials. 2014;35:3786-93.

25. Pinto AR, Ilinykh A, Ivey MJ, Kuwabara JT, D'Antoni ML, Debuque R, Chandran A, Wang L, Arora K, Rosenthal NA and Tallquist MD. Revisiting Cardiac Cellular Composition. 2016;118:400-409.

26. Li W, Germain RN and Gerner MY. High-dimensional cell-level analysis of tissues with Ce3D multiplex volume imaging. Nature Protocols. 2019;14:1708-1733.

27. Sowell B and Fast VG. Ionic mechanism of shock-induced arrhythmias: role of intracellular calcium. Heart Rhythm. 2012;9:96-104.

28. Linkermann A, Kunzendorf U and Krautwald S. Phosphorylated MLKL causes plasma membrane rupture. Mol Cell Oncol. 2014;1:e29915-e29915.

29. Negroni A, Colantoni E, Pierdomenico M, Palone F, Costanzo M, Oliva S, Tiberti A, Cucchiara S and Stronati L. RIP3 AND pMLKL promote necroptosis-induced inflammation and alter membrane permeability in intestinal epithelial cells. Digestive and Liver Disease. 2017;49:1201-1210.

30. Gillan L, Matei D, Fishman DA, Gerbin CS, Karlan BY and Chang DD. Periostin secreted by epithelial ovarian carcinoma is a ligand for alpha(V)beta(3) and alpha(V)beta(5) integrins and promotes cell motility. Cancer research. 2002;62:5358-64.

31. Allen DL and Leinwand LA. Postnatal Myosin Heavy Chain Isoform Expression in Normal Mice and Mice Null for IIb or IId Myosin Heavy Chains. Developmental Biology. 2001;229:383-395.

32. Everett AW, Sinha AM, Umeda PK, Jakovcic S, Rabinowitz M and Zak R. Regulation of myosin synthesis by thyroid hormone: relative change in the .alpha.- and .beta.-myosin heavy chain mRNA levels in rabbit heart. Biochemistry. 1984;23:1596-1599.

33. Van der Velden J, Moorman AF and Stienen GJ. Age-dependent changes in myosin composition correlate with enhanced economy of contraction in guinea-pig hearts. The Journal of physiology. 1998;507 (Pt 2):497-510.

34. Reiser PJ, Portman MA, Ning X-H and Moravec CS. Human cardiac myosin heavy chain isoforms in fetal and failing adult atria and ventricles. 2001;280:H1814-H1820.

35. LaBarge W, Mattappally S, Kannappan R, Fast VG, Pretorius D, Berry JL and Zhang J. Maturation of three-dimensional, hiPSC-derived cardiomyocyte spheroids utilizing cyclic, uniaxial stretch and electrical stimulation. PloS one. 2019;14:e0219442-e0219442.

36. Mihic A, Li J, Miyagi Y, Gagliardi M, Li S-H, Zu J, Weisel RD, Keller G and Li R-K. The effect of cyclic stretch on maturation and 3D tissue formation of human embryonic stem cell-derived cardiomyocytes. Biomaterials. 2014;35:2798-2808.

37. Ruan J-L, Tulloch NL, Saiget M, Paige SL, Razumova MV, Regnier M, Tung KC, Keller G, Pabon L, Reinecke H and Murry CE. Mechanical Stress Promotes Maturation of Human Myocardium From Pluripotent Stem Cell-Derived Progenitors. 2015;33:2148-2157.

38. Ng SY, Wong CK and Tsang SY. Differential gene expressions in atrial and ventricular myocytes: insights into the road of applying embryonic stem cell-derived cardiomyocytes for future therapies. 2010;299:C1234-C1249.

39. Wendel JS, Ye L, Tao R, Zhang J, Zhang J, Kamp TJ and Tranquillo RT. Functional Effects of a Tissue-Engineered Cardiac Patch From Human Induced Pluripotent Stem Cell-Derived Cardiomyocytes in a Rat Infarct Model. Stem Cells Transl Med. 2015;4:1324-1332.

40. Bax NAM, van Marion MH, Shah B, Goumans M-J, Bouten CVC and van der Schaft DWJ. Matrix production and remodeling capacity of cardiomyocyte progenitor cells during in vitro differentiation. Journal of molecular and cellular cardiology. 2012;53:497-508.

41. Mecham RP, Madaras J, McDonald JA and Ryan U. Elastin production by cultured calf pulmonary artery endothelial cells. Journal of cellular physiology. 1983;116:282-8.

42. L'Heureux N, Pâquet S, Labbé R, Germain L and Auger FA. A completely biological tissue-engineered human blood vessel. FASEB journal : official publication of the Federation of American Societies for Experimental Biology. 1998;12:47-56.

43. Eghbali M. Cardiac fibroblasts: function, regulation of gene expression, and phenotypic modulation. Basic research in cardiology. 1992;87 Suppl 2:183-9.

44. Norris RA, Damon B, Mironov V, Kasyanov V, Ramamurthi A, Moreno-Rodriguez R, Trusk T, Potts JD, Goodwin RL, Davis J, Hoffman S, Wen X, Sugi Y, Kern CB, Mjaatvedt CH, Turner DK, Oka T, Conway SJ, Molkentin JD, Forgacs G and Markwald RR. Periostin regulates collagen fibrillogenesis and the biomechanical properties of connective tissues. Journal of cellular biochemistry. 2007;101:695-711.

45. Takayama G, Arima K, Kanaji T, Toda S, Tanaka H, Shoji S, McKenzie AN, Nagai H, Hotokebuchi T and Izuhara K. Periostin: a novel component of subepithelial fibrosis of bronchial asthma downstream of IL-4 and IL-13 signals. The Journal of allergy and clinical immunology. 2006;118:98-104.

46. Kennedy A, Dong H, Chen D and Chen WT. Elevation of seprase expression and promotion of an invasive phenotype by collagenous matrices in ovarian tumor cells. International journal of cancer. 2009;124:27-35.

47. Savchenko E, Teku GN, Boza-Serrano A, Russ K, Berns M, Deierborg T, Lamas NJ, Wichterle H, Rothstein J, Henderson CE, Vihinen M and Roybon L. FGF family members differentially regulate maturation and proliferation of stem cell-derived astrocytes. Scientific Reports. 2019;9:9610.

48. Rich CB, Nugent MA, Stone P and Foster JA. Elastase Release of Basic Fibroblast Growth Factor in Pulmonary Fibroblast Cultures Results in Down-regulation of Elastin Gene Transcription: A ROLE FOR BASIC FIBROBLAST GROWTH FACTOR IN REGULATING LUNG REPAIR*. Journal of Biological Chemistry. 1996;271:23043-23048.

49. Ronaldson-Bouchard K, Ma SP, Yeager K, Chen T, Song L, Sirabella D, Morikawa K, Teles D, Yazawa M and Vunjak-Novakovic G. Advanced maturation of human cardiac tissue grown from pluripotent stem cells. Nature. 2018;556:239-243.

50. Ruan JL, Tulloch NL, Razumova MV, Saiget M, Muskheli V, Pabon L, Reinecke H, Regnier M and Murry CE. Mechanical Stress Conditioning and Electrical Stimulation Promote Contractility and Force Maturation of Induced Pluripotent Stem Cell-Derived Human Cardiac Tissue. Circulation. 2016;134:1557-1567.

51. Yang X and Murry CE. One Stride Forward: Maturation and Scalable Production of Engineered Human Myocardium. Circulation. 2017;135:1848-1850.

52. Shadrin IY, Allen BW, Qian Y, Jackman CP, Carlson AL, Juhas ME and Bursac N. Cardiopatch platform enables maturation and scale-up of human pluripotent stem cell-derived engineered heart tissues. Nat Commun. 2017;8:1825.

53. Liu X, Wu H, Byrne M, Krane S and Jaenisch R. Type III collagen is crucial for collagen I fibrillogenesis and for normal cardiovascular development. 1997;94:1852-1856.

54. George EL, Georges-Labouesse EN, Patel-King RS, Rayburn H and Hynes RO. Defects in mesoderm, neural tube and vascular development in mouse embryos lacking fibronectin. Development (Cambridge, England). 1993;119:1079-91.

55. Hochman-Mendez C, Curty E and Taylor DA. Change the Laminin, Change the Cardiomyocyte: Improve Untreatable Heart Failure. International journal of molecular sciences. 2020;21.

56. Peter AK, Cheng H, Ross RS, Knowlton KU and Chen J. The costamere bridges sarcomeres to the sarcolemma in striated muscle. Progress in pediatric cardiology. 2011;31:83-88.

57. Hochman-Mendez C, Pereira de Campos DB, Pinto RS, Mendes B, Rocha GM, Monnerat G, Weissmuller G, Sampaio LC, Carvalho AB, Taylor DA and de Carvalho ACC. Tissue-engineered human embryonic stem cell-containing cardiac patches: evaluating recellularization of decellularized matrix. J Tissue Eng. 2020;11:2041731420921482.

58. Kanisicak O, Khalil H, Ivey MJ, Karch J, Maliken BD, Correll RN, Brody MJ, J. Lin S-C, Aronow BJ, Tallquist MD and Molkentin JD. Genetic lineage tracing defines myofibroblast origin and function in the injured heart. Nature Communications. 2016;7:12260.

59. Mecham RP, Madaras J, McDonald JA and Ryan U. Elastin production by cultured calf pulmonary artery endothelial cells. 1983;116:282-288.

60. Stennard FA, Costa MW, Lai D, Biben C, Furtado MB, Solloway MJ, McCulley DJ, Leimena C, Preis JI, Dunwoodie SL, Elliott DE, Prall OW, Black BL, Fatkin D and Harvey RP. Murine T-box transcription factor Tbx20 acts as a repressor during heart development, and is essential for adult heart integrity, function and adaptation. Development (Cambridge, England). 2005;132:2451-62.

61. Singh MK, Christoffels VM, Dias JM, Trowe MO, Petry M, Schuster-Gossler K, Bürger A, Ericson J and Kispert A. Tbx20 is essential for cardiac chamber differentiation and repression of Tbx2. Development (Cambridge, England). 2005;132:2697-707.

62. Chakraborty S and Yutzey KE. Tbx20 regulation of cardiac cell proliferation and lineage specialization during embryonic and fetal development in vivo. Developmental Biology. 2012;363:234-246.

63. Zhou Y, Tang Y, Fast VG, Zhao L, Lu R and Zhang J. Abstract 103: TBX20 Activates Cardiac Maturation Gene Programs Promoting Direct Human Cardiac Reprogramming. 2020;127:A103-A103.

64. Ieda M, Tsuchihashi T, Ivey KN, Ross RS, Hong TT, Shaw RM and Srivastava D. Cardiac fibroblasts regulate myocardial proliferation through beta1 integrin signaling. Developmental cell. 2009;16:233-44.

65. Wang B, Borazjani A, Tahai M, Curry AL, Simionescu DT, Guan J, To F, Elder SH and Liao J. Fabrication of cardiac patch with decellularized porcine myocardial scaffold and bone marrow mononuclear cells. Journal of biomedical materials research Part A. 2010;94:1100-10.

66. Little R and Wead W. Diastolic viscoelastic properties of active and quiescent cardiac muscle. 1971;221:1120-1125.

67. Tsaturyan AK, Izacov VJ, Zhelamsky SV and Bykov BL. Extracellular fluid filtration as the reason for the viscoelastic behaviour of the passive myocardium. Journal of Biomechanics. 1984;17:749-755.

68. Miller CE and Wong CL. Trabeculated embryonic myocardium shows rapid stress relaxation and non-quasi-linear viscoelastic behavior. Journal of Biomechanics. 2000;33:615-622.

Supplementary Material

Flow cytometry analysis

Flow cytometry analysis was performed as described previously [13, 19]. Briefly, cells were dissociated using 0.25 % trypsin and resuspended as single cells, permeabilized in 0.1 % Triton X-100 at 4 °C for 10 min, then incubated with primary and secondary antibodies for 30 min at 4 °C with 3 x 5 min wash in between. Finally, cells were resuspended in 2% fetal bovine serum/phosphate-buffered saline (FBS/PBS) containing 5 μL of propidium iodide (10 μg/mL) and evaluated with a FACS Aria instrument (BD Biosciences, USA). Antibodies used, along with dilutions, are listed Supplementary Table S1.

Cardiomyocyte proliferation assay

Cardiomyocyte proliferation was tested using a proliferation assay from CyQUANT Direct Cell Proliferation Assay Kit (Invitrogen, Cat# C35011). Briefly, CM proliferation was determined via green fluorescent nucleic acid staining of the nucleus, after which the fluorescence intensity of the readout was obtained 60 min after reagent addition via microplate reader in a 96-well plate (10 000 cells/well). Based on the results, there was no significant difference between the proliferation of 6-hour-old and 14-day-old hiPSC-CMs (see Supplementary Figure S2). Student t-test was performed, $p = 0.783$ ($n = 9$).

Image analyses

All image quantification analyses were performed with ImageJ. Where indicated, arbitrary units (A.U) are representative of a pixel count and intensity for each sample. All samples were stained and imaged under similar conditions to allow for a comparative study.

Tube-formation assay

Tube-formation in thick LbL engineered cardiac tissue was analyzed by incubating tissue in their optimized DMEM media with 0.05% FBS for 2 hours at 37 °C. Following incubation, media was removed and replaced with normal optimized DMEM media containing 2% FBS + Dil-Ac-LDL (10 µg/mL final concentration, Thermo Fisher # L35354) and incubated for 4 hours at 37 °C. Tube formation was then visualized using confocal microscope.

Supplementary Tables

Table S1: Antibodies used for flow cytometry, FACS, and immunofluorescent staining.

Antibody Name	**Application**	**Company**	**Catalog Number**
Alexa Fluor® 647 Mouse Anti-Human CD31	FACS	BD Biosciences	561654
Cardiac Troponin T Monoclonal Antibody (13-11)	Flow Analysis	Invitrogen	MA5-12960
Anti-alpha smooth muscle Actin antibody	Immunofluorescent Staining	Abcam	21027
Rabbit Anti-Cardiac Troponin T antibody [EPR3695]	Immunofluorescent Staining	Abcam	91605
Mouse Anti-Cardiac Troponin T antibody [1F11]	Immunofluorescent Staining	Abcam	10214
Goat anti-Mouse IgG Secondary Antibody, Alexa Fluor 555	Immunofluorescent Staining	Invitrogen	A32727
Donkey anti-Mouse IgG Secondary Antibody, Alexa Fluor 488	Immunofluorescent Staining	Invitrogen	A21202
Donkey anti-Rabbit IgG Secondary Antibody, Alexa Fluor 488	Immunofluorescent Staining	Invitrogen	A21206
Donkey anti-Rabbit IgG Secondary Antibody, Alexa Fluor 555	Immunofluorescent Staining	Invitrogen	A31572
Rabbit Anti-Collagen I antibody	Immunofluorescent Staining	Abcam	34710
Mouse Anti-CD31 antibody [JC/70A]	Immunofluorescent Staining	Abcam	9498
Rabbit Anti-Fibrinogen beta chain antibody	Immunofluorescent Staining	Abcam	137830
Rabbit Anti-Collagen III antibody	Immunofluorescent Staining	Abcam	7778
Rabbit Anti-Fibronectin antibody	Immunofluorescent Staining	Abcam	2413
Rabbit Anti-Collagen IV antibody	Immunofluorescent Staining	Abcam	6586
Rabbit Anti-Laminin antibody	Immunofluorescent Staining	Abcam	11575
Rabbit Anti-VE Cadherin	Immunofluorescent Staining	Abcam	33168
Mouse Anti-VWF Antibody (F8/86)	Immunofluorescent Staining	Santa Cruz Biotech	53466
Rabbit Anti-N-Cadherin	Immunofluorescent Staining	Abcam	18203
Anti-Alpha Actinin	Immunofluorescent Staining	Sigma	A7811
Anti-Connexin 43 / GJA1 antibody - Intercellular Junction Marker	Immunofluorescent Staining	Abcam	11370
Mouse Anti-Ryanodine Receptor antibody [C3-33]	Immunofluorescent Staining	Abcam	2827
JPH2 Polyclonal Antibody	Immunofluorescent Staining	Thermo Fisher	40-5300
Recombinant Anti-Cardiac Troponin T antibody	FACS	Abcam	91605

Mouse anti-Human CD144	FACS	BD Biosciences	560410
Anti-Fibroblasts Antibody	FACS	Millipore Sigma	CBL271

Table S2: Formulation of cardiac fibroblast differentiation basal medium (CFBM)

Components	**Final concentration**
DMEM, high glucose (4.5 g/L)	basal medium
HLL Supplement: HSA (human serum albumin), linoleic acid and lecithin	HSA: 500 µg/mL Linoleic Acid: 0.6 µM Lecithin: 0.6 µg/mL
Ascorbic Acid	50 µg/mL
GlutaMAX	7.5 mM
Hydrocortisone Hemisuccinate	1.0 µg/mL
rh Insulin	5 µg/mL

Table S3: Primers used for RNA analyses

Target Gene	Forward Primer	Reverse Primer
cTnT	TTCACCAAA-GATCTGCTCCTCGCT	TTATTACTGGTGTGGAG-TGGGTGTGG
CD31	TCAGACGTGCAGTACACGGA	GGGAGCCTTCCGTTCTAGAGT
Alpha SMA	TATCCCCGGGACTAAGACGG	CACCATCACCCCCTGATGTC
Periostin	AGGTCACCAAGGTCAC-CAAATTC	CTCACGGGTGTGTCTCCCTG
Vimentin	CCTCCGGGAGAAATTGCAGG	TCAAGGTCAAGACGTGCCAG
FAP	AGGGATGGTCATTGCCTTGG	ATCCTCCATAGGACCAGCCC
Alpha MHC	CTCCGTGAAGGGATAACCAGG	TTCACAGTCACCGTCTTCCC
Beta MHC	ACCAACCTGTCCAAGTTCCG	TCATTCAAGCCCTTCGTGCC
MLC2a	GGAGTTCAAAGAA-GCCTTCAGC	AAAGAGCGTGAGGAAGACGG
MLC2v	ACATCATCACCCACGGAGAA-GAGA	ATTGGAACATGGCCTCTG-GATGGA
Collagen 1	TGACGAGACCAAGAACTGCC	GCACCATCATTTCCACGAGC
Collagen 3	GGATGGTTGCACGAAACACAC	GGTAGTCTCACAGCCTTGCG
Collagen 4	GGCAGATTCGGACCACTAGG	GCGTCTGTGGCAATACTAGC
Fibronectin	TCGTGCTTTGACCCCTACAC	CGGGAATCTTCTCTGTCAGCC
Laminin	ACTTGAGTATGAAA-GCAAGGCCAG	GGAGAGCTCCACAAAACCAGG
Elastin	GTGTCTGCAGGTGCGGTG	CTGGGTATACACCTGGCAGC
SERCA	TCACCTGTGAGAATTGACTGG	AGAAAGAGTGTGCAGCGGAT
RyR2	TTGGAAGTGGACTCCAAGAAA	CGAAGACGAGATCCAGTTCC
CACNA1C	TGATTCCAACGCCACCAATTC	GAGGAGTCCATAGGCGATTACT
JPH2	CCAAGTATGAGGGCACCTGG	GCCTTGGTACGTCCCTCCAT
Cx43	GGTGACTGGAGCGCCTTAG	GCGCACATGAGAGATTGGGA
Tbx20	ATTCCTATGCACGCTCACCC	TGTTGTAAAGGCTGACCCTCG

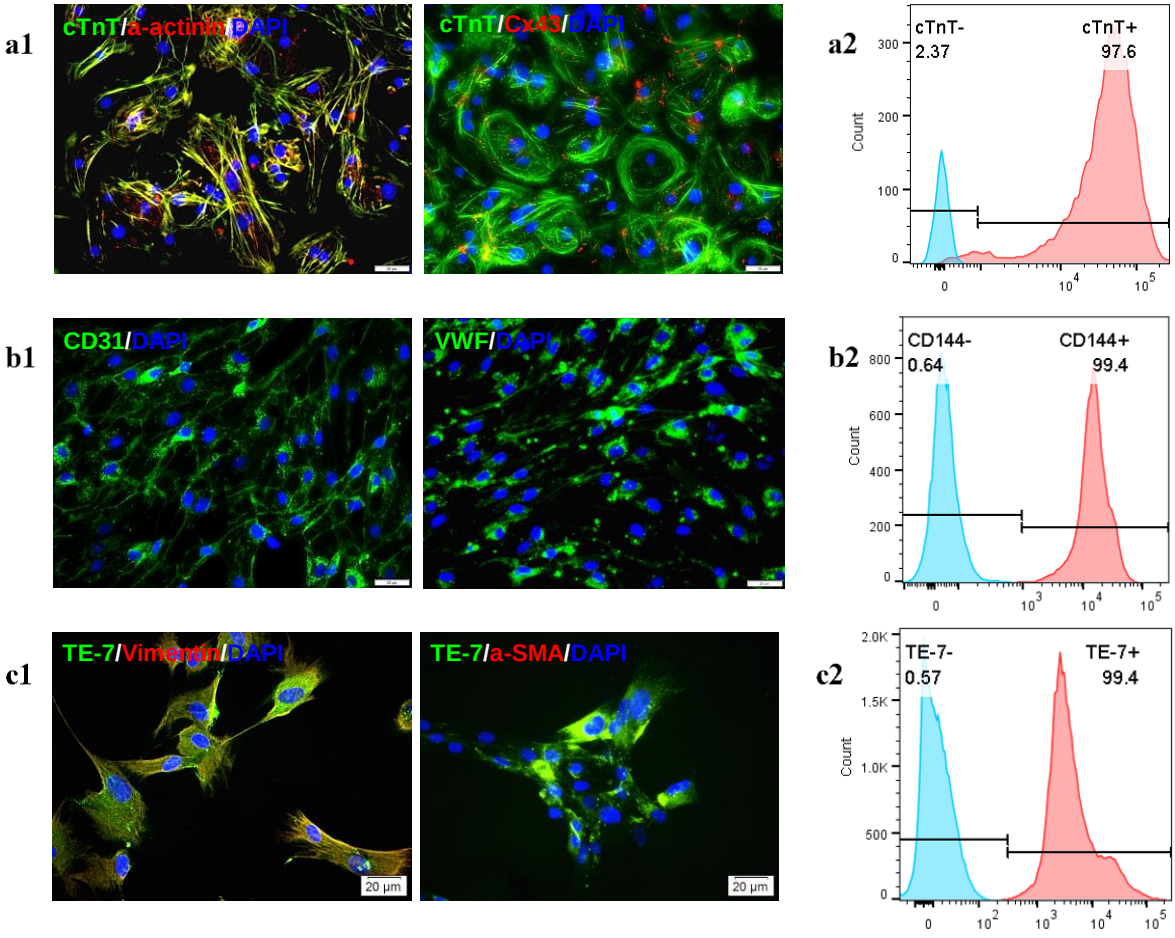

Figure S1: **Characterization of hiPSC-derived cells**. Characterization data confirming differentiation and purification of iCMs (a), iECs (b) and cFBs (c) using immunofluorescent staining (1) and flow cytometry (2) analysis.

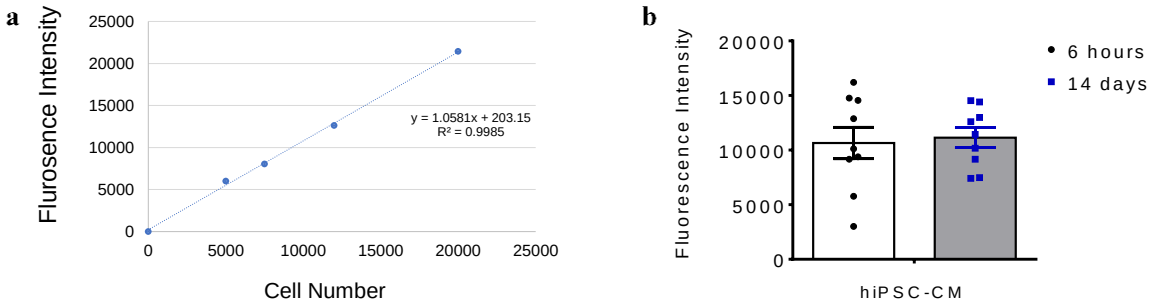

Figure S2: **Fluorescence-based cell proliferation assay.** (a) Standard curve and (b) the resulting measurements at 6 hours of hiPSC-CMs culture in a 96-well plate (10,000 cells/well) as well as measurements after 14 days of culture. p = 0.783, n = 9

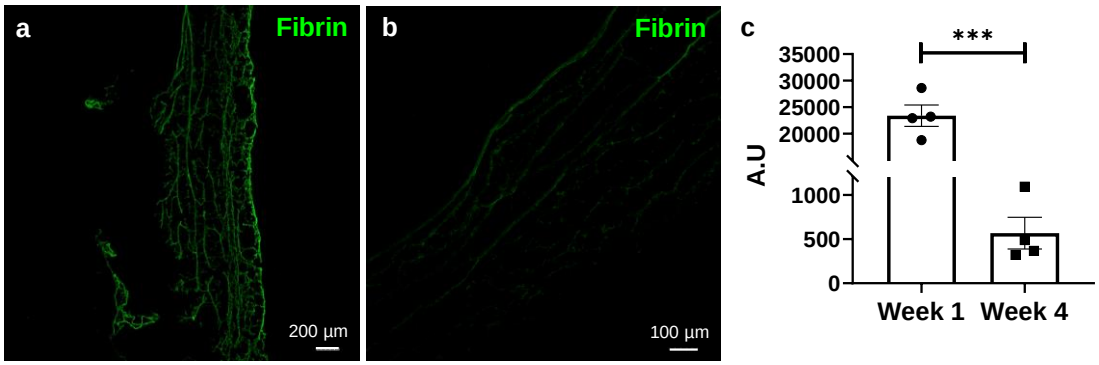

Figure S3: Fibrin degradation. Representative confocal images of fibrin degradation over a 4-week period, with (a) showing fibrin expression levels at week 1, (b) showing fibrin expression levels at week 2, and (c) showing quantification of relative expression levels at each time point (n = 4, ***p < 0.001)

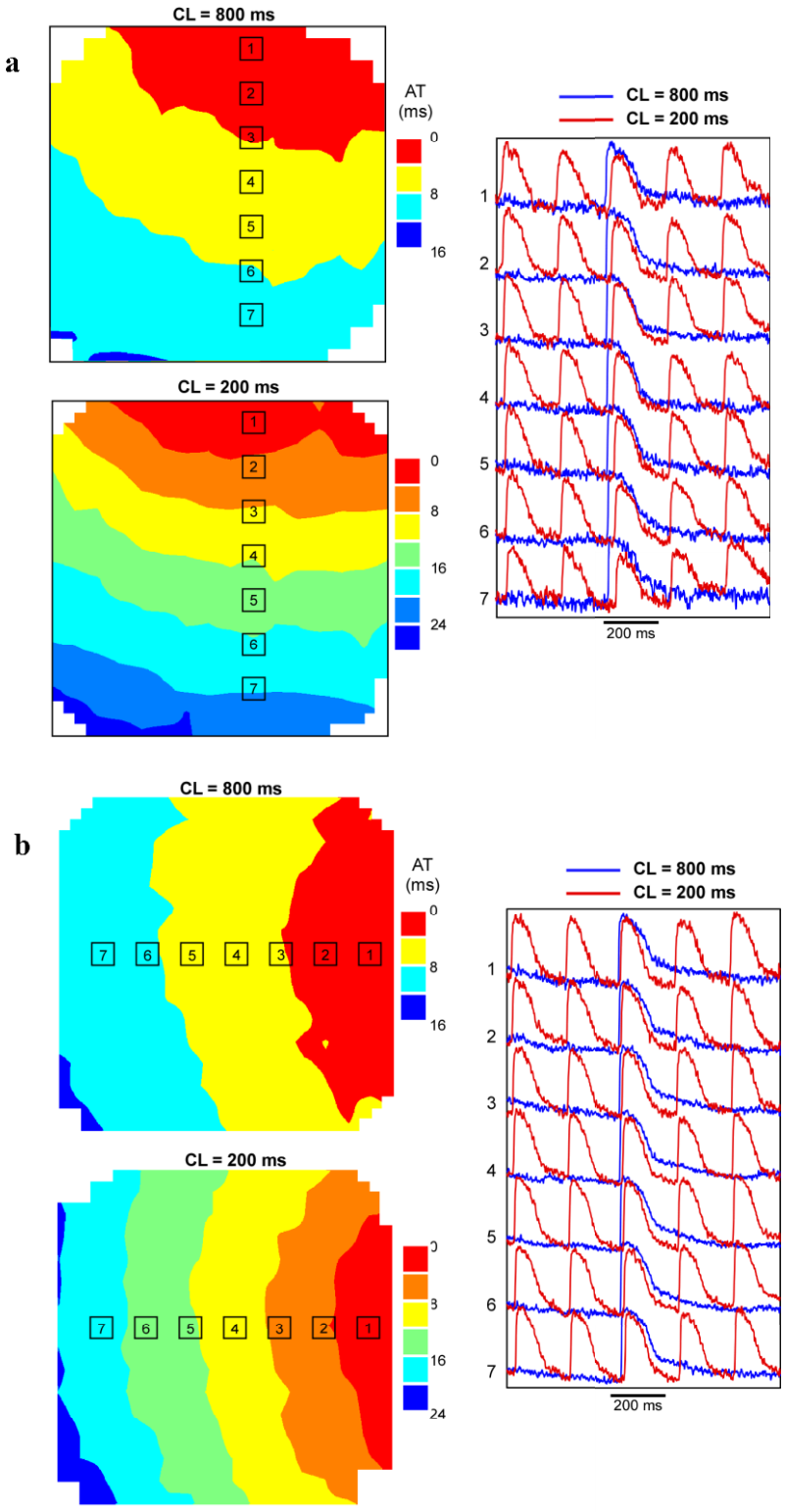

Figure S4: **Optical mapping results**. Representative isochronal maps of engineered tissue conduction capabilities, with representative signal propagation as well as pacing at both 200 ms (red) and 800 ms (blue) for (a) week 2, and (b) week 4 samples

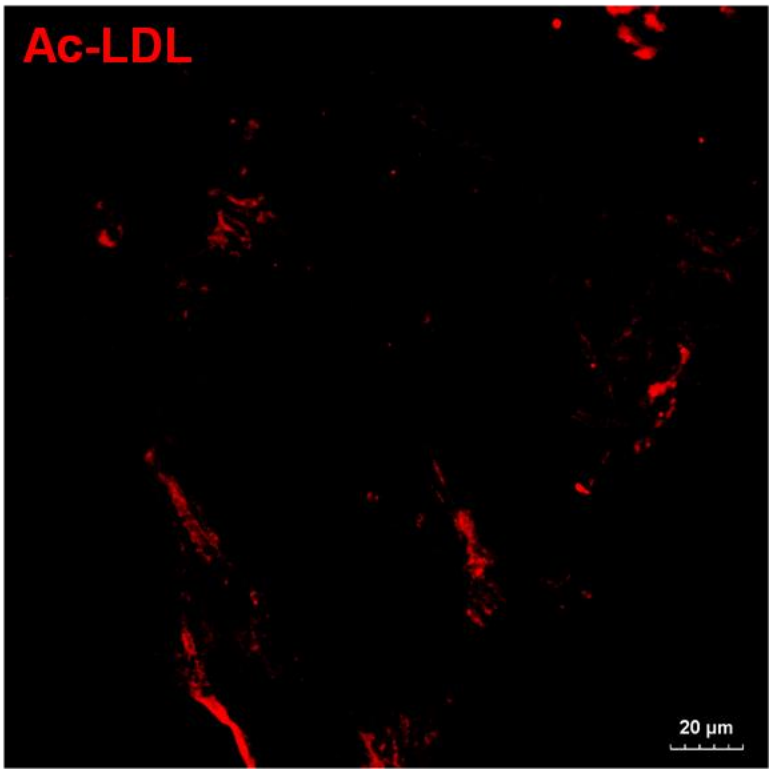

Figure S5: **Ac-LDL assay showing vessel-like structures**. These structures formed throughout the thick LbL engineered tissue after 10 days in culture.

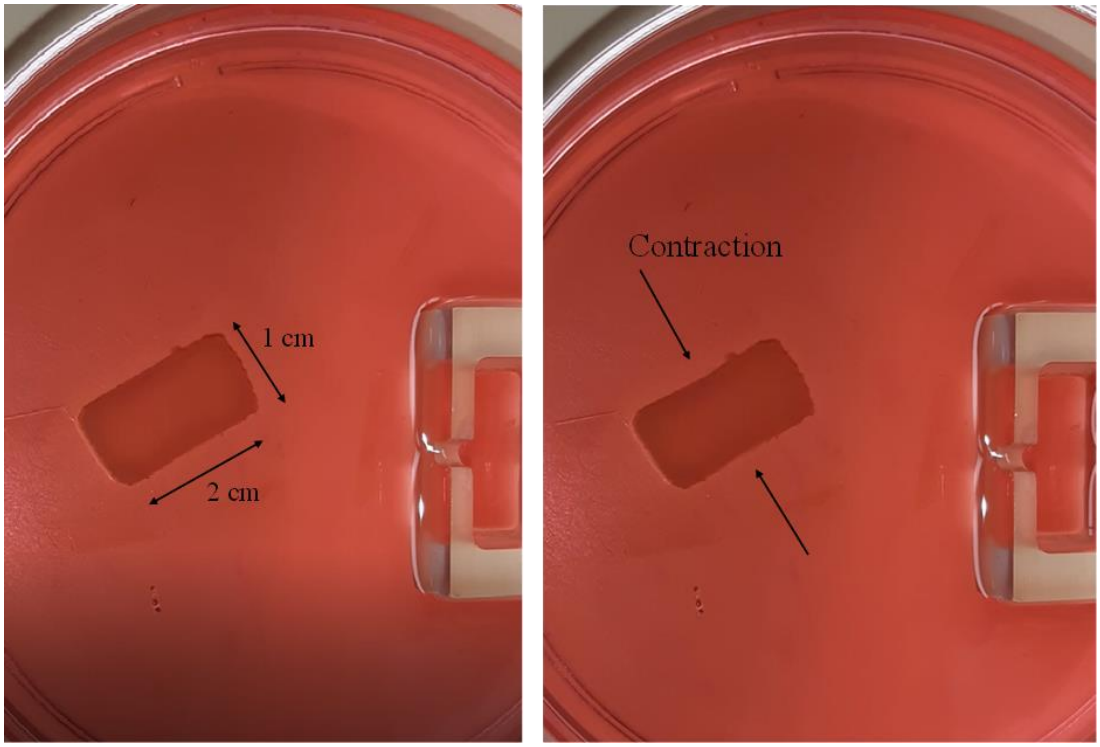

Figure S6: **Image of the thick 1x2 cm^2 thick LbL engineered cardiac tissue outside of its frame**

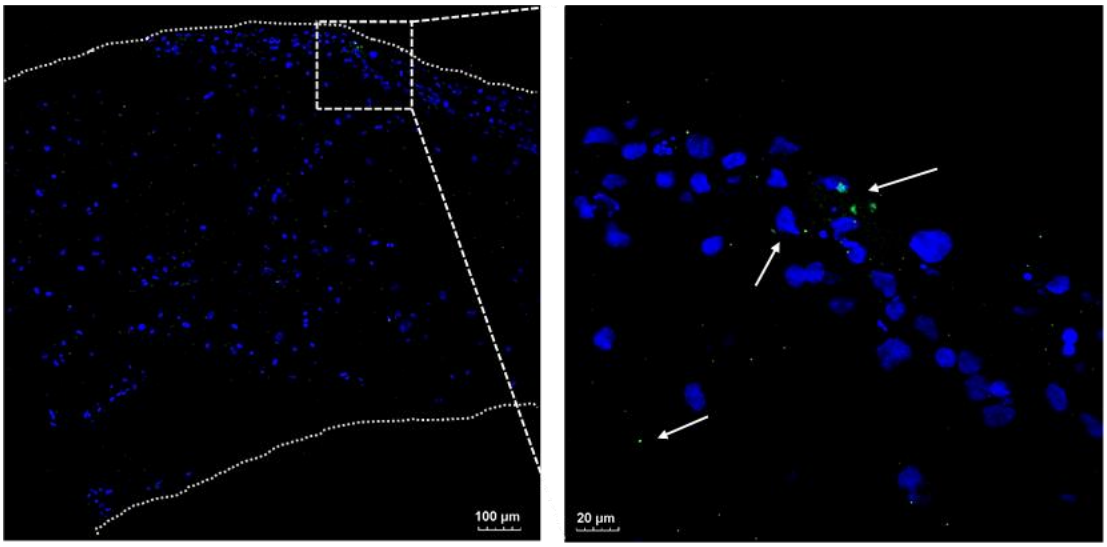

Figure S7: **Tri-lineage structure viability at 2 weeks.** Representative confocal micrograph of engineered LbL cardiac tissue displaying necrotic cells identified by the necrosis marker phosphorylated MLKL (Ser358, pMLKL) at week 2 of culture. Border indicated with short dashed line

All videos associated with this work, clips 1 and 2, are available online under doi:

10.3389/fcell.2021.670504

CHAPTER 4

DISCUSSION

Project Summary and Future Directions

In vitro models using hiPSC-derived cells that accurately mimic the native myocardium are exceptionally valuable tools for mechanistic studies, allowing for the modelling of complex interaction between cells as well as cells and their dynamic ECM surroundings. Moreover, these models are also promising therapeutic agents, though their full clinical potential is yet to be reached due to limitations associated with engineered tissue thickness, related to inadequate vascularization and subsequent nutrient limitations, mechanical mismatch between engineered tissues and the host environment and the immature nature of hiPSC-CMs, all of which contribute to structures that are not physiologically competitive. Herein, the development and characterization of a novel *in vitro* cardiac tissue engineering fabrication method utilizing hiPSC-derived cells has been described (see Chapters 2 for experimental setup), resulting in thick, viable cardiac tissue surrogates up to four weeks in culture. Full characterization of engineered cardiac tissue included histological analysis, determination of viscoelastic properties, analysis of tissue surrogate ultrastructure, as well as functional analysis via optical and electromechanical mapping.

In Chapter 3, additional the cellular representation of the native myocardium was mimicked further with the addition of cardiac FBs generated from hiPSCs (cFBs). Utilizing the LbL fabrication process developed and optimized in Chapter 2, the addition of cFBs yielded engineered cardiac tissue structures that surpassed any previously published reports in terms of thickness (~ 2.12 mm after 1 week in culture), while showing minimal evidence of necrosis (< 6 % after 4 weeks in culture). Furthermore, this fabrication method allowed for the generation of physiologically relevant conduction velocities, with velocities in excess of 40 cm/s recorded after 2 weeks in culture, finally almost reaching 50 cm/s after 4 weeks in culture (the highest ever recorded in 3D hiPSC-derived cellular structures).

A great deal of the future clinical success of cardiac patch treatments can, however, be broken up into the following subcategories: system optimization, relevant *in vivo* studies and their implications, and large scale manufacturing (see **Figure 1**).

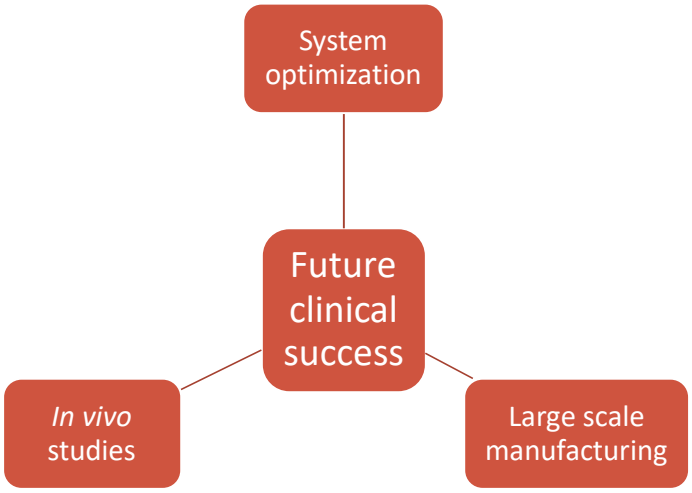

Figure 1: Considerations for future clinical success of cardiac patch treatments.

To further optimize the LbL system developed here and maximize its clinical potential, the immature nature of hiPSC-CMs needs to be addressed, certain mechanisms need to be elucidated, system mechanical properties need to be characterized further, and the potential *in vivo* implications of implanting this system need to be considered.

hiPSC-CM maturation

hiPSC-CM maturation can generally be achieved by either one or a combination of the following methods: mechanical stimulation, electrical stimulation, addition of small molecules, culturing in 3D/ECM interactions and extending culture periods [123, 148, 155, 160, 205-207]. Employing physical stimulation, whether through mechanical or electrical means, can accelerate hiPSC-CM maturation by promoting expression of contractile proteins and structural organization [123] , similar to what has been observed during natural development [208].

Mechanical stimulation. Tissues are commonly stimulated physically via either passive (also referred to as resistance to deformation) or active strain. Over the past decade, the application of passive stain has varied in approach, with one of the most readily used approaches being the mounting of fabricated tissues on top of posts with varying elasticity and ultimately resist deformation [209-211]. It has been shown that passive strain treatment of hiPSC-CM 3D engineered cardiac tissue promoted cell- and ECM alignment, enhanced myofibrillogenesis and sarcomeric banding, while also enhancing contractile protein expression, and force generation in comparison to control tissues [160]. Increasing the strain experienced by the engineered tissues in a stepwise fashion post-fabrication, also referred to as afterload, has been shown to further enhance engineered cardiac tissue conditioning yielding hypertrophic models [123, 212, 213]. These hypertrophic

models are associated with enhanced twitch force, sarcomeric length, CM size in terms of length and area as well as overall improvements in calcium handling ability.

Another method of mechanically stimulating cardiac tissue, to more closely mimic the repeated stresses experienced *in vivo*, is to employ cyclic strain and actively stimulate the structures. Numerous strains and frequencies have been applied to improve the maturation of hiPSC-CMs and their derived tissues [154, 214]. Devices and bioreactors have been designed to optimize hemodynamic loads experienced *in vivo* to more accurately recapitulate pressure/volume changes associated with heart development [215, 216]. These cyclic straining experiments have yielded enhancements in cellular and ECM alignment, significant enhancement in genes associated with physiological hypertrophy and ventricular CM development, enhanced ultrastructure development as well as potential changes to cellular metabolism.

Electrical stimulation. A vital property of CMs is their electromechanical excitability, where mechanical contraction and force generation are triggered by electrical depolarization [217]. Further mimicking of physical *in vivo* environments includes electrical stimulation, as these electrical signals are present throughout early development and later stages in life [218, 219].

To enhance cellular coupling and overall maturity of iPSC-CMs in engineered cardiac tissues, varying magnitudes and regimens of electrical stimulation have been investigated [220-222]. This electrical stimulation, or pacing, has been shown to be a very useful tool in manipulating the electrophysiological properties of cardiomyocytes, such as action potential, beat rate, action potential duration and conduction velocity [223]. Pacing

during *in vitro* culturing has been noted be of both structural and functional benefit to engineered cardiac tissue structures. hiPSC-CMs in 3D embryoid body format were stimulated for 7 days at frequencies ranging between 0.5 and 2 Hz, with unstimulated structures used as controls [223]. Electrically stimulated CM structures showed enhances gap junction expression levels, sarcomeric structure development, while also possessing the ability to tolerate rapid electrical pacing. The effect of electrical stimulation on some variations of thick cardiac engineered tissues, around 1 mm at the initiation of the stimulation protocol, has also been recorded. These constructs were exposed to progressively increasing stimulation frequencies over a 7-day period, from 1 Hz to 3 Hz (low frequency) or from 1 Hz to 6 Hz (high frequency) distinguish between any potential differences that stimulation rate may have on CM maturation [224]. Results obtained from the progressive increase from 1 to 6 Hz yielded the optimal results regarding cellular alignment, functional properties related to electrophysiology (conduction velocity, maximum capture rate) and subsequent calcium handling machinery, as well as ultrastructure development, demonstrating the causal relationship between stimulation rate and cardiac maturation.

Combined stimulation approaches. Under physiological conditions, cardiomyocytes experience cardiac electrical and mechanical stimuli as a result of various well-orchestrated physiological cues [225]. Combinations of these stimuli-based maturation regimens have been employed to optimize cardiac maturation past the capabilities of a single technique or approach, yielding more physiologically relevant CM morphologies, cardiac gene expression levels and force generation profiles [155, 226, 227]. Passive mechanical stimulation of thick cardiac engineered tissue (1.8 mm in diameter initially) in combination constant stimulation (2 Hz) or intensity training (initiated at 2 Hz, increased to 6 Hz over

a 3 week period) was compared to no stimulation [155]. Tissues from the intensity-training group showed compact and well-defined cardiac muscle structures as well as and significant changes in gene expression levels associated with more mature electrophysiological properties, including calcium handling machinery and subsequent conduction velocities. Ruan *et al*. [154] have also demonstrated combined approaches, specifically in the form of static stress conditioning combined with electrical stimulation, resulting in enhanced contractile function and maturation protein expression levels.

With this in mind, preliminary experiments were performed, using the LbL method, to fabricate thick (> 2 mm) hiPSC-CM-only cardiac engineered tissue as a platform for future, faster, more robust maturation approaches. Here we utilized passive mechanical stimulation (resistance to deformation) along with chronic biphasic electrical stimulation (C-Pace, IonOptix) [228-230] over a 7 day period, post tissue fabrication, to enhance the maturation of the hiPSC-CMs as well as the tissue overall. Four groups were evaluated, a control group (no stimulation), a stretch group (resistance to deformation only), a stretch + low voltage group (2 ms pulses, 2 Hz, 15 V) and a stretch + high voltage group (2 ms pulses, 2 Hz, 22 V). These relatively high voltages were employed to ensure signal capturing. Passive mechanical stimulation was achieved by mounting tissue (2 x 1 cm^2 in surface area) on to an array of stainless steel needles mounted in a PDMS base (**Figure 2** a). Tissue thickness post-fabrication was measured with a caliper (**Figure 2** b, n = 5), protein expression levels were qualified via confocal microscopy and whole-mount staining (See Chapters 2 and 3 for Materials and Methods), maturation markers

and relative protein expression levels were quantified via RT-PCR, while ultrastructure analysis was done through TEM.

Whole-mount staining showed structural alignment and protein expression were maximized with a combination of both resistance to deformation (stretch) and high voltage electrical stimulation treatment (**Figure 3** d). Sarcomeres became more delineated as indicated by cTnT and alpha actinin staining (**Figure 3**), suggestive of maturation.

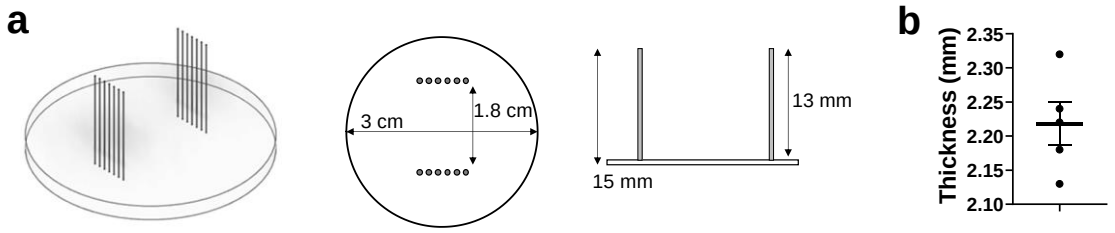

Figure 2: Maturation of thick, layered, hiPSC-CM-only tissue. (a) Passive mechanical stimulation of engineered cardiac tissues measuring 2x1 cm^2 can easily achieved by mounting onto highly flexible stainless steel needles. (b) hiPSC-CM-only tissue thickness post-fabrication, prior to initiation of maturation regimen, n = 5.

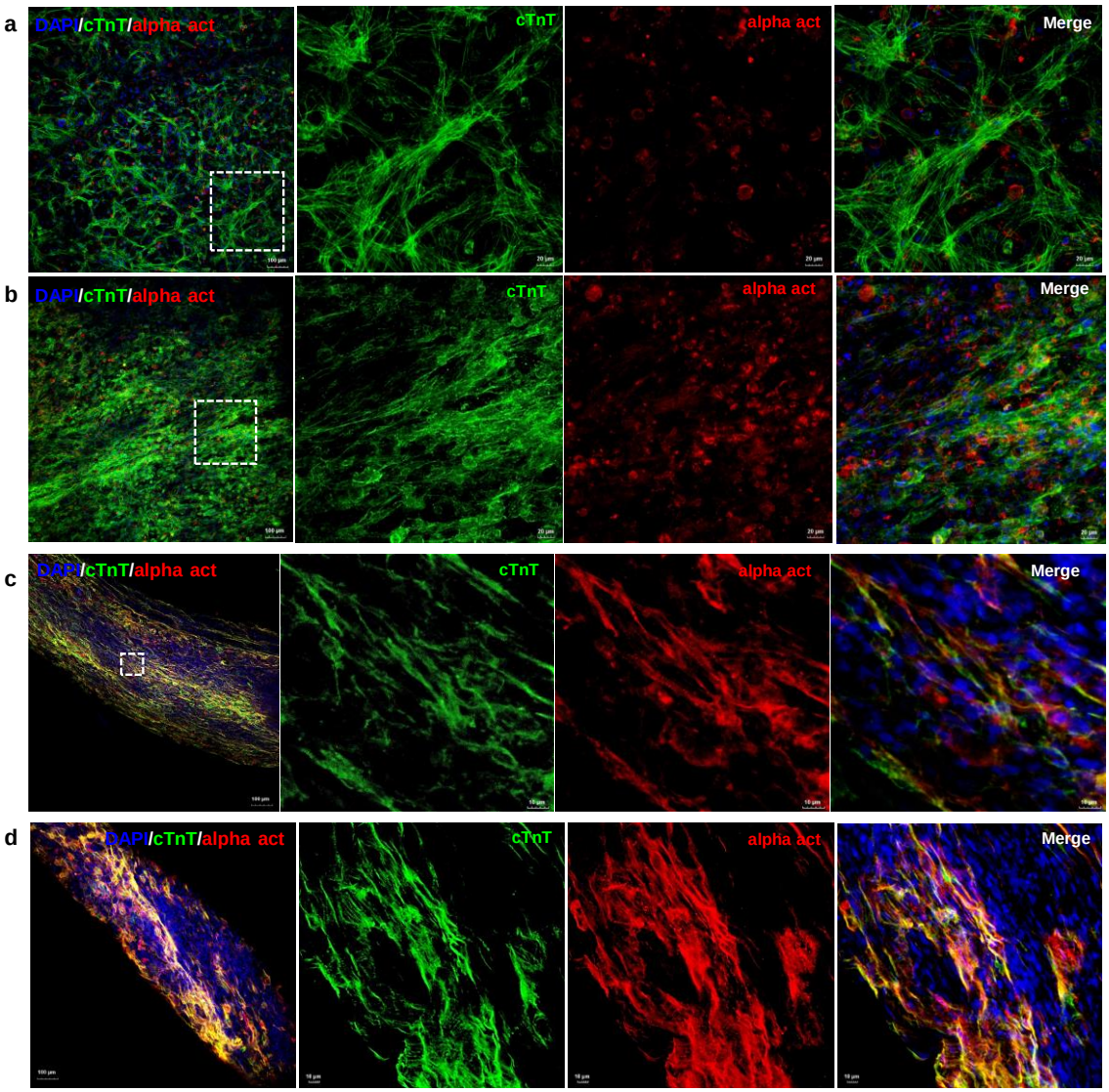

Figure 3: Whole-mount staining of thick hiPSC-CM-only tissue with DAPI, cTnT and alpha actinin of respective maturation approaches. (a) Control tissue, (b) resistance to deformation (stretch) tissue, (c) stretch + low voltage and (d) stretch + high voltage treatment.

Preliminary RNA analysis was performed on control samples as well as samples exposed to stretch + high voltage stimulation (n = 3 each, **Figure 4**). Quantitative comparison between these samples yielded significant improvement associated with stretch + high voltage treatment with respect to protein levels associated with muscle structure

development and contractility (**Figure 4** a), the development of calcium handling machinery and gap junctions (**Figure 4** b), as well as certain metabolic markers (**Figure 4** c). Specifically, decreased expression in α-MHC, along with enhancement in the ratio of β-MHC:α-MHC were noted, suggesting slower stronger contractions [150, 151]. Further phenotypic alterations were recorded with the downregulation of MLC2a and subsequent relative increase in the expression of MLC2v:MLC2a, showing a switch from a more atrial to a more ventricular phenotype [13, 15]. Upregulation of electromechanical coupling proteins such as N-cadherin was noted, suggesting enhanced maturation [153, 231]. Enhanced calcium handling machinery was evident in the stimulated engineered tissues by the increases in the expression levels of calsequestrin as well as the inward-rectifier potassium ion channel $K_{ir2.1}$, expressed by the gene KCNJ2 [232-234]. Even though there weren't statistically significant differences in the metabolic activity of the stimulated tissues (**Figure 4** c), the notable increased expression in PPARα (peroxisome proliferator activated receptor α), a fatty acid oxidation activator, is associated with cardiomyocyte maturation [161, 235, 236].

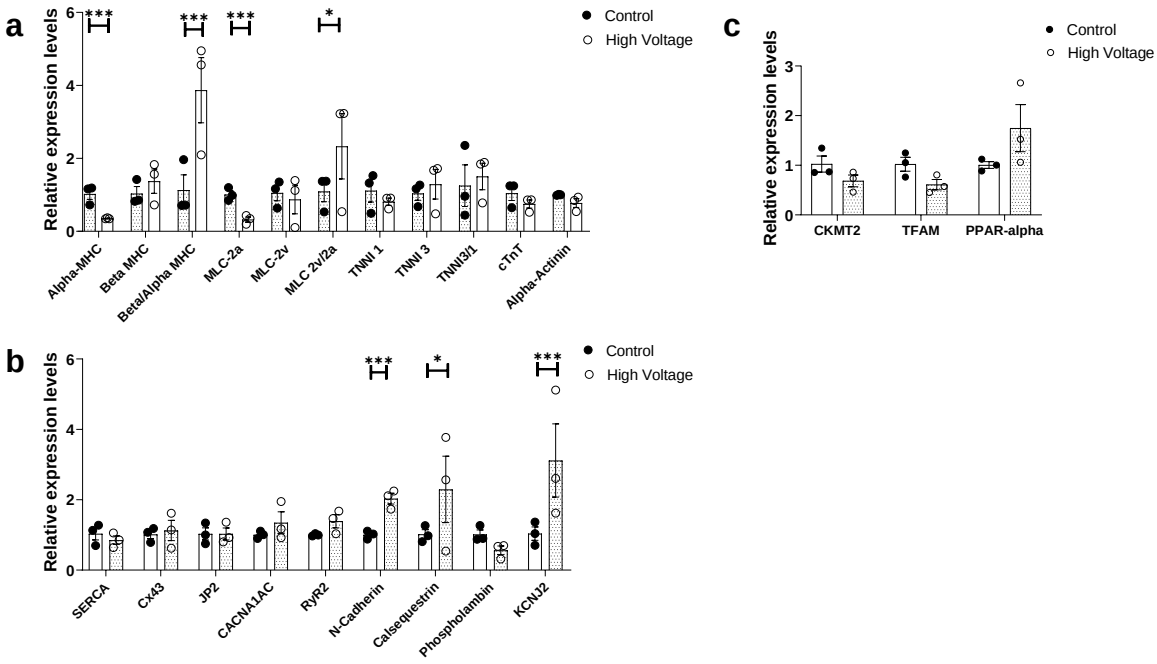

Figure 4: Protein expression levels of hiPSC-CM-only samples in control tissue versus tissue exposed to stretch + high voltage stimulation. The protein expression panels show the relative expression levels of each component normalized to GAPDH for (a) muscle structure and contractility associated proteins, (b) calcium handling machinery and jap junction development and, (c) metabolic markers, (n = 3, *p < 0.05, ***p < 0.005)

Functional analysis of the thick hiPSC-CM-only structures included ultrastructure analysis via TEM (**Figure 5**, n = 25). Qualitatively, stimulation, both mechanically and electrically, yielded enhanced structural alignment and ECM production. Quantitative analysis showed that the stimulation treatments all resulted in enhanced sarcomeric lengths as well, with control samples yielding 1.64 ± 0.02 µm, stretch samples 1.78 ± 0.06 µm, with both low and high voltage samples yielding physiologically relevant sarcomeric lengths [146, 147] at 1.80 ± 0.04 µm and 1.91 ± 0.02 µm, respectively (**Figure 5** e). In **Figure 5**, ZL represents Z-Lines, MC the mitochondria, GJ the gap junctions and N the nucleus.

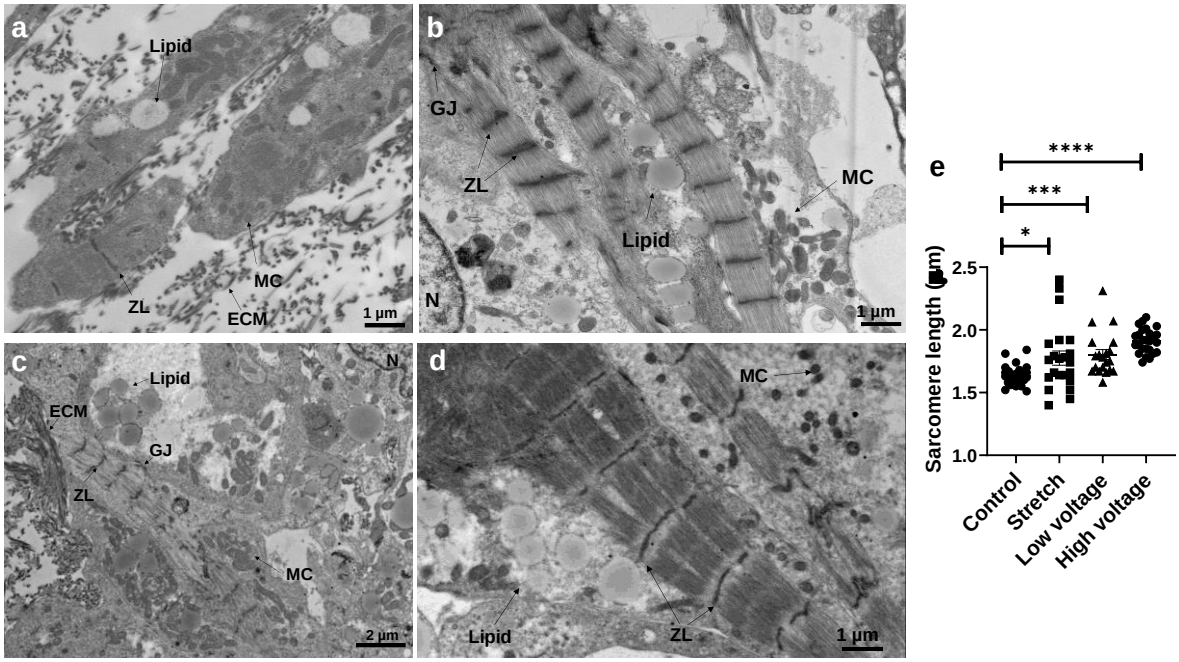

Figure 5: TEM analysis from respective hiPSC-CM-only maturation approaches. (a) Control tissue, (b) resistance to deformation (stretch) tissue, (c) stretch + low voltage, (d) stretch + high voltage treatment, and (e) the sarcomeric lengths of each treatment (n = 25, *p < 0.05, ***p < 0.005, ****p < 0.0001). ZL represents Z-Lines, MC the mitochondria, GJ the gap junctions and N the nucleus.

Moving forward, incorporation of supporting cell types, such as ECs, will be utilized to enhance vascularization potential of the tissues prior to employment of maturation regimens. Immunofluorescent staining for cell migration, cellular fate and system viability will be done to determine what the optimal maturation protocol for the LbL system is, and the degree of functional maturation as will be assessed by way of optical mapping, electromechanical mapping, and force generation capabilities.

Cell and molecular mechanisms

Further studies are, however, required to develop a better understanding of cellular interactions and how each cell type influences the engineered cardiac tissue, its development and remodeling as a whole [237-239]. Cardiac development is greatly influenced by supportive non-cardiac cells, such as FBs, ECs, SMCs, neural cells and immune cells, all

of which actively contribute to CM maturation through various cell-cell interactions and/or paracrine signaling [240-246]. Cardiac FBs, for example, have been shown to have stage-specific functions: early embryonic FBs promote CM proliferation via secretion of ECM factors, such as fibronectin, collagen and periostin, whereas adult FBs induce CM hypertrophy and sarcomere organization by secreting growth-related cytokines, such as interleukin 1 alpha (IL-1α) [241]. Co-culture of ECs with CMs has been shown to induce the upregulation of certain miRNAs in CMs [247]. When a cocktail of these miRNAs were introduced to human embryonic stem cell derived CMs, a more mature phenotype was induced. Tri-lineage 3D microtissues consisting of hiPSC-CMs, -ECs and -FBs have been used to study some of the cellular mechanisms between cardiac FBs, cardiac ECs and their specific effects on hiPSC-CMs [246]. Cultures containing cardiac FBs demonstrated enhanced sarcomeric structures with T-tubules, improved contractility and mitochondrial respiration and were also more electrophysiologically mature than those without cardiac FBs. Interactions allowing for this maturation included coupling between hiPSC-CMs and FBs via Cx43 gap junctions as well as upregulated intracellular cyclic AMP (cAMP, cyclic adenosine monophosphate). Not only are the exact molecular mechanisms that distinguish the LbL fabrication method from co-culture methods still unknown, but so too are the exact mechanisms driving the enhanced performance behind this optimized fabrication method. Moving forward, the potential paracrine signaling from hiPSC-ECs and hiPSC-FBs on thick 3D hiPSC-CM structures will be assessed via the addition of conditioned media from respective EC-only, FB-only, EC/FB, EC/CM, FB/CM, or CM/EC/FB cultures [248-251].

Mechanical testing and modeling

The mechanical properties of the heart can be studied and modeled under both passive and active conditions. In order to understand and model the active contractions of this complex organ – or even a subsection of the organ, such as one of its ventricle walls effectively – a clear understanding must first be gained under passive conditions [252]. Ideally, tissue engineered structures must exhibit tissue-like functional properties, including mechanical behavior comparable to the native tissues they are intended to replace. Moreover, the ability to reversibly undergo large strains can help to promote and guide tissue growth, and prevent potential mechanical mismatch [253]. Soft tissues consisting mostly of collagen, especially collagen 1, exhibit an exponential-like stress-strain response [254], primarily due to the straightening of the collagen fibers under increasing loads, with elastin contributing to the load-bearing in the low-strain region [255]. With the major increases noted in collagen production with the tri-lineage LbL engineered cardiac tissue, future in *ex vivo* mechanical testing and viscoelastic modeling will be performed through utilization of stress-relaxation tests in tension-mode [256-259].

In vivo whole-heart mechanical properties under active conditions, pre- and post-implantation of engineered cardiac tissue, will be assessed via pressure-volume (PV) loop measurement, by inserting a PV catheter into the ventricle lumen [260]. Chamber compliance, defined as the ratio of ventricular volume change over pressure change during a cardiac cycle ($\Delta V/\Delta P$) will be used to describe ventricular stiffness [261-263].

In vivo implications

During the culturing process, stresses exerted by iCMs and cFBs allow for compaction and alignment in the LbL engineered cardiac tissues. This alignment, although

optimal for tissue maturation, could influence the outcome of the structures when employed *in vivo*. Previous studies have shown that inappropriate transplantation methods yield regional heterogeneity and myofiber misalignment between the host and the implanted cells, resulting in lethal arrhythmia [264, 265]. The degree of alignment, or lack thereof, when implanted has also been found to greatly affect the degree of therapeutic improvement associated with cardiac muscle patches [266]. CMs and ECs were seeded on non-biodegradable nanofibrous electrospun patches created in two formats, one aligned with the direction of the heart's myofibers and one randomly oriented (**Figure 6**).

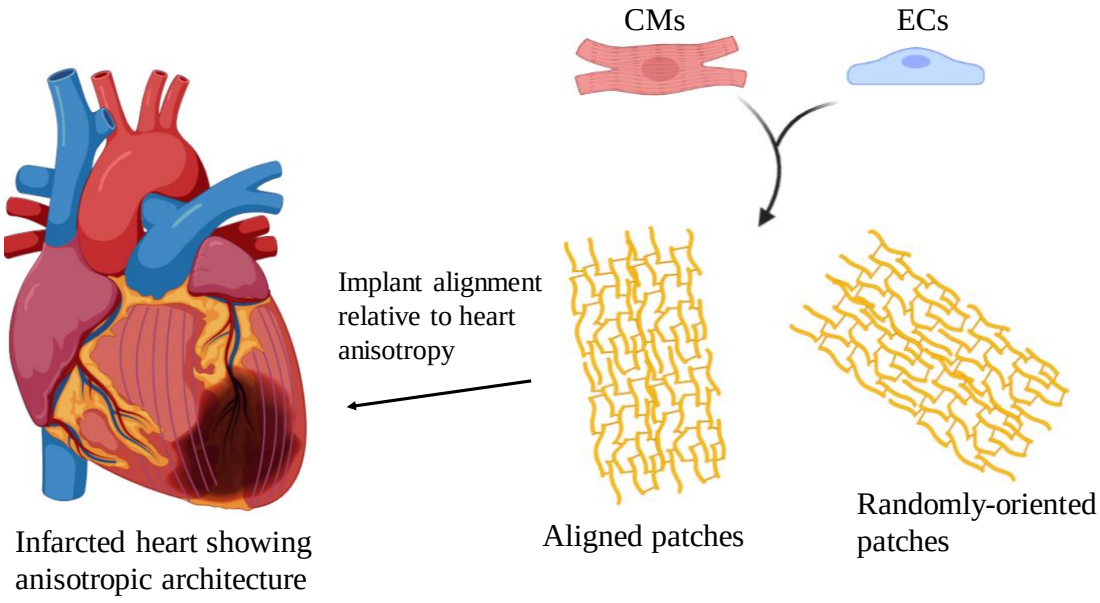

Figure 6: The anisotropic nature of the heart and how the architecture of implanted structures can affect it.

Analysis via atomic force microscopy (AFM) showed that CMs seeded on the aligned patches demonstrated enhanced beating frequency and amplitude than those seeded on randomly seeded patches. Implantation of these structures into an MI-mouse model showed that even though both structures provided mechanical support, alleviating cardiac remodeling, aligned patches resulted in significantly smaller infarct sizes 2

months post-MI. Further functional importance of alignment was demonstrated with *ex vivo* electrophysiological studies 7 days post-MI. Implantation of aligned patches preserved not only the anisotropic electro-conduction pattern, but also the conduction velocity, while randomly oriented patches resulted in conduction blocks between the host myocardium and the implanted tissue. Additionally, pacing of randomly oriented patch animals also resulted in ventricular tachycardia more frequently than animals with aligned patches.

Enhanced cellular and ECM alignment have not only been associated with enhanced electrophysiological properties, such as conduction velocities and action potential propagation, but also with enhanced isometric twitch force generation capabilities [267, 268]. Similar to the effect that tissue alignment has on the functional outcome and therapeutic success of the implanted structure, the effect of implantation orientation in terms of force generation needs to be considered as well, especially considering the complex anisotropic nature of the heart as a contractile organ.

Large scale manufacturing

In order to make engineered cardiac tissue patches a more economical solution in the future, certain considerations such as large scale production and long-term storage capabilities need to be considered. The use of cell-products, such as growth factors, RNAs and exosomes for example, as opposed to livings cells in these structures may offer one solution to some of the restrictions faced in this regard at present (**Figure 7**).

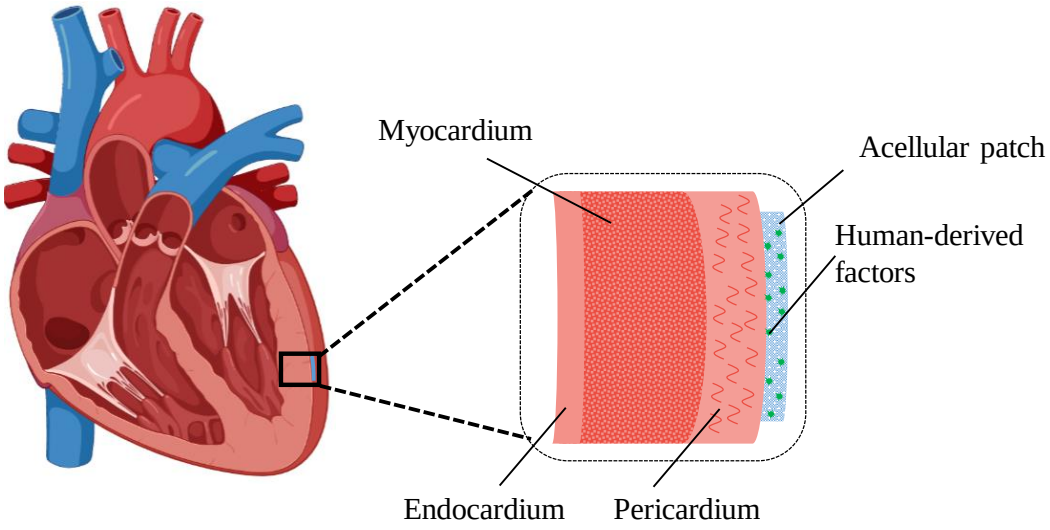

Figure 7: Acellular cardiac patch impregnated with human-derived factors enhances the possibilities of large scale manufacturing

By employing cell-products rather than cells, the potential for contamination and immune responses are reduced, the host's native cells can be recruited to the site of injury, and the engineered tissue constructs would be easier to store.

Conclusions

CVD is the leading cause of deaths globally, with patients suffering MIs representing almost 50 % of those deaths. At present, limited long-term viable treatment options exist for patients, yet with the discovery of and subsequent development of stem cell-based therapies, potential to remuscularize and revascularize the damaged myocardium has become more realistic and attainable.

Despite major strides made in the field of tissue engineering, the ability to generate tissues of a clinically relevant thickness has been hampered by diffusion limits of oxygen and nutrients, with tissue becoming necrotic within 100 – 200 μm of the boundary

conditions. Employing a LbL fabrication method, has however allowed for the production of cardiac tissue constructs from hiPSC-derived cells that exceed 2 mm in thickness with minimal necrosis (< 6 % after weeks in culture), while also mimicking the native myocardium in both form and function. Tri-lineage engineered cardiac tissues consisting of hiPSC-CMs, -ECs, and -FBs yielded physiologically relevant conduction velocities (> 30 cm/s) after 2 weeks in culture, with samples generating velocities as high as 49 cm/s after 4 weeks in culture.

Future directions associated with this research involve 1) the maturation of these hiPSC-derived structures with a combination of both electrical and mechanical stimulation, 2) elucidating the cellular and molecular mechanisms behind the enhanced electrophysiological performance observed with the addition of cFBs to the system, 3) determining the viscoelastic properties of the structures *in vitro* and how they are affected *in vivo*, 4) determining whether alignment and implantation orientation affect active mechanical properties such as twitch force generation capabilities and then determining what the optimal implantation orientation of these structures would be *in vivo* and 5) developing methods that would allow for large scale production of these engineered constructs.

GENERAL LIST OF REFERENCES

1. National Research Council Committee on AFfDaNToD. The National Academies Collection: Reports funded by National Institutes of Health *Toward Precision Medicine: Building a Knowledge Network for Biomedical Research and a New Taxonomy of Disease* Washington (DC): National Academies Press (US); 2011.

2. Ginsburg GS and Phillips KA. Precision Medicine: From Science To Value. *Health Aff (Millwood)*. 2018;37:694-701.

3. Nassar SF, Raddassi K, Ubhi B, Doktorski J and Abulaban A. Precision Medicine: Steps along the Road to Combat Human Cancer. *Cells*. 2020;9:2056.

4. Saidi RF and Hejazii Kenari SK. Challenges of organ shortage for transplantation: solutions and opportunities. *Int J Organ Transplant Med*. 2014;5:87-96.

5. Levitt M. Could the organ shortage ever be met? *Life Sciences, Society and Policy*. 2015;11:6.

6. Abouna GM. Organ shortage crisis: problems and possible solutions. *Transplantation proceedings*. 2008;40:34-8.

7. Goerler H, Simon A, Gohrbandt B, Hagl C, Oppelt P, Haverich A and Strueber M. Cardiac retransplantation: is it justified in times of critical donor organ shortage? Long-term single-center experience. *European Journal of Cardio-Thoracic Surgery*. 2008;34:1185-1190.

8. Everly MJ. Cardiac transplantation in the United States: an analysis of the UNOS registry. *Clinical transplants*. 2008:35-43.

9. Wang X, Yan Y and Zhang R. Recent trends and challenges in complex organ manufacturing. *Tissue engineering Part B, Reviews*. 2010;16:189-97.

10. Lenas P, Luyten FP, Doblare M, Nicodemou-Lena E and Lanzara AE. Modularity in Developmental Biology and Artificial Organs: A Missing Concept in Tissue Engineering. 2011;35:656-662.

11. Noor N, Shapira A, Edri R, Gal I, Wertheim L and Dvir T. 3D Printing of Personalized Thick and Perfusable Cardiac Patches and Hearts. 2019;6:1900344.

12. Burstein B, Libby E, Calderone A and Nattel S. Differential Behaviors of Atrial Versus Ventricular Fibroblasts. 2008;117:1630-1641.

13. Ng SY, Wong CK and Tsang SY. Differential gene expressions in atrial and ventricular myocytes: insights into the road of applying embryonic stem cell-derived cardiomyocytes for future therapies. 2010;299:C1234-C1249.

14. Cyganek L, Tiburcy M, Sekeres K, Gerstenberg K, Bohnenberger H, Lenz C, Henze S, Stauske M, Salinas G, Zimmermann W-H, Hasenfuss G and Guan K. Deep phenotyping of human induced pluripotent stem cell-derived atrial and ventricular cardiomyocytes. *JCI insight*. 2018;3:e99941.

15. Goldfracht I, Protze S, Shiti A, Setter N, Gruber A, Shaheen N, Nartiss Y, Keller G and Gepstein L. Generating ring-shaped engineered heart tissues from ventricular and atrial human pluripotent stem cell-derived cardiomyocytes. *Nature Communications*. 2020;11:75.

16. Boyett MR, Honjo H and Kodama I. The sinoatrial node, a heterogeneous pacemaker structure. *Cardiovasc Res*. 2000;47:658-687.

17. Unudurthi SD, Wolf RM and Hund TJ. Role of sinoatrial node architecture in maintaining a balanced source-sink relationship and synchronous cardiac pacemaking. 2014;5.

18. Laird RJ and Irwin S. Chapter 1 - Cardiovascular Structure and Function. In: S. Irwin and J. S. Tecklin, eds. *Cardiopulmonary Physical Therapy (Fourth Edition)* Saint Louis: Mosby; 2004: 3-38.

19. Greenbaum RA, Ho SY, Gibson DG, Becker AE and Anderson RH. Left ventricular fibre architecture in man. *Br Heart J*. 1981;45:248-263.

20. Balakumar P, Maung UK and Jagadeesh G. Prevalence and prevention of cardiovascular disease and diabetes mellitus. *Pharmacological research*. 2016;113:600-609.

21. Joseph P, Leong D, McKee M, Anand SS, Schwalm JD, Teo K, Mente A and Yusuf S. Reducing the Global Burden of Cardiovascular Disease, Part 1: The Epidemiology and Risk Factors. *Circ Res*. 2017;121:677-694.

22. Benjamin EJ, Blaha MJ, Chiuve SE, Cushman M, Das SR, Deo R, Ferranti SDd, Floyd J, Fornage M, Gillespie C, Isasi CR, Jiménez MC, Jordan LC, Judd SE, Lackland D, Lichtman JH, Lisabeth L, Liu S, Longenecker CT, Mackey RH, Matsushita K, Mozaffarian D, Mussolino ME, Nasir K, Neumar RW, Palaniappan L, Pandey DK, Thiagarajan RR, Reeves MJ, Ritchey M, Rodriguez CJ, Roth GA, Rosamond WD, Sasson C, Towfighi A, Tsao CW, Turner MB, Virani SS, Voeks JH, Willey JZ, Wilkins JT, Wu JH, Alger HM, Wong SS and Muntner P. Heart Disease and Stroke Statistics, 2014 - 2017 Update: A Report From the American Heart Association. 2017;135:e146-e603.

23. Thygesen K, Alpert JS and White HD. Universal Definition of Myocardial Infarction. 2007;116:2634-2653.

24. Libby P and Theroux P. Pathophysiology of Coronary Artery Disease. 2005;111:3481-3488.

25. Prabhu SD and Frangogiannis NG. The Biological Basis for Cardiac Repair After Myocardial Infarction: From Inflammation to Fibrosis. *Circ Res*. 2016;119:91-112.

26. Tzahor E and Poss KD. Cardiac regeneration strategies: Staying young at heart. *Science (New York, NY)*. 2017;356:1035-1039.

27. Mollova M, Bersell K, Walsh S, Savla J, Das LT, Park S-Y, Silberstein LE, dos Remedios CG, Graham D, Colan S and Kühn B. Cardiomyocyte proliferation contributes to heart growth in young humans. 2013;110:1446-1451.

28. Vadakke-Madathil S and Chaudhry HW. Cardiac Regeneration. 2018;123:24-26.

29. van Nieuwenhoven FA and Turner NA. The role of cardiac fibroblasts in the transition from inflammation to fibrosis following myocardial infarction. *Vascular Pharmacology*. 2013;58:182-188.

30. Sutton MGSJ and Sharpe N. Left Ventricular Remodeling After Myocardial Infarction. 2000;101:2981-2988.

31. Firth BG and Dunnmon PM. Left ventricular dilatation and failure post-myocardial infarction: pathophysiology and possible pharmacologic interventions. *Cardiovascular drugs and therapy*. 1990;4:1363-74.

32. Rumberger JA. Ventricular dilatation and remodeling after myocardial infarction. *Mayo Clinic proceedings*. 1994;69:664-74.

33. Di Napoli P, Taccardi AA, Grilli A, Felaco M, Balbone A, Angelucci D, Gallina S, Calafiore AM, De Caterina R and Barsotti A. Left ventricular wall stress as a direct correlate of cardiomyocyte apoptosis in patients with severe dilated cardiomyopathy. *American heart journal*. 2003;146:1105-11.

34. French BA and Kramer CM. Mechanisms of Post-Infarct Left Ventricular Remodeling. *Drug Discov Today Dis Mech*. 2007;4:185-196.

35. Ong SB, Hernández-Reséndiz S, Crespo-Avilan GE, Mukhametshina RT, Kwek XY, Cabrera-Fuentes HA and Hausenloy DJ. Inflammation following acute myocardial infarction: Multiple players, dynamic roles, and novel therapeutic opportunities. *Pharmacology & therapeutics*. 2018;186:73-87.

36. Bhar-Amato J, Davies W and Agarwal S. Ventricular Arrhythmia after Acute Myocardial Infarction: 'The Perfect Storm'. *Arrhythmia & electrophysiology review*. 2017;6:134-139.

37. Nguyen HL, Saczynski JS, Gore JM, Waring ME, Lessard D, Yarzebski J, Reed G, Spencer FA, Li SX and Goldberg RJ. Long-term trends in short-term outcomes in acute myocardial infarction. *The American journal of medicine*. 2011;124:939-46.

38. Maher JF, Mallory GK and Laurenz GA. Rupture of the Heart after Myocardial Infarction. 1956;255:1-10.

39. Fletcher AP, Alkjaersig N, Smyrniotis FE and Sherry S. The treatment of patients suffering from early myocardial infarction with massive and prolonged streptokinase therapy. *Transactions of the Association of American Physicians*. 1958;71:287-296.

40. Manning AS and Hearse DJ. Reperfusion-induced arrhythmias: mechanisms and prevention. *Journal of molecular and cellular cardiology*. 1984;16:497-518.

41. Braunwald E and Kloner RA. Myocardial reperfusion: a double-edged sword? *J Clin Invest*. 1985;76:1713-9.

42. Murphy E and Steenbergen C. Mechanisms Underlying Acute Protection From Cardiac Ischemia-Reperfusion Injury. 2008;88:581-609.

43. Verma S, Fedak PWM, Weisel RD, Butany J, Rao V, Maitland A, Li R-K, Dhillon B and Yau TM. Fundamentals of Reperfusion Injury for the Clinical Cardiologist. 2002;105:2332-2336.

44. Miura T and Miki T. Limitation of myocardial infarct size in the clinical setting: current status and challenges in translating animal experiments into clinical therapy. *Basic research in cardiology*. 2008;103:501-13.

45. Yellon DM and Hausenloy DJ. Myocardial Reperfusion Injury. 2007;357:1121-1135.

46. Huang S and Frangogiannis NG. Anti-inflammatory therapies in myocardial infarction: failures, hopes and challenges. 2018;175:1377-1400.

47. May MRL, Wells GA, Labinaz M, Davies RF, Turek M, Leddy D, Maloney J, McKibbin T, Quinn B, Beanlands RS, Glover C, Marquis J-F, O'Brien ER, Williams WL and Higginson LA. Combined Angioplasty and Pharmacological Intervention Versus Thrombolysis Alone in Acute Myocardial Infarction (CAPITAL AMI Study). 2005;46:417-424.

48. Cantor WJ, Fitchett D, Borgundvaag B, Ducas J, Heffernan M, Cohen EA, Morrison LJ, Langer A, Dzavik V, Mehta SR, Lazzam C, Schwartz B, Casanova A and Goodman SG. Routine Early Angioplasty after Fibrinolysis for Acute Myocardial Infarction. 2009;360:2705-2718.

49. Kulik A, Ruel M, Jneid H, Ferguson TB, Hiratzka LF, Ikonomidis JS, Lopez-Jimenez F, McNallan SM, Patel M, Roger VL, Sellke FW, Sica DA and Zimmerman L. Secondary Prevention After Coronary Artery Bypass Graft Surgery. 2015;131:927-964.

50. Henderson R, Bucknall C, Timmis A, Karani S, Dritsas A and Sowton E. Clinical outcome of coronary angioplasty for single-vessel disease. *The Lancet*. 1989;334:546-550.

51. Kilic A, Acker MA and Atluri P. Dealing with surgical left ventricular assist device complications. *Journal of thoracic disease*. 2015;7:2158-64.

52. Ranganath NK, Nafday HB, Zias E, Hisamoto K, Chen S, Kon ZN, Galloway AC, Moazami N and Smith DE. Concomitant temporary mechanical support in high-risk coronary artery bypass surgery. *Journal of cardiac surgery*. 2019;34:1569-1572.

53. Chachques JC, Jegaden O, Mesana T, Glock Y, Grandjean PA and Carpentier AF. Cardiac bioassist: results of the French multicenter cardiomyoplasty study. *Asian cardiovascular & thoracic annals*. 2009;17:573-80.

54. Lembcke A, Dushe S, Enzweiler CNH, Kloeters C, Wiese TH, Hermann K-GA, Hamm B and Konertz WF. Passive external cardiac constraint improves segmental left ventricular wall motion and reduces akinetic area in patients with non-ischemic dilated cardiomyopathy. *European Journal of Cardio-Thoracic Surgery*. 2004;25:84-90.

55. Raman JS, Power JM, Buxton BF, Alferness C and Hare D. Ventricular containment as an adjunctive procedure in ischemic cardiomyopathy: early results. *The Annals of Thoracic Surgery*. 2000;70:1124-1126.

56. Raman JS, Hata M, Storer M, Power JM, Buxton BF, Alferness C and Hare D. The mid-term results of ventricular containment (ACORN WRAP) for end-stage ischemic cardiomyopathy. *Annals of thoracic and cardiovascular surgery : official journal of the Association of Thoracic and Cardiovascular Surgeons of Asia*. 2001;7:278-81.

57. Konertz WF, Shapland JE, Hotz H, Dushe S, Braun JP, Stantke K and Kleber FX. Passive Containment and Reverse Remodeling by a Novel Textile Cardiac Support Device. 2001;104:I-270-I-275.

58. Speziale G, Nasso G, Piancone F, Generali K, Paterno C, Miccoli A, Fiore F, Del Prete A, Del Prete G, Lopriore V, Spirito F, Caldarola P, Paparella D, Massari F and Tavazzi L. One-year results after implantation of the CorCap for dilated cardiomyopathy and heart failure. *Ann Thorac Surg*. 2011;91:1356-62.

59. Park J, Choi S, Janardhan AH, Lee S-Y, Raut S, Soares J, Shin K, Yang S, Lee C, Kang K-W, Cho HR, Kim SJ, Seo P, Hyun W, Jung S, Lee H-J, Lee N, Choi SH, Sacks M, Lu N, Josephson ME, Hyeon T, Kim D-H and Hwang HJ. Electromechanical cardioplasty using a wrapped elasto-conductive epicardial mesh. 2016;8:344ra86-344ra86.

60. Goonoo N, Bhaw-Luximon A, Bowlin GL and Jhurry D. An assessment of biopolymer- and synthetic polymer-based scaffolds for bone and vascular tissue engineering. 2013;62:523-533.

61. Zhu J and Marchant RE. Design properties of hydrogel tissue-engineering scaffolds. *Expert Review of Medical Devices*. 2011;8:607-626.

62. Yamazaki Y, Eguchi S, Miyamura H, Hayashi J, Fukuda J, Ozeki H, Yoshimura T, Fujita Y and Tsuchiya A. Replacement of myocardium with a Dacron prosthesis for complications of acute myocardial infarction. *The Journal of cardiovascular surgery*. 1989;30:277-80.

63. Liu Y, He T and Gao C. Surface modification of poly(ethylene terephthalate) via hydrolysis and layer-by-layer assembly of chitosan and chondroitin sulfate to construct cytocompatible layer for human endothelial cells. *Colloids and Surfaces B: Biointerfaces*. 2005;46:117-126.

64. Cristallini C, Vaccari G, Barbani N, Cibrario Rocchietti E, Barberis R, Falzone M, Cabiale K, Perona G, Bellotti E, Rastaldo R, Pascale S, Pagliaro P and Giachino C. Cardioprotection of PLGA/gelatine cardiac patches functionalised with adenosine in a large animal model of ischaemia and reperfusion injury: A feasibility study. 2019;13:1253-1264.

65. Noori A, Ashrafi SJ, Vaez-Ghaemi R, Hatamian-Zaremi A and Webster TJ. A review of fibrin and fibrin composites for bone tissue engineering. *Int J Nanomedicine*. 2017;12:4937-4961.

66. Linnes MP, Ratner BD and Giachelli CM. A fibrinogen-based precision microporous scaffold for tissue engineering. *Biomaterials*. 2007;28:5298-5306.

67. Kitsara M, Joanne P, Boitard SE, Ben Dhiab I, Poinard B, Menasché P, Gagnieu C, Forest P, Agbulut O and Chen Y. Fabrication of cardiac patch by using electrospun collagen fibers. *Microelectronic Engineering*. 2015;144:46-50.

68. Miyagi Y, Chiu LLY, Cimini M, Weisel RD, Radisic M and Li R-K. Biodegradable collagen patch with covalently immobilized VEGF for myocardial repair. *Biomaterials*. 2011;32:1280-1290.

69. Weisel JW. Structure of fibrin: impact on clot stability. 2007;5:116-124.

70. Feng X, Clark RAF, Galanakis D and Tonnesen MG. Fibrin and Collagen Differentially Regulate Human Dermal Microvascular Endothelial Cell Integrins: Stabilization of αv/β3 mRNA by Fibrin1. *Journal of Investigative Dermatology*. 1999;113:913-919.

71. Chung E, Rytlewski JA, Merchant AG, Dhada KS, Lewis EW and Suggs LJ. Fibrin-based 3D matrices induce angiogenic behavior of adipose-derived stem cells. *Acta Biomaterialia*. 2015;17:78-88.

72. Morin KT and Tranquillo RT. In vitro models of angiogenesis and vasculogenesis in fibrin gel. *Experimental Cell Research*. 2013;319:2409-2417.

73. Tang J, Vandergriff A, Wang Z, Hensley MT, Cores J, Allen TA, Dinh P-U, Zhang J, Caranasos TG and Cheng K. A Regenerative Cardiac Patch Formed by Spray Painting of Biomaterials onto the Heart. *Tissue Eng Part C Methods*. 2017;23:146-155.

74. Badylak SF, Lantz GC, Coffey A and Geddes LA. Small intestinal submucosa as a large diameter vascular graft in the dog. *The Journal of surgical research*. 1989;47:74-80.

75. Badylak SF. Xenogeneic extracellular matrix as a scaffold for tissue reconstruction. *Transplant immunology*. 2004;12:367-77.

76. Robinson KA, Li J, Mathison M, Redkar A, Cui J, Chronos NA, Matheny RG and Badylak SF. Extracellular matrix scaffold for cardiac repair. *Circulation*. 2005;112:I135-43.

77. Badylak SF and Gilbert TW. Immune response to biologic scaffold materials. *Seminars in Immunology*. 2008;20:109-116.

78. Ott HC, Matthiesen TS, Goh SK, Black LD, Kren SM, Netoff TI and Taylor DA. Perfusion-decellularized matrix: using nature's platform to engineer a bioartificial heart. *Nat Med*. 2008;14:213-21.

79. Song JJ and Ott HC. Organ engineering based on decellularized matrix scaffolds. *Trends in Molecular Medicine*. 2011;17:424-432.

80. Bursac N, Papadaki M, Cohen RJ, Schoen FJ, Eisenberg SR, Carrier R, Vunjak-Novakovic G and Freed LE. Cardiac muscle tissue engineering: toward an in vitro model for electrophysiological studies. 1999;277:H433-H444.

81. Baar K, Birla R, Boluyt MO, Borschel GH, Arruda EM and Dennis RG. Self-organization of rat cardiac cells into contractile 3-D cardiac tissue. 2005;19:1-21.

82. Rau T, Nose M, Remmers U, Weil J, Weiβmüller A, Davia K, Harding S, Peppel K, Koch WJ and Eschenhagen T. Overexpression of wild-type Gαi-2 suppresses β-adrenergic signaling in cardiac myocytes. 2003;17:1-23.

83. Zong X, Bien H, Chung C-Y, Yin L, Fang D, Hsiao BS, Chu B and Entcheva E. Electrospun fine-textured scaffolds for heart tissue constructs. *Biomaterials*. 2005;26:5330-5338.

84. Engelmayr GC, Jr., Cheng M, Bettinger CJ, Borenstein JT, Langer R and Freed LE. Accordion-like honeycombs for tissue engineering of cardiac anisotropy. *Nature materials*. 2008;7:1003-10.

85. Li RK, Jia ZQ, Weisel RD, Mickle DA, Choi A and Yau TM. Survival and function of bioengineered cardiac grafts. *Circulation*. 1999;100:Ii63-9.

86. Zimmermann WH, Fink C, Kralisch D, Remmers U, Weil J and Eschenhagen T. Three-dimensional engineered heart tissue from neonatal rat cardiac myocytes. *Biotechnology and bioengineering*. 2000;68:106-14.

87. Zimmermann WH, Melnychenko I, Wasmeier G, Didié M, Naito H, Nixdorff U, Hess A, Budinsky L, Brune K, Michaelis B, Dhein S, Schwoerer A, Ehmke H and Eschenhagen T. Engineered heart tissue grafts improve systolic and diastolic function in infarcted rat hearts. *Nat Med*. 2006;12:452-8.

88. Furuta A, Miyoshi S, Itabashi Y, Shimizu T, Kira S, Hayakawa K, Nishiyama N, Tanimoto K, Hagiwara Y, Satoh T, Fukuda K, Okano T and Ogawa S. Pulsatile Cardiac Tissue Grafts Using a Novel Three-Dimensional Cell Sheet Manipulation Technique Functionally Integrates With the Host Heart, In Vivo. 2006;98:705-712.

89. Menasché P. Cell therapy trials for heart regeneration — lessons learned and future directions. *Nature Reviews Cardiology*. 2018;15:659-671.

90. Yanamandala M, Zhu W, Garry DJ, Kamp TJ, Hare JM, Jun H-w, Yoon Y-s, Bursac N, Prabhu SD, Dorn GW, Bolli R, Kitsis RN and Zhang J. Overcoming the Roadblocks to Cardiac Cell Therapy Using Tissue Engineering. *Journal of the American College of Cardiology*. 2017;70:766-775.

91. Sánchez PL, Fernández-Santos ME, Costanza S, Climent AM, Moscoso I, Gonzalez-Nicolas MA, Sanz-Ruiz R, Rodríguez H, Kren SM, Garrido G, Escalante JL, Bermejo J, Elizaga J, Menarguez J, Yotti R, Pérez del Villar C, Espinosa MA, Guillem MS, Willerson JT, Bernad A, Matesanz R, Taylor DA and Fernández-Avilés F. Acellular human heart matrix: A critical step toward whole heart grafts. *Biomaterials*. 2015;61:279-89.

92. Bissell MJ and Aggeler J. Dynamic reciprocity: how do extracellular matrix and hormones direct gene expression? *Progress in clinical and biological research*. 1987;249:251-62.

93. Chagastelles PC and Nardi NB. Biology of stem cells: an overview. *Kidney International Supplements*. 2011;1:63-67.

94. Messina E, Angelis LD, Frati G, Morrone S, Chimenti S, Fiordaliso F, Salio M, Battaglia M, Latronico MVG, Coletta M, Vivarelli E, Frati L, Cossu G and Giacomello A. Isolation and Expansion of Adult Cardiac Stem Cells From Human and Murine Heart. 2004;95:911-921.

95. Zhang JZ, Guo H and Wu JC. Applications of genetically engineered human pluripotent stem cell reporters in cardiac stem cell biology. *Current Opinion in Biotechnology*. 2018;52:66-73.

96. Bolli R, Hare JM, March KL, Pepine CJ, Willerson JT, Perin EC, Yang PC, Henry TD, Traverse JH, Mitrani RD, Khan A, Hernandez-Schulman I, Taylor DA, DiFede DL, Lima JAC, Chugh A, Loughran J, Vojvodic RW, Sayre SL, Bettencourt J, Cohen M, Moyé L, Ebert RF and Simari RD. Rationale and Design of the CONCERT-HF Trial (Combination of Mesenchymal and c-kit Cardiac Stem Cells As Regenerative Therapy for Heart Failure). 2018;122:1703-1715.

97. Torella D, Ellison GM, Nadal-Ginard B and Indolfi C. Cardiac Stem and Progenitor Cell Biology for Regenerative Medicine. *Trends in Cardiovascular Medicine*. 2005;15:229-236.

98. Wu SM, Chien KR and Mummery C. Origins and Fates of Cardiovascular Progenitor Cells. *Cell*. 2008;132:537-543.

99. Xia H, Li X, Gao W, Fu X, Fang RH, Zhang L and Zhang K. Tissue repair and regeneration with endogenous stem cells. *Nature Reviews Materials*. 2018;3:174-193.

100. Weissman IL. Stem cells: units of development, units of regeneration, and units in evolution. *Cell*. 2000;100:157-68.

101. Evans MJ and Kaufman MH. Establishment in culture of pluripotential cells from mouse embryos. *Nature*. 1981;292:154-156.

102. Thomson JA, Itskovitz-Eldor J, Shapiro SS, Waknitz MA, Swiergiel JJ, Marshall VS and Jones JM. Embryonic stem cell lines derived from human blastocysts. *Science (New York, NY)*. 1998;282:1145-7.

103. Itskovitz-Eldor J, Schuldiner M, Karsenti D, Eden A, Yanuka O, Amit M, Soreq H and Benvenisty N. Differentiation of human embryonic stem cells into embryoid bodies compromising the three embryonic germ layers. *Molecular medicine (Cambridge, Mass)*. 2000;6:88-95.

104. Takahashi K and Yamanaka S. Induction of Pluripotent Stem Cells from Mouse Embryonic and Adult Fibroblast Cultures by Defined Factors. *Cell*. 2006;126:663-676.

105. Yu J, Vodyanik MA, Smuga-Otto K, Antosiewicz-Bourget J, Frane JL, Tian S, Nie J, Jonsdottir GA, Ruotti V, Stewart R, Slukvin, II and Thomson JA. Induced pluripotent stem cell lines derived from human somatic cells. *Science (New York, NY)*. 2007;318:1917-20.

106. Boyer LA, Lee TI, Cole MF, Johnstone SE, Levine SS, Zucker JP, Guenther MG, Kumar RM, Murray HL, Jenner RG, Gifford DK, Melton DA, Jaenisch R and Young RA. Core transcriptional regulatory circuitry in human embryonic stem cells. *Cell*. 2005;122:947-56.

107. Balsam LB, Wagers AJ, Christensen JL, Kofidis T, Weissman IL and Robbins RC. Haematopoietic stem cells adopt mature haematopoietic fates in ischaemic myocardium. *Nature*. 2004;428:668-673.

108. Murry CE, Soonpaa MH, Reinecke H, Nakajima H, Nakajima HO, Rubart M, Pasumarthi KB, Virag JI, Bartelmez SH, Poppa V, Bradford G, Dowell JD, Williams DA and Field LJ. Haematopoietic stem cells do not transdifferentiate into cardiac myocytes in myocardial infarcts. *Nature*. 2004;428:664-8.

109. Asahara T, Masuda H, Takahashi T, Kalka C, Pastore C, Silver M, Kearne M, Magner M and Isner JM. Bone marrow origin of endothelial progenitor cells responsible for postnatal vasculogenesis in physiological and pathological neovascularization. *Circ Res*. 1999;85:221-8.

110. Assmus B, Schächinger V, Teupe C, Britten M, Lehmann R, Döbert N, Grünwald F, Aicher A, Urbich C, Martin H, Hoelzer D, Dimmeler S and Zeiher AM. Transplantation of Progenitor Cells and Regeneration Enhancement in Acute Myocardial Infarction (TOPCARE-AMI). *Circulation*. 2002;106:3009-17.

111. Schächinger V, Erbs S, Elsässer A, Haberbosch W, Hambrecht R, Hölschermann H, Yu J, Corti R, Mathey DG, Hamm CW, Süselbeck T, Assmus B, Tonn T, Dimmeler S and Zeiher AM. Intracoronary bone marrow-derived progenitor cells in acute myocardial infarction. *The New England journal of medicine*. 2006;355:1210-21.

112. Niebruegge S, Bauwens CL, Peerani R, Thavandiran N, Masse S, Sevaptisidis E, Nanthakumar K, Woodhouse K, Husain M, Kumacheva E and Zandstra PW. Generation of human embryonic stem cell-derived mesoderm and cardiac cells using size-specified aggregates in an oxygen-controlled bioreactor. *Biotechnology and bioengineering*. 2009;102:493-507.

113. Niebruegge S, Nehring A, Bär H, Schroeder M, Zweigerdt R and Lehmann J. Cardiomyocyte production in mass suspension culture: embryonic stem cells as a source for great amounts of functional cardiomyocytes. *Tissue engineering Part A*. 2008;14:1591-601.

114. Bursac N. Cardiac tissue engineering using stem cells. *IEEE engineering in medicine and biology magazine : the quarterly magazine of the Engineering in Medicine & Biology Society*. 2009;28:80, 82, 84-6, 88-9.

115. Zimmermann W-H and Eschenhagen T. Embryonic Stem Cells for Cardiac Muscle Engineering. *Trends in Cardiovascular Medicine*. 2007;17:134-140.

116. Morizane A, Doi D, Kikuchi T, Okita K, Hotta A, Kawasaki T, Hayashi T, Onoe H, Shiina T, Yamanaka S and Takahashi J. Direct comparison of autologous and allogeneic transplantation of iPSC-derived neural cells in the brain of a non-human primate. *Stem Cell Reports*. 2013;1:283-92.

117. Li C, Chen S, Zhou Y, Zhao Y, Liu P and Cai J. Application of induced pluripotent stem cell transplants: Autologous or allogeneic? *Life Sciences*. 2018;212:145-149.

118. Gao L, Gregorich ZR, Zhu W, Mattapally S, Oduk Y, Lou X, Kannappan R, Borovjagin AV, Walcott GP, Pollard AE, Fast VG, Hu X, Lloyd SG, Ge Y and Zhang J. Large Cardiac Muscle Patches Engineered From Human Induced-Pluripotent Stem Cell-Derived Cardiac Cells Improve Recovery From Myocardial Infarction in Swine. *Circulation*. 2018;137:1712-1730.

119. Zhang J, Tao R, Campbell KF, Carvalho JL, Ruiz EC, Kim GC, Schmuck EG, Raval AN, da Rocha AM, Herron TJ, Jalife J, Thomson JA and Kamp TJ. Functional cardiac fibroblasts derived from human pluripotent stem cells via second heart field progenitors. *Nature Communications*. 2019;10:2238.

120. Ye L, Basu J and Zhang J. Fabrication of a myocardial patch with cells differentiated from human-induced pluripotent stem cells. *Methods in molecular biology (Clifton, NJ)*. 2015;1299:103-14.

121. Zhang J, Wilson GF, Soerens AG, Koonce CH, Yu J, Palecek SP, Thomson JA and Kamp TJ. Functional cardiomyocytes derived from human induced pluripotent stem cells. *Circ Res*. 2009;104:e30-41.

122. Lemoine MD, Krause T, Koivumäki JT, Prondzynski M, Schulze ML, Girdauskas E, Willems S, Hansen A, Eschenhagen T and Christ T. Human Induced Pluripotent Stem Cell-Derived Engineered Heart Tissue as a Sensitive Test System for QT Prolongation and Arrhythmic Triggers. 2018;11:e006035.

123. Leonard A, Bertero A, Powers JD, Beussman KM, Bhandari S, Regnier M, Murry CE and Sniadecki NJ. Afterload promotes maturation of human induced pluripotent stem cell derived cardiomyocytes in engineered heart tissues. *Journal of molecular and cellular cardiology*. 2018;118:147-158.

124. Mannhardt I, Breckwoldt K, Letuffe-Brenière D, Schaaf S, Schulz H, Neuber C, Benzin A, Werner T, Eder A, Schulze T, Klampe B, Christ T, Hirt Marc N, Huebner N, Moretti A, Eschenhagen T and Hansen A. Human Engineered Heart Tissue: Analysis of Contractile Force. *Stem Cell Reports*. 2016;7:29-42.

125. Schaaf S, Eder A, Vollert I, Stöhr A, Hansen A and Eschenhagen T. Generation of strip-format fibrin-based engineered heart tissue (EHT). *Methods in molecular biology (Clifton, NJ)*. 2014;1181:121-9.

126. Wang Q, Yang H, Bai A, Jiang W, Li X, Wang X, Mao Y, Lu C, Qian R, Guo F, Ding T, Chen H, Chen S, Zhang J, Liu C and Sun N. Functional engineered human cardiac patches prepared from nature's platform improve heart function after acute myocardial infarction. *Biomaterials*. 2016;105:52-65.

127. Weinberger F, Breckwoldt K, Pecha S, Kelly A, Geertz B, Starbatty J, Yorgan T, Cheng K-H, Lessmann K, Stolen T, Scherrer-Crosbie M, Smith G, Reichenspurner H, Hansen A and Eschenhagen T. Cardiac repair in guinea pigs with human engineered heart tissue from induced pluripotent stem cells. 2016;8:363ra148-363ra148.

128. Wendel JS, Ye L, Tao R, Zhang J, Zhang J, Kamp TJ and Tranquillo RT. Functional Effects of a Tissue-Engineered Cardiac Patch From Human Induced Pluripotent Stem Cell-Derived Cardiomyocytes in a Rat Infarct Model. *Stem Cells Transl Med*. 2015;4:1324-1332.

129. Khan M, Xu Y, Hua S, Johnson J, Belevych A, Janssen PML, Gyorke S, Guan J and Angelos MG. Evaluation of Changes in Morphology and Function of Human Induced Pluripotent Stem Cell Derived Cardiomyocytes (HiPSC-CMs) Cultured on an Aligned-Nanofiber Cardiac Patch. *PloS one*. 2015;10:e0126338.

130. Ye L, Chang YH, Xiong Q, Zhang P, Zhang L, Somasundaram P, Lepley M, Swingen C, Su L, Wendel JS, Guo J, Jang A, Rosenbush D, Greder L, Dutton JR, Zhang J, Kamp TJ, Kaufman DS, Ge Y and Zhang J. Cardiac repair in a porcine model of acute myocardial infarction with human induced pluripotent stem cell-derived cardiovascular cells. *Cell Stem Cell*. 2014;15:750-61.

131. Gao L, Kupfer ME, Jung JP, Yang L, Zhang P, Sie YD, Tran Q, Ajeti V, Freeman BT, Fast VG, Campagnola PJ, Ogle BM and Zhang J. Myocardial Tissue Engineering With Cells Derived From Human-Induced Pluripotent Stem Cells and a Native-Like, High-Resolution, 3-Dimensionally Printed Scaffold. 2017;120:1318-1325.

132. Devalla HD, Schwach V, Ford JW, Milnes JT, El-Haou S, Jackson C, Gkatzis K, Elliott DA, Chuva de Sousa Lopes SM, Mummery CL, Verkerk AO and Passier R. Atrial-like cardiomyocytes from human pluripotent stem cells are a robust preclinical model for assessing atrial-selective pharmacology. *EMBO molecular medicine*. 2015;7:394-410.

133. Lee JH, Protze SI, Laksman Z, Backx PH and Keller GM. Human Pluripotent Stem Cell-Derived Atrial and Ventricular Cardiomyocytes Develop from Distinct Mesoderm Populations. *Cell Stem Cell*. 2017;21:179-194.e4.

134. Chen Z, Xian W, Bellin M, Dorn T, Tian Q, Goedel A, Dreizehnter L, Schneider CM, Ward-van Oostwaard D, Ng JK, Hinkel R, Pane LS, Mummery CL, Lipp P, Moretti A, Laugwitz KL and Sinnecker D. Subtype-specific promoter-driven action potential imaging for precise disease modelling and drug testing in hiPSC-derived cardiomyocytes. *European heart journal*. 2017;38:292-301.

135. Protze SI, Liu J, Nussinovitch U, Ohana L, Backx PH, Gepstein L and Keller GM. Sinoatrial node cardiomyocytes derived from human pluripotent cells function as a biological pacemaker. *Nature Biotechnology*. 2017;35:56-68.

136. Abdelwahid E, Kalvelyte A, Stulpinas A, de Carvalho KA, Guarita-Souza LC and Foldes G. Stem cell death and survival in heart regeneration and repair. *Apoptosis : an international journal on programmed cell death*. 2016;21:252-68.

137. Bolli R. Repeated Cell Therapy: A Paradigm Shift Whose Time Has Come. *Circ Res*. 2017;120:1072-1074.

138. Fishbein MC, Maclean D and Maroko PR. Experimental myocardial infarction in the rat: qualitative and quantitative changes during pathologic evolution. *The American journal of pathology*. 1978;90:57-70.

139. Synnergren J, Améen C, Jansson A and Sartipy P. Global transcriptional profiling reveals similarities and differences between human stem cell-derived cardiomyocyte clusters and heart tissue. *Physiological genomics*. 2012;44:245-58.

140. Robertson C, Tran DD and George SC. Concise review: maturation phases of human pluripotent stem cell-derived cardiomyocytes. *Stem cells (Dayton, Ohio)*. 2013;31:829-37.

141. Yang X, Pabon L and Murry CE. Engineering Adolescence. 2014;114:511-523.

142. Tu C, Chao BS and Wu JC. Strategies for Improving the Maturity of Human Induced Pluripotent Stem Cell-Derived Cardiomyocytes. 2018;123:512-514.

143. Scuderi GJ and Butcher J. Naturally Engineered Maturation of Cardiomyocytes. *Front Cell Dev Biol*. 2017;5:50-50.

144. Feric NT and Radisic M. Maturing human pluripotent stem cell-derived cardiomyocytes in human engineered cardiac tissues. *Advanced drug delivery reviews*. 2016;96:110-34.

145. Mollova M, Bersell K, Walsh S, Savla J, Das LT, Park SY, Silberstein LE, Dos Remedios CG, Graham D, Colan S and Kühn B. Cardiomyocyte proliferation contributes to heart growth in young humans. *Proceedings of the National Academy of Sciences of the United States of America*. 2013;110:1446-51.

146. Renshaw A. Rubin's Pathology. Clinicopathologic Foundations of Medicine. 2008;15:125.

147. Ribeiro MC, Tertoolen LG, Guadix JA, Bellin M, Kosmidis G, D'Aniello C, Monshouwer-Kloots J, Goumans MJ, Wang YL, Feinberg AW, Mummery CL and Passier R. Functional maturation of human pluripotent stem cell derived cardiomyocytes in vitro--correlation between contraction force and electrophysiology. *Biomaterials*. 2015;51:138-150.

148. Lundy SD, Zhu WZ, Regnier M and Laflamme MA. Structural and functional maturation of cardiomyocytes derived from human pluripotent stem cells. *Stem cells and development*. 2013;22:1991-2002.

149. Kotini M, Barriga EH, Leslie J, Gentzel M, Rauschenberger V, Schambony A and Mayor R. Gap junction protein Connexin-43 is a direct transcriptional regulator of N-cadherin in vivo. *Nature Communications*. 2018;9:3846.

150. Reiser PJ, Portman MA, Ning X-H and Moravec CS. Human cardiac myosin heavy chain isoforms in fetal and failing adult atria and ventricles. 2001;280:H1814-H1820.

151. Allen DL and Leinwand LA. Postnatal Myosin Heavy Chain Isoform Expression in Normal Mice and Mice Null for IIb or IId Myosin Heavy Chains. *Developmental Biology*. 2001;229:383-395.

152. Sottas V, Wahl CM, Trache MC, Bartolf-Kopp M, Cambridge S, Hecker M and Ullrich ND. Improving electrical properties of iPSC-cardiomyocytes by enhancing Cx43 expression. *Journal of molecular and cellular cardiology*. 2018;120:31-41.

153. Lou X, Zhao M, Fan C, Fast VG, Valarmathi MT, Zhu W and Zhang J. N-cadherin overexpression enhances the reparative potency of human-induced pluripotent stem cell-derived cardiac myocytes in infarcted mouse hearts. *Cardiovasc Res*. 2020;116:671-685.

154. Ruan JL, Tulloch NL, Razumova MV, Saiget M, Muskheli V, Pabon L, Reinecke H, Regnier M and Murry CE. Mechanical Stress Conditioning and Electrical Stimulation Promote Contractility and Force Maturation of Induced Pluripotent Stem Cell-Derived Human Cardiac Tissue. *Circulation*. 2016;134:1557-1567.

155. Ronaldson-Bouchard K, Ma SP, Yeager K, Chen T, Song L, Sirabella D, Morikawa K, Teles D, Yazawa M and Vunjak-Novakovic G. Advanced maturation of human cardiac tissue grown from pluripotent stem cells. *Nature*. 2018;556:239-243.

156. Lee P, Klos M, Bollensdorff C, Hou L, Ewart P, Kamp TJ, Zhang J, Bizy A, Guerrero-Serna G, Kohl P, Jalife J and Herron TJ. Simultaneous Voltage and Calcium Mapping of Genetically Purified Human Induced Pluripotent Stem Cell-Derived Cardiac Myocyte Monolayers. 2012;110:1556-1563.

157. Valderrábano M. Influence of anisotropic conduction properties in the propagation of the cardiac action potential. *Progress in Biophysics and Molecular Biology*. 2007;94:144-168.

158. Keung W, Boheler KR and Li RA. Developmental cues for the maturation of metabolic, electrophysiological and calcium handling properties of human pluripotent stem cell-derived cardiomyocytes. *Stem Cell Research & Therapy*. 2014;5:17.

159. Itzhaki I, Rapoport S, Huber I, Mizrahi I, Zwi-Dantsis L, Arbel G, Schiller J and Gepstein L. Calcium handling in human induced pluripotent stem cell derived cardiomyocytes. *PloS one*. 2011;6:e18037.

160. Tulloch NL, Muskheli V, Razumova MV, Korte FS, Regnier M, Hauch KD, Pabon L, Reinecke H and Murry CE. Growth of engineered human myocardium with mechanical loading and vascular coculture. *Circ Res*. 2011;109:47-59.

161. Lopaschuk GD and Jaswal JS. Energy metabolic phenotype of the cardiomyocyte during development, differentiation, and postnatal maturation. *Journal of cardiovascular pharmacology*. 2010;56:130-40.

162. Horikoshi Y, Yan Y, Terashvili M, Wells C, Horikoshi H, Fujita S, Bosnjak ZJ and Bai X. Fatty Acid-Treated Induced Pluripotent Stem Cell-Derived Human Cardiomyocytes Exhibit Adult Cardiomyocyte-Like Energy Metabolism Phenotypes. *Cells*. 2019;8.

163. Ho SY. Anatomy and myoarchitecture of the left ventricular wall in normal and in disease. *European journal of echocardiography : the journal of the Working Group on Echocardiography of the European Society of Cardiology*. 2009;10:iii3-7.

164. Lee PT, Dweck MR, Prasher S, Shah A, Humphries SE, Pennell DJ, Montgomery HE and Payne JR. Left Ventricular Wall Thickness and the Presence of Asymmetric Hypertrophy in Healthy Young Army Recruits. 2013;6:262-267.

165. Richardson JJ, Björnmalm M and Caruso F. Technology-driven layer-by-layer assembly of nanofilms. 2015;348:aaa2491.

166. Zhang X, Chen H and Zhang H. Layer-by-layer assembly: from conventional to unconventional methods. *Chemical Communications*. 2007:1395-1405.

167. Kirkland JJ. Porous Thin-Layer Modified Glass Bead Supports for Gas Liquid Chromatography. *Analytical Chemistry*. 1965;37:1458-1461.

168. Jin W, Toutianoush A and Tieke B. Use of Polyelectrolyte Layer-by-Layer Assemblies as Nanofiltration and Reverse Osmosis Membranes. *Langmuir*. 2003;19:2550-2553.

169. Siepmann J and Peppas NAJPR. Hydrophilic Matrices for Controlled Drug Delivery: An Improved Mathematical Model to Predict the Resulting Drug Release Kinetics (the “sequential Layer” Model). 2000;17:1290-1298.

170. Donath E, Sukhorukov GB, Caruso F, Davis SA and Möhwald H. Novel Hollow Polymer Shells by Colloid-Templated Assembly of Polyelectrolytes. 1998;37:2201-2205.

171. Dreaden EC, Morton SW, Shopsowitz KE, Choi J-H, Deng ZJ, Cho N-J and Hammond PT. Bimodal Tumor-Targeting from Microenvironment Responsive Hyaluronan Layer-by-Layer (LbL) Nanoparticles. *ACS Nano*. 2014;8:8374-8382.

172. Cui J, Liu Y and Hao J. Multiwalled Carbon-Nanotube-Embedded Microcapsules and Their Electrochemical Behavior. *The Journal of Physical Chemistry C*. 2009;113:3967-3972.

173. Lulevich VV, Andrienko D and Vinogradova OI. Elasticity of polyelectrolyte multilayer microcapsules. 2004;120:3822-3826.

174. Best JP, Neubauer MP, Javed S, Dam HH, Fery A and Caruso F. Mechanics of pH-Responsive Hydrogel Capsules. *Langmuir*. 2013;29:9814-9823.

175. Shimizu T, Yamato M, Kikuchi A and Okano T. Two-Dimensional Manipulation of Cardiac Myocyte Sheets Utilizing Temperature-Responsive Culture Dishes Augments the Pulsatile Amplitude. 2001;7:141-151.

176. Okano T, Yamada N, Sakai H and Sakurai Y. A novel recovery system for cultured cells using plasma-treated polystyrene dishes grafted with poly(N-isopropylacrylamide). *Journal of biomedical materials research*. 1993;27:1243-51.

177. Bischofberger I and Trappe V. New aspects in the phase behaviour of poly-N-isopropyl acrylamide: systematic temperature dependent shrinking of PNiPAM assemblies well beyond the LCST. *Scientific Reports*. 2015;5:15520.

178. Shimizu T, Yamato M, Isoi Y, Akutsu T, Setomaru T, Abe K, Kikuchi A, Umezu M and Okano T. Fabrication of Pulsatile Cardiac Tissue Grafts Using a Novel 3-Dimensional Cell Sheet Manipulation Technique and Temperature-Responsive Cell Culture Surfaces. 2002;90:e40-e48.

179. Haraguchi Y, Shimizu T, Yamato M, Kikuchi A and Okano T. Electrical coupling of cardiomyocyte sheets occurs rapidly via functional gap junction formation. *Biomaterials*. 2006;27:4765-74.

180. Kawamura M, Miyagawa S, Miki K, Saito A, Fukushima S, Higuchi T, Kawamura T, Kuratani T, Daimon T, Shimizu T, Okano T and Sawa Y. Feasibility, safety, and therapeutic efficacy of human induced pluripotent stem cell-derived cardiomyocyte sheets in a porcine ischemic cardiomyopathy model. *Circulation*. 2012;126:S29-37.

181. Matsuo T, Masumoto H, Tajima S, Ikuno T, Katayama S, Minakata K, Ikeda T, Yamamizu K, Tabata Y, Sakata R and Yamashita JK. Efficient long-term survival of cell grafts after myocardial infarction with thick viable cardiac tissue entirely from pluripotent stem cells. *Scientific Reports*. 2015;5:16842.

182. Qasim M, Haq F, Kang MH and Kim JH. 3D printing approaches for cardiac tissue engineering and role of immune modulation in tissue regeneration. *Int J Nanomedicine*. 2019;14:1311-1333.

183. Ong CS, Fukunishi T, Zhang H, Huang CY, Nashed A, Blazeski A, DiSilvestre D, Vricella L, Conte J, Tung L, Tomaselli GF and Hibino N. Biomaterial-Free Three-

Dimensional Bioprinting of Cardiac Tissue using Human Induced Pluripotent Stem Cell Derived Cardiomyocytes. *Scientific Reports*. 2017;7:4566.

184. Fleischer S, Feiner R and Dvir T. Cutting-edge platforms in cardiac tissue engineering. *Current Opinion in Biotechnology*. 2017;47:23-29.

185. LaBarge W, Morales A, Pretorius D, Kahn-Krell AM, Kannappan R and Zhang J. Scaffold-Free Bioprinter Utilizing Layer-By-Layer Printing of Cellular Spheroids. *Micromachines*. 2019;10.

186. Tsukamoto Y, Akagi T and Akashi M. Vascularized cardiac tissue construction with orientation by layer-by-layer method and 3D printer. *Scientific Reports*. 2020;10:5484.

187. Yeung E, Fukunishi T, Bai Y, Bedja D, Pitaktong I, Mattson G, Jeyaram A, Lui C, Ong CS, Inoue T, Matsushita H, Abdollahi S, Jay SM and Hibino N. Cardiac regeneration using human-induced pluripotent stem cell-derived biomaterial-free 3D-bioprinted cardiac patch in vivo. 2019;13:2031-2039.

188. Vihola H, Laukkanen A, Valtola L, Tenhu H and Hirvonen J. Cytotoxicity of thermosensitive polymers poly(N-isopropylacrylamide), poly(N-vinylcaprolactam) and amphiphilically modified poly(N-vinylcaprolactam). *Biomaterials*. 2005;26:3055-3064.

189. Cooperstein MA and Canavan HE. Assessment of cytotoxicity of (N-isopropyl acrylamide) and poly(N-isopropyl acrylamide)-coated surfaces. *Biointerphases*. 2013;8:19.

190. Capella V, Rivero RE, Liaudat AC, Ibarra LE, Roma DA, Alustiza F, Mañas F, Barbero CA, Bosch P, Rivarola CR and Rodriguez N. Cytotoxicity and bioadhesive properties of poly-N-isopropylacrylamide hydrogel. *Heliyon*. 2019;5:e01474.

191. Yogev S, Shabtay-Orbach A, Nyska A and Mizrahi B. Local Toxicity of Topically Administrated Thermoresponsive Systems: In Vitro Studies with In Vivo Correlation. 2019;47:426-432.

192. Oliver Cassell CS, Stefan Hofer OP, Morrison WA and Knight KR. Vascularisation of tissue-engineered grafts: the regulation of angiogenesis in reconstructive surgery and in disease states. *British Journal of Plastic Surgery*. 2002;55:603-610.

193. Risau W. Mechanisms of angiogenesis. *Nature*. 1997;386:671-674.

194. Ishaug-Riley SL, Crane-Kruger GM, Yaszemski MJ and Mikos AG. Three-dimensional culture of rat calvarial osteoblasts in porous biodegradable polymers. *Biomaterials*. 1998;19:1405-1412.

195. Radisic M, Yang L, Boublik J, Cohen RJ, Langer R, Freed LE and Vunjak-Novakovic G. Medium perfusion enables engineering of compact and contractile cardiac tissue. 2004;286:H507-H516.

196. Radisic M, Malda J, Epping E, Geng W, Langer R and Vunjak-Novakovic G. Oxygen gradients correlate with cell density and cell viability in engineered cardiac tissue. 2006;93:332-343.

197. Shadrin IY, Allen BW, Qian Y, Jackman CP, Carlson AL, Juhas ME and Bursac N. Cardiopatch platform enables maturation and scale-up of human pluripotent stem cell-derived engineered heart tissues. *Nature Communications*. 2017;8:1825.

198. Griffith CK, Miller C, Sainson RC, Calvert JW, Jeon NL, Hughes CC and George SC. Diffusion limits of an in vitro thick prevascularized tissue. *Tissue engineering*. 2005;11:257-66.

199. Radisic M, Marsano A, Maidhof R, Wang Y and Vunjak-Novakovic G. Cardiac tissue engineering using perfusion bioreactor systems. *Nat Protoc*. 2008;3:719-38.

200. Brown MA, Iyer RK and Radisic M. Pulsatile perfusion bioreactor for cardiac tissue engineering. 2008;24:907-920.

201. Jackman CP, Ganapathi AM, Asfour H, Qian Y, Allen BW, Li Y and Bursac N. Engineered cardiac tissue patch maintains structural and electrical properties after epicardial implantation. *Biomaterials*. 2018;159:48-58.

202. Almeida SO, Skelton RJ, Adigopula S and Ardehali R. Arrhythmia in stem cell transplantation. *Cardiac electrophysiology clinics*. 2015;7:357-70.

203. Huang NF, Serpooshan V, Morris VB, Sayed N, Pardon G, Abilez OJ, Nakayama KH, Pruitt BL, Wu SM, Yoon Y-s, Zhang J and Wu JC. Big bottlenecks in cardiovascular tissue engineering. *Communications Biology*. 2018;1:199.

204. Bursac N, Loo Y, Leong K and Tung L. Novel anisotropic engineered cardiac tissues: studies of electrical propagation. *Biochemical and biophysical research communications*. 2007;361:847-853.

205. Kamakura T, Makiyama T, Sasaki K, Yoshida Y, Wuriyanghai Y, Chen J, Hattori T, Ohno S, Kita T, Horie M, Yamanaka S and Kimura T. Ultrastructural maturation of human-induced pluripotent stem cell-derived cardiomyocytes in a long-term culture. *Circulation journal : official journal of the Japanese Circulation Society*. 2013;77:1307-14.

206. McDevitt TC, Laflamme MA and Murry CE. Proliferation of cardiomyocytes derived from human embryonic stem cells is mediated via the IGF/PI 3-kinase/Akt signaling pathway. *Journal of molecular and cellular cardiology*. 2005;39:865-73.

207. Parikh SS, Blackwell DJ, Gomez-Hurtado N, Frisk M, Wang L, Kim K, Dahl CP, Fiane A, Tønnessen T, Kryshtal DO, Louch WE and Knollmann BC. Thyroid and Glucocorticoid Hormones Promote Functional T-Tubule Development in Human-Induced Pluripotent Stem Cell-Derived Cardiomyocytes. *Circ Res*. 2017;121:1323-1330.

208. Damon BJ, Rémond MC, Bigelow MR, Trusk TC, Xie W, Perucchio R, Sedmera D, Denslow S and Thompson RP. Patterns of muscular strain in the embryonic heart wall. *Developmental dynamics : an official publication of the American Association of Anatomists*. 2009;238:1535-46.

209. Boudou T, Legant WR, Mu A, Borochin MA, Thavandiran N, Radisic M, Zandstra PW, Epstein JA, Margulies KB and Chen CS. A microfabricated platform to measure and manipulate the mechanics of engineered cardiac microtissues. *Tissue engineering Part A*. 2012;18:910-9.

210. Abilez OJ, Tzatzalos E, Yang H, Zhao MT, Jung G, Zöllner AM, Tiburcy M, Riegler J, Matsa E, Shukla P, Zhuge Y, Chour T, Chen VC, Burridge PW, Karakikes I, Kuhl E, Bernstein D, Couture LA, Gold JD, Zimmermann WH and Wu JC. Passive Stretch Induces Structural and Functional Maturation of Engineered Heart Muscle as Predicted by Computational Modeling. *Stem cells (Dayton, Ohio)*. 2018;36:265-277.

211. Rodriguez ML, Graham BT, Pabon LM, Han SJ, Murry CE and Sniadecki NJ. Measuring the contractile forces of human induced pluripotent stem cell-derived cardiomyocytes with arrays of microposts. *J Biomech Eng*. 2014;136:051005.

212. Hirt MN, Sörensen NA, Bartholdt LM, Boeddinghaus J, Schaaf S, Eder A, Vollert I, Stöhr A, Schulze T, Witten A, Stoll M, Hansen A and Eschenhagen T. Increased afterload induces pathological cardiac hypertrophy: a new in vitro model. *Basic research in cardiology*. 2012;107:307.

213. Werner TR, Kunze A-C, Stenzig J, Eschenhagen T and Hirt MN. Blockade of miR-140-3p prevents functional deterioration in afterload-enhanced engineered heart tissue. *Scientific Reports*. 2019;9:11494.

214. Mihic A, Li J, Miyagi Y, Gagliardi M, Li S-H, Zu J, Weisel RD, Keller G and Li R-K. The effect of cyclic stretch on maturation and 3D tissue formation of human embryonic stem cell-derived cardiomyocytes. *Biomaterials*. 2014;35:2798-2808.

215. Rogers AJ, Fast VG and Sethu P. Biomimetic Cardiac Tissue Model Enables the Adaption of Human Induced Pluripotent Stem Cell Cardiomyocytes to Physiological Hemodynamic Loads. *Anal Chem*. 2016;88:9862-9868.

216. Rogers AJ, Kannappan R, Abukhalifeh H, Ghazal M, Miller JM, El-Baz A, Fast VG and Sethu P. Hemodynamic Stimulation Using the Biomimetic Cardiac Tissue Model (BCTM) Enhances Maturation of Human Induced Pluripotent Stem Cell-Derived Cardiomyocytes. *Cells, tissues, organs*. 2018;206:82-94.

217. Satin J, Kehat I, Caspi O, Huber I, Arbel G, Itzhaki I, Magyar J, Schroder EA, Perlman I and Gepstein L. Mechanism of spontaneous excitability in human embryonic stem cell derived cardiomyocytes. 2004;559:479-496.

218. Olson EN and Srivastava D. Molecular Pathways Controlling Heart Development. 1996;272:671-676.

219. Hirota A, Kamino K, Komuro H, Sakai T and Yada T. Early events in development of electrical activity and contraction in embryonic rat heart assessed by optical recording. 1985;369:209-227.

220. Tandon N, Cannizzaro C, Chao P-HG, Maidhof R, Marsano A, Au HTH, Radisic M and Vunjak-Novakovic G. Electrical stimulation systems for cardiac tissue engineering. *Nature Protocols*. 2009;4:155-173.

221. Tandon N, Marsano A, Maidhof R, Wan L, Park H and Vunjak-Novakovic G. Optimization of electrical stimulation parameters for cardiac tissue engineering. *J Tissue Eng Regen Med*. 2011;5:e115-25.

222. Hirt MN, Boeddinghaus J, Mitchell A, Schaaf S, Bornchen C, Muller C, Schulz H, Hubner N, Stenzig J, Stoehr A, Neuber C, Eder A, Luther PK, Hansen A and Eschenhagen

T. Functional improvement and maturation of rat and human engineered heart tissue by chronic electrical stimulation. *Journal of molecular and cellular cardiology*. 2014;74:151-61.

223. Eng G, Lee BW, Protas L, Gagliardi M, Brown K, Kass RS, Keller G, Robinson RB and Vunjak-Novakovic G. Autonomous beating rate adaptation in human stem cell-derived cardiomyocytes. *Nature Communications*. 2016;7:10312.

224. Nunes SS, Miklas JW, Liu J, Aschar-Sobbi R, Xiao Y, Zhang B, Jiang J, Massé S, Gagliardi M, Hsieh A, Thavandiran N, Laflamme MA, Nanthakumar K, Gross GJ, Backx PH, Keller G and Radisic M. Biowire: a platform for maturation of human pluripotent stem cell–derived cardiomyocytes. *Nature Methods*. 2013;10:781.

225. Stoppel WL, Kaplan DL and Black LD, 3rd. Electrical and mechanical stimulation of cardiac cells and tissue constructs. *Advanced drug delivery reviews*. 2016;96:135-55.

226. Godier-Furnémont AF, Tiburcy M, Wagner E, Dewenter M, Lämmle S, El-Armouche A, Lehnart SE, Vunjak-Novakovic G and Zimmermann WH. Physiologic force-frequency response in engineered heart muscle by electromechanical stimulation. *Biomaterials*. 2015;60:82-91.

227. Visone R, Talò G, Occhetta P, Cruz-Moreira D, Lopa S, Pappalardo OA, Redaelli A, Moretti M and Rasponi M. A microscale biomimetic platform for generation and electro-mechanical stimulation of 3D cardiac microtissues. *APL Bioeng*. 2018;2:046102.

228. Berger HJ, Prasad SK, Davidoff AJ, Pimental D, Ellingsen O, Marsh JD, Smith TW and Kelly RA. Continual electric field stimulation preserves contractile function of adult ventricular myocytes in primary culture. *The American journal of physiology*. 1994;266:H341-9.

229. Kato S, Ivester CT, Cooper Gt, Zile MR and McDermott PJ. Growth effects of electrically stimulated contraction on adult feline cardiocytes in primary culture. *The American journal of physiology*. 1995;268:H2495-504.

230. Ivester CT, Kent RL, Tagawa H, Tsutsui H, Imamura T, Cooper Gt and McDermott PJ. Electrically stimulated contraction accelerates protein synthesis rates in adult feline cardiocytes. *The American journal of physiology*. 1993;265:H666-74.

231. Bian W, Badie N, Himel HD and Bursac N. Robust T-tubulation and maturation of cardiomyocytes using tissue-engineered epicardial mimetics. *Biomaterials*. 2014;35:3819-3828.

232. Liu J, Lieu DK, Siu CW, Fu JD, Tse HF and Li RA. Facilitated maturation of Ca2+ handling properties of human embryonic stem cell-derived cardiomyocytes by calsequestrin expression. *American journal of physiology Cell physiology*. 2009;297:C152-9.

233. Li M, Kanda Y, Ashihara T, Sasano T, Nakai Y, Kodama M, Hayashi E, Sekino Y, Furukawa T and Kurokawa J. Overexpression of KCNJ2 in induced pluripotent stem cell-derived cardiomyocytes for the assessment of QT-prolonging drugs. *Journal of Pharmacological Sciences*. 2017;134:75-85.

234. Jiang Y, Park P, Hong SM and Ban K. Maturation of Cardiomyocytes Derived from Human Pluripotent Stem Cells: Current Strategies and Limitations. *Molecules and cells*. 2018;41:613-621.

235. Ellen Kreipke R, Wang Y, Miklas JW, Mathieu J and Ruohola-Baker H. Metabolic remodeling in early development and cardiomyocyte maturation. *Seminars in cell & developmental biology*. 2016;52:84-92.

236. Gentillon C, Li D, Duan M, Yu WM, Preininger MK, Jha R, Rampoldi A, Saraf A, Gibson GC, Qu CK, Brown LA and Xu C. Targeting HIF-1α in combination with PPARα activation and postnatal factors promotes the metabolic maturation of human induced pluripotent stem cell-derived cardiomyocytes. *Journal of molecular and cellular cardiology*. 2019;132:120-135.

237. Hui EE and Bhatia SN. Micromechanical control of cell–cell interactions. 2007;104:5722-5726.

238. Deb A. Cell–cell interaction in the heart via Wnt/β-catenin pathway after cardiac injury. *Cardiovasc Res*. 2014;102:214-223.

239. Howard CM and Baudino TA. Dynamic cell–cell and cell–ECM interactions in the heart. *Journal of molecular and cellular cardiology*. 2014;70:19-26.

240. Brutsaert DL. Cardiac endothelial-myocardial signaling: its role in cardiac growth, contractile performance, and rhythmicity. *Physiological reviews*. 2003;83:59-115.

241. Ieda M, Tsuchihashi T, Ivey KN, Ross RS, Hong TT, Shaw RM and Srivastava D. Cardiac fibroblasts regulate myocardial proliferation through beta1 integrin signaling. *Developmental cell*. 2009;16:233-44.

242. Tirziu D, Giordano FJ and Simons M. Cell communications in the heart. *Circulation*. 2010;122:928-37.

243. Fountoulaki K, Dagres N and Iliodromitis EK. Cellular Communications in the Heart. *Cardiac failure review*. 2015;1:64-68.

244. Bergmann O, Zdunek S, Felker A, Salehpour M, Alkass K, Bernard S, Sjostrom SL, Szewczykowska M, Jackowska T, Dos Remedios C, Malm T, Andrä M, Jashari R, Nyengaard JR, Possnert G, Jovinge S, Druid H and Frisén J. Dynamics of Cell Generation and Turnover in the Human Heart. *Cell*. 2015;161:1566-75.

245. Pinto AR, Ilinykh A, Ivey MJ, Kuwabara JT, D'Antoni ML, Debuque R, Chandran A, Wang L, Arora K, Rosenthal NA and Tallquist MD. Revisiting Cardiac Cellular Composition. *Circ Res*. 2016;118:400-9.

246. Giacomelli E, Meraviglia V, Campostrini G, Cochrane A, Cao X, van Helden RWJ, Krotenberg Garcia A, Mircea M, Kostidis S, Davis RP, van Meer BJ, Jost CR, Koster AJ, Mei H, Míguez DG, Mulder AA, Ledesma-Terrón M, Pompilio G, Sala L, Salvatori DCF, Slieker RC, Sommariva E, de Vries AAF, Giera M, Semrau S, Tertoolen LGJ, Orlova VV, Bellin M and Mummery CL. Human-iPSC-Derived Cardiac Stromal Cells Enhance Maturation in 3D Cardiac Microtissues and Reveal Non-cardiomyocyte Contributions to Heart Disease. *Cell Stem Cell*. 2020;26:862-879.e11.

247. Lee Desy S, Chen J-H, Lundy David J, Liu C-H, Hwang S-M, Pabon L, Shieh R-C, Chen C-C, Wu S-N, Yan Y-T, Lee S-T, Chiang P-M, Chien S, Murry Charles E and Hsieh Patrick CH. Defined MicroRNAs Induce Aspects of Maturation in Mouse and Human Embryonic-Stem-Cell-Derived Cardiomyocytes. *Cell Reports*. 2015;12:1960-1967.

248. Pedrotty DM, Klinger RY, Kirkton RD and Bursac N. Cardiac fibroblast paracrine factors alter impulse conduction and ion channel expression of neonatal rat cardiomyocytes. *Cardiovasc Res*. 2009;83:688-697.

249. Ohnishi S, Sumiyoshi H, Kitamura S and Nagaya N. Mesenchymal stem cells attenuate cardiac fibroblast proliferation and collagen synthesis through paracrine actions. *FEBS Letters*. 2007;581:3961-3966.

250. Bang C, Batkai S, Dangwal S, Gupta SK, Foinquinos A, Holzmann A, Just A, Remke J, Zimmer K, Zeug A, Ponimaskin E, Schmiedl A, Yin X, Mayr M, Halder R, Fischer A, Engelhardt S, Wei Y, Schober A, Fiedler J and Thum T. Cardiac fibroblast–derived microRNA passenger strand-enriched exosomes mediate cardiomyocyte hypertrophy. *The Journal of Clinical Investigation*. 2014;124:2136-2146.

251. Ceccato TL, Starbuck RB, Hall JK, Walker CJ, Brown TE, Killgore JP, Anseth KS and Leinwand LA. Defining the Cardiac Fibroblast Secretome in a Fibrotic Microenvironment. 2020;9:e017025.

252. Pinto JG and Fung YC. Mechanical properties of the heart muscle in the passive state. *Journal of Biomechanics*. 1973;6:597-616.

253. Wang B, Borazjani A, Tahai M, Curry AL, Simionescu DT, Guan J, To F, Elder SH and Liao J. Fabrication of cardiac patch with decellularized porcine myocardial scaffold and bone marrow mononuclear cells. *Journal of biomedical materials research Part A*. 2010;94:1100-10.

254. Fung YC. *Biomechanics: Mechanical Properties of Living Tissues*. New York: Springer-Verlag; 1993.

255. Lanir Y. Constitutive equations for fibrous connective tissues. *Journal of Biomechanics*. 1983;16:1-12.

256. Little R and Wead W. Diastolic viscoelastic properties of active and quiescent cardiac muscle. 1971;221:1120-1125.

257. Tsaturyan AK, Izacov VJ, Zhelamsky SV and Bykov BL. Extracellular fluid filtration as the reason for the viscoelastic behaviour of the passive myocardium. *Journal of Biomechanics*. 1984;17:749-755.

258. Miller CE and Wong CL. Trabeculated embryonic myocardium shows rapid stress relaxation and non-quasi-linear viscoelastic behavior. *Journal of Biomechanics*. 2000;33:615-622.

259. Sommer G, Schriefl AJ, Andrä M, Sacherer M, Viertler C, Wolinski H and Holzapfel GA. Biomechanical properties and microstructure of human ventricular myocardium. *Acta Biomaterialia*. 2015;24:172-192.

260. Nguyen-Truong M and Wang Z. Biomechanical Properties and Mechanobiology of Cardiac ECM. *Advances in experimental medicine and biology*. 2018;1098:1-19.

261. Wang Z and Chesler NC. Pulmonary Vascular Wall Stiffness: An Important Contributor to the Increased Right Ventricular Afterload with Pulmonary Hypertension. 2011;1:212-223.

262. Wang Z and Chesler NC. Pulmonary vascular mechanics: important contributors to the increased right ventricular afterload of pulmonary hypertension. 2013;98:1267-1273.

263. Wang Z, Schreier DA, Hacker TA and Chesler NC. Progressive right ventricular functional and structural changes in a mouse model of pulmonary arterial hypertension. 2013;1:e00184.

264. Fukushima S, Coppen SR, Lee J, Yamahara K, Felkin LE, Terracciano CM, Barton PJ, Yacoub MH and Suzuki K. Choice of cell-delivery route for skeletal myoblast transplantation for treating post-infarction chronic heart failure in rat. *PloS one*. 2008;3:e3071.

265. Chen HS, Kim C and Mercola M. Electrophysiological challenges of cell-based myocardial repair. *Circulation*. 2009;120:2496-508.

266. Lin YD, Ko MC, Wu ST, Li SF, Hu JF, Lai YJ, Harn HI, Laio IC, Yeh ML, Yeh HI, Tang MJ, Chang KC, Su FC, Wei EI, Lee ST, Chen JH, Hoffman AS, Wu WT and Hsieh PC. A nanopatterned cell-seeded cardiac patch prevents electro-uncoupling and improves the therapeutic efficacy of cardiac repair. *Biomaterials science*. 2014;2:567-80.

267. Bian W, Jackman CP and Bursac N. Controlling the structural and functional anisotropy of engineered cardiac tissues. *Biofabrication*. 2014;6:024109.

268. Black LD, 3rd, Meyers JD, Weinbaum JS, Shvelidze YA and Tranquillo RT. Cell-induced alignment augments twitch force in fibrin gel-based engineered myocardium via gap junction modification. *Tissue engineering Part A*. 2009;15:3099-108.

APPENDIX A

IACUC APPROVAL FORM

From: Office of IACUC UAB <iacuc@uab.edu>
Sent: Wednesday, February 26, 2020 4:54 PM
To: Zhang, Jianyi (Jay)
Cc: Hillard, Kelly; Gregory P Walcott
Subject: IACUC Approval for Modification of Animal Protocol Number (APN): IACUC-20216

DO NOT Reply or Reply All to this email!

Protocol PI: Jianyi Zhang
Title: Myocardial Repair Using Human iPSC Derived Cardiac Muscle Patch
Sponsor: National Heart, Lung, and Blood Institute/NIH/DHHS
Animal Project Number (APN): IACUC-20216

On 2/26/2020, the UAB Institutional Animal Care and Use Committee (IACUC) approved the proposed modification: Personel: Danielle Pretorius. The sponsor for this project may require notification of modification(s) approved by the IACUC, but not included in the original grant proposal/experimental plan; please inform the sponsor if necessary.
Approval from the IACUC must be obtained before implementing any changes or modifications in the approved animal use. Refer to APN IACUC-20216 when ordering animals or in any correspondence with the IACUC or Animal Resources Program (ARP) offices regarding this study. If you have concerns or questions regarding this notice, please call the IACUC office at (205) 934-7692.

IACUC Office